

**SYNTHESIS AND CHARACTERIZATION OF SILVER AND SILVER
SELENIDE NANOPARTICLES AND THEIR INCORPORATION INTO
POLYMER FIBRES USING ELECTROSPINNING TECHNIQUE**

A Dissertation

by

Dikeledi Selinah More

20478330

**Submitted to the faculty of Applied and Computer Science in fulfilment of the
requirements for the degree of**

MASTERS

IN

CHEMISTRY

in the

DEPARTMENT OF CHEMISTRY

VAAL UNIVERSITY OF TECHNOLOGY

Supervisor : Prof. M. J. Moloto (PhD Chemistry) (VUT)

Co-supervisor : Dr. N. Moloto (PhD Chemistry) (WITS UNIVERSITY)

DECLARATION

I hereby declare that the work on “Synthesis and characterization of silver and silver selenide nanoparticles and their incorporation into polymer fibres using electrospinning technique” is my own, and has not been submitted for any degree or examination in any other university.

Name: Dikeledi Selinah More

Date: -----

Signature: -----

DEDICATION

I would like to dedicate this work to my grandfather who passed away last year. He was my strength whenever I was feeling down. He used to support and guide me to all the things I was doing. I would also like to dedicate this dissertation to my family for what they have done for me through these years. I would not have been able to get to where I am today without their love and support. Lastly dedication to God almighty for making this work to be possible and for providing all the necessary resources required.

ACKNOWLEDGEMENTS

I would like to thank my supervisor, Prof M. J. Moloto, for his advice on my research and for the valuable help during my difficult times. I also would like to thank Dr. N. Moloto for her kindness and helpful discussion. My deepest thanks to Vaal University of Technology for letting me use their resources and helping me with financial support. I also thank NRF for their financial support. I would like to express my gratitude to Dr. K. P. Matabola from Mintek for being a good mentor for electrospinning. Finally, thanks to Mr Siyasanga Mpelane at Mintek for characterization of my samples. Many thanks to my group members for helping me especially Mr Bonginkosi Sibokoza.

CONFERENCES AND PUBLICATIONS

Conferences

1. NanoAfrica International Conference (Poster presentation), TOPO-capped Ag₂Se nanoparticles and their incorporation into polymer fibres using electrospinning technique. Held at Quest conference estates, Vanderbijlpark, 30 - 2 March 2014.
2. SACI Conference (Oral presentation), TOPO-capped Ag₂Se nanoparticles and their incorporation into polymer fibres using electrospinning technique. Walter Sisulu University, East London, 1-6 December 2013.
3. SANI Symposium (Oral presentation), TOPO-capped Ag₂Se nanoparticles and their incorporation into poly (vinyl pyrrolidone) (PVP) nanofibres using electrospinning technique. Held at CSIR, Pretoria, 8th November 2013.
4. Inorganic Conference (Poster presentation), Synthesis and characterization of Ag₂Se nanoparticles and their incorporation into poly (vinyl pyrrolidone) (PVP) nanofibres using electrospinning technique. Held at Southern Sun Elangeni Hotel, Durban, 30-4 July 2013.
5. Year-end function hosted by Bioscience department (Oral presentation), Synthesis and characterization of TOPO/HDA-capped Ag₂Se nanoparticles. Held at GW 103 Vaal University of Technology, 29 November 2012.

Publications

1. D. S. More, M. J. Moloto, N. Moloto, K.P. Matabola, TOPO-capped silver selenide nanoparticles and their incorporation into polymer nanofibres using electrospinning technique, Materials Research Bulletin, 65 (2015) 14-22.
2. D. S. More, M. J. Moloto, N. Moloto, Synthesis and Characterization of HDA-capped Ag₂Se nanoparticles, Manuscript under construction, 2015.

ABSTRACT

Here, we report the synthesis and characterization of silver (Ag) and silver selenide (Ag_2Se) nanoparticles using the metal-organic route method. This method involves the reduction of selenium powder and silver nitrate in the presence of trioctylphosphine as a solvent. Tri-n-octylphosphine oxide (TOPO) and hexadecylamine (HDA) were used in the study as capping molecules. The optical properties of the as-prepared nanoparticles were studied using UV-Visible and photoluminescence spectroscopy (PL). Transmission electron microscopy (TEM) and X-ray powder diffraction (XRD) were used to study the structural properties. The effect of capping molecules and temperature were investigated on the growth of the nanoparticles. The prepared nanoparticles seem to depend on the reaction temperature where the increase in temperature led to an increase in particle sizes. The growth of the as-prepared TOPO-capped Ag_2Se nanoparticles was influenced by temperature, this was evident when the temperature was increased, the nanoparticles evolved from sphere to hexagonal shape. TOPO-capped nanoparticles showed the tendency of agglomeration with increase in temperature compared to HDA-capped nanoparticles. The X-ray diffraction results showed peaks which were identified as due to α - Ag_2Se body centered cubic compound for both TOPO/HDA-capped Ag_2Se nanoparticles. Some evidence of impurities were observed in the XRD analysis and indexed to metallic silver.

HDA-capped Ag nanoparticles were found to be affected by temperature variation. The prepared nanoparticles were characterized with UV-Vis spectroscopy and transmission electron microscopy. XRD analysis was not performed due to small yield obtained. The absorption spectra of HDA-capped Ag nanoparticles at different temperatures show a surface Plasmon resonance (SPR) band in the regions 418 - 428 nm. Uniform spherical shapes were obtained for both 130 and 190 °C and fewer particles were obtained at 160 °C. The synthesis of TOPO-capped Ag nanoparticles was unsuccessful since none of the particles were isolated from the solution due to its lower capping ability or it may be that TOPO is binding too strongly to Ag.

The polymer nanofibres were electrospun using electrospinning technique. Parameters such as concentration and voltage were investigated. These parameters significantly affect the formation of fibre morphology. PVP and PMMA polymers were used for this study. The electrospun composite fibres were characterized using UV-Visible spectroscopy, scanning electron microscopy (SEM), Thermal gravimetric analysis (TGA), X-ray diffraction (XRD) and Fourier transformer infrared (FTIR) spectroscopy. The SEM results show that increasing the polymer concentration resulted in increased fibre diameters. Hence increasing the voltage decreases the fibre diameters. Ag₂Se nanoparticles were incorporated into PVP and PMMA and electrospun using electrospinning to produce composite fibres. Their addition into PVP polymer fibres improved the fibre's uniformity and further decreased their diameters. The SEM of composite fibres for PMMA is not shown. The absorption bands for PVP composites fibres show a blue shift from the pure Ag₂Se nanoparticles, whereas the one for PMMA show a red shift from the pure Ag₂Se nanoparticles. Both the composite fibres for PVP and PMMA show a blue shift from the bulk of Ag₂Se. The XRD analysis of the composite fibres shows no significant effect upon addition of Ag₂Se nanoparticles on the amorphous peak of the PVP polymer, whereas on the PMMA, it shows peaks which were due to the face centered cubic phase of Ag. The FTIR spectra of the composite fibres and pure polymers (PVP and PMMA) gave almost identical features. TGA curves show no significant effect on the thermal properties of the PVP polymer and its composites, however, on the PMMA composite fibres it show an increase in the thermal stability of the polymers upon addition of Ag₂Se nanoparticles. The study was based on silver nanoparticles and its antibacterial activities. One of the synthetic challenges for silver nanoparticles is their solubility and yield. Selenide was introduced in the study to improve such shortcomings of silver nanoparticles and also for possible improved properties, chemical stability and increased activity against bacteria. The selenide group on the metal also provides stronger chemical interaction between the nanoparticles and the polymer. Therefore, the intension was to use these nanoparticles into polymer fibres for potential use in wound dressing.

TABLE OF CONTENTS

DECLARATION	i
DEDICATION	ii
ACKNOWLEDGEMENTS	iii
CONFERENCES AND PUBLICATIONS.....	iv
ABSTRACT	v
TABLE OF CONTENTS.....	vii
LIST OF FIGURES	xiii
LIST OF ABBREVIATIONS.....	xvi
DISSERTATION OUTLINE.....	xvii
CHAPTER 1	1
INTRODUCTION	1

1.1	Nanotechnology	1
1.1.1	Silver and silver selenide nanoparticles	2
1.2	Polymer nanocomposites	4
1.3	Electrospinning	5
1.3.1	Electrospinning: History and process setup	7
1.3.2	Jet initiation	9
1.3.3	Continuous flow of the jet towards the ground collector	9
1.3.4	Bending instability of the jet	10
1.3.5	Parameters affecting electrospinning process	10
1.3.6	Solution parameters.....	11
1.3.6.1	Concentration	11
1.3.6.2	Viscosity	11
1.3.6.3	Molecular weight.....	12
1.3.6.4	Conductivity/Surface Charge Density.....	12
1.3.6.5	Surface tension	13
1.3.7	Process parameters	13
1.3.7.1	Applied voltage	13
1.3.7.2	Distance between the tip and the collector.....	14
1.3.7.3	Flow rate.....	14
1.3.8	Ambient parameters	15
1.3.8.1	Temperature (Ambient temperature).....	15
1.3.8.2	Humidity.....	15
1.4	Motivation statement	16
1.5	Aim and Objectives of the study.....	16
1.6	References.....	18

CHAPTER 2	22
LITERATURE REVIEW	22
2.1 Silver metal nanoparticles.....	22
2.1.2 Silver selenide semiconductor nanoparticles (Ag_2Se)	23
2.2 Synthetic methods for the preparation of nanoparticles	24
2.2.1 Colloidal route.....	25
2.2.2 Metal-organic routes	25
2.2.3 Solvothermal Method.....	26
2.2.4 Synthesis in confined matrices	26
2.2.5 Chemical precipitation method	26
2.2.6 Sol-Gel process	27
2.3 Applications of nanoparticles	27
2.3.1 Applications of Ag nanoparticles.....	27
2.3.1.1 Antibacterial Application	27
2.3.1.2 Catalytic Application.....	28
2.3.1.3 Optical Application	28
2.3.2 Applications of Ag_2Se nanoparticles.....	28
2.3.2.1 Photovoltaic devices.....	28
2.3.2.2 Light emitting devices	29
2.3.2.3 Biological Applications.....	29
2.3.3 Applications of Electrospinning.....	30
2.3.3.1 Filtration applications.....	30
2.3.3.2 Textile applications	31
2.3.3.3 Catalysis	31
2.3.4 Medical Applications	32

2.3.4.1	Tissue engineering scaffolds	32
2.3.4.2	Wound healing	32
2.3.4.3	Nanosensors	33
2.4	References.....	34
 CHAPTER 3		37
MATERIALS AND METHODS.....		37
3.1	Materials	37
3.2	Instrumentation	37
3.2.1	Optical characterization.....	37
3.2.2	Transmission electron microscopy (TEM).....	38
3.2.3	X-ray diffraction (XRD).....	38
3.2.4	Scanning electron microscopy (SEM).....	38
3.2.5	Infrared spectrophotometer	38
3.2.6	Thermogravimetric analysis (TGA)	38
3.2.7	Electrospinning.....	39
3.3	Experimental procedures	39
3.3.1	Synthesis of Ag nanoparticles	39
3.3.2	Synthesis of Ag ₂ Se nanoparticles.....	39
3.3.3	Electrospinning of Ag ₂ Se/PVP/PMMA	40
 RESULTS AND DISCUSSIONS		42
CHAPTER 4		42
NANOPARTICLES.....		42
4.1	Synthesis and characterization of Ag ₂ Se nanoparticles	42

4.1.1	Capping molecules	42
4.2	TOPO-capped Ag ₂ Se nanoparticles	43
4.2.1	Effect of temperature.....	43
4.2.1.1	Optical properties	43
4.2.1.2	Structural characterization.....	45
4.3	HDA-capped Ag ₂ Se nanoparticles.....	48
4.3.1	Effect of temperature.....	48
4.3.1.1	Optical properties	48
4.3.1.2	Structural characterization.....	50
4.4	Ag Nanoparticles	53
4.4.1	Effect of temperature.....	54
4.4.1.1	Optical properties	54
4.4.1.2	Structural properties	55
4.5	Conclusions.....	57
4.6	References.....	58
CHAPTER 5		59
POLYMER FIBRES		59
5.1	Properties of PVP and PMMA polymers	59
5.2	Electrospinning of PVP and PMMA polymer fibers	60
5.2.1	Polymer nanofibers	60
5.2.2	Effect of PVP and PMMA concentration the electrospun polymer fibers	61
5.3	Effect of applied voltage	64
5.4	PVP/PMMA/Ag ₂ Se composite fibres	66
5.4.1	Incorporation of TOPO-capped Ag ₂ Se nanoparticles into PVP and PMMA nanofibers	66

5.4.2	Structural properties of the composite fibres	66
5.4.2.1	SEM analysis of the composite fibres	66
5.4.2.2	XRD analysis of the pure polymer and the composite fibres.....	69
5.4.2.3	FTIR spectral analysis of the polymer and the composites fibres.....	70
5.5	Thermogravimetric analysis (TGA) of the polymers and the composites fibres.....	71
5.6	Optical properties of the polymer and the composite fibres	73
5.7	Incorporation of HDA-capped Ag ₂ Se nanoparticles into PVP and PMMA nanofibers....	74
5.7.1	XRD analysis of the pure polymer and the composite fibres.....	75
5.7.1.2	FTIR spectral analysis of the polymer and the composites fibres.....	76
5.8	Thermogravimetric analysis (TGA) of the polymers and the composites fibers.....	77
5.9	Optical properties of the polymers and the composite fibres	79
5.10	Conclusions.....	81
5.11	References.....	83
CHAPTER 6		85
SUMMARY AND RECOMMENDATION		85
6.1	Summary	85
6.2	Recommendations.....	86

LIST OF FIGURES

Figure 1: Schematic diagram of electrospinning technique for producing nanofibres	6
Figure 2: Schematic diagram showing the synthesis Ag ₂ Se nanoparticles.....	40
Figure 3: schematic illustration of the nanoparticles incorporated into PVP and PMMA polymers	41
Figure 4: Structures of coordinating solvent (a) TOPO (trioctylphosphine oxide) and (b) HDA (hexadecylamine).....	43
Figure 5:(a) Absorption and (b) Emission spectra of TOPO-capped Ag ₂ Se nanoparticles prepared at different temperatures (i) 180 °C (ii) 200 °C and (iii) 250 °C	45
Figure 6: TEM images and histogram of TOPO-capped Ag ₂ Se nanoparticles prepared at different temperatures (a, b) 180 °C, (c, d) 200 °C and (e, f) 250 °C.....	46
Figure 7:X-ray diffraction patterns of TOPO–capped Ag ₂ Se nanoparticles at different temperatures (a) 180 °C, (b) 200 °C and (c) 250 °C	48
Figure 8: (a) Absorption and (b) emission spectra of HDA-capped Ag ₂ Se nanoparticles prepared at different temperatures (i) 130 °C, (ii) 160 °C and (iii) 190 °C	50
Figure 9: TEM images of HDA-capped Ag ₂ Se nanoparticles prepared at different temperatures (a, b) 130 °C, (c, d) 160 °C and (e, f) 190 °C	51
Figure 10: XRD pattern of HDA-capped Ag ₂ Se nanoparticles prepared at different temperatures (a) 130 °C, (b) 160 °C and (c) 190 °C.	52

Figure 11: Absorption spectra of HDA-capped Ag nanoparticles prepared at different temperatures (i) 130, (ii) 160 and (iii) 190 °C.....	55
Figure 12: TEM images of HDA-capped Ag nanoparticles prepared at different temperatures (a, b) 130 °C, (c, d) 160 °C and (e, f) 190 °C	56
Figure 13: Structure of (a) PVP and (b) PMMA polymers.....	60
Figure 14: SEM images and average fiber distribution of PVP nanofibers at different polymer concentrations of (a) 35 wt%, (b) 40 wt% and (c) 45 wt%.....	63
Figure 15: SEM images and fibres distribution of 40 wt% PVP at different voltages (a) 11 kV, (b) 13 kV, (c) 15 kV, (d) 17 kV and (e) 20 kV (f) Fibre size distribution.....	65
Figure 16: SEM images and fibre distribution of (40 wt%) PVP with different loading of the nanoparticles (a) 0 wt% (b) 0.2 wt% and (c) 0.6 wt%.....	68
Figure 17: XRD patterns of (a) PVP, (i) 0wt%, (ii) 0.2 wt% and (iii) 0.6 wt% and (b) PMMA, (i) 0 wt%, (ii) 0.2 wt% and (iii) 0.6 wt% Ag ₂ Se/ PVP/PMMA.....	69
Figure 18: FTIR spectra of (a) PVP, (i) 0 wt%, (ii) 0.2 wt% and (iii) 0.6 wt% and (b) PMMA, (i) 0 wt%, (ii) 0.2 wt% and (iii) 0.6 wt% Ag ₂ Se/ PVP/PMMA.....	71
Figure 19: TGA curve of (a) PVP, (i) 0 wt%, (ii) 0.2 wt% and (iii) 0.6 wt% and (b) PMMA, (i) 0 wt%, (ii) 0.2 wt% and (iii) 0.6 wt% Ag ₂ Se/ PVP/PMMA.....	72
Figure 20: Absorption spectra of (a) PVP, (i) 0 wt%, (ii) 0.2 wt% and (iii) 0.6 wt% and (b) PMMA, (i) 0 wt%, (ii) 0.2 wt% and (iii) 0.6 wt% Ag ₂ Se/ PVP/PMMA	73
Figure 21: XRD patterns of (a) PVP, (i) 0 wt%, (ii) 0.2 wt% and (iii) 0.6 wt% and (b) PMMA, (i) 0 wt %, (ii) 0.2 wt% and (iii) 0.6 wt% Ag ₂ Se/ PVP/PMMA	75

Figure 22: FTIR spectra of (a) PVP, (i) 0 wt%, (ii) 0.2 wt% and (iii) 0.6 wt% and (b) PMMA, (i) 0 wt%, (ii) 0.2 wt% and (iii) 0.6 wt% Ag₂Se/ PVP/PMMA..... 76

Figure 23:TGA curve of (a) PVP, (i) 0 wt%, (ii) 0.2 wt% and (iii) 0.6 wt% and (b) PMMA, (i) 0 wt%, (ii) 0.2 wt% and (iii) 0.6 wt% Ag₂Se/ PVP/PMMA..... 78

Figure 24: Absorption spectra of (a) PVP, (i) 0 wt%, (ii) 0.2 wt% and (iii) 0.6 wt% and (b) PMMA, (i) 0 wt%, (ii) 0.2 wt% and (iii) 0.6 wt% Ag₂Se/ PVP/PMMA 79

LIST OF ABBREVIATIONS

TOPO	Trioctylphosphine oxide
HDA	Hexadecylamine
TOP	Trioctylphosphine
PVP	Poly (vinylpyrrolidone)
PMMA	poly (methyl methacrylate)
PU	Polyurethane
PAN	Polyacrylonitrile
PLLA	Poly-l-lactic acid
PLC	Polymer liquid crystal
PLA	Polylactic acid
a.u	Arbitrary units
nm	Nanometre
FTIR	Fourier transformer infrared spectroscopy
TEM	Transmission electron microscopy
UV/Vis	Ultra violet visible spectroscopy
PL	Photoluminescence
XRD	X-ray powder diffraction
SEM	Scanning electron microscopy
TGA	Thermal gravimetric analysis

DISSERTATION OUTLINE

This dissertation is divided into six chapters. The outlines for each chapter are presented as follows:

Chapter 1

Chapter deals with short discussion which covers a general background on nanotechnology, inorganic material used to synthesize the nanoparticles, nanocomposites and electrospinning. History of electrospinning and process parameters is discussed in detail in this chapter. The motivation statement, aim and objectives of the study are also stated in this chapter.

Chapter 2

Chapter two presents a literature review of the overall study. Metal and semiconductors nanoparticles are discussed in this chapter. Synthetic method and applications of nanoparticles are also discussed. Applications of polymer nanofibres are also stated.

Chapter 3

This chapter explains the synthesis of nanoparticles and their incorporation into polymer fibres using electrospinning technique. Characterization techniques were also stated in this chapter. The chemicals used for this study were also stated.

Chapter 4

The results and discussions are covered in this chapter as well as the conclusions.

Chapter 5

This chapter presents results and discussions with more emphasis on the electrospun fibres. It also highlights the properties of the chosen polymers.

Chapter 6

The overall conclusions and recommendations are fully discussed in this chapter.

CHAPTER 1

INTRODUCTION

1.1 Nanotechnology

Nanotechnology is an important field of modern research dealing with design, synthesis, characterization, exploration and manipulation of particles structure ranging from approximately (1-100 nm). It deals with the materials whose structures exhibit significantly novel and improved physical, chemical, and biological properties, phenomena, and functionality due to their nanoscaled size. Nanotechnology also takes advantage of the fact that when a solid material becomes very small, its specific surface area increases, which leads to an increase in the surface reactivity and quantum-related effects. The physical and chemical properties of nanomaterials can become very different from those of the same material in larger bulk form. The history of nanotechnology dates back in 1959 where a physicist called Richard Feynman in his speech, he stated that “There’s plenty of room at the bottom” [1]. Feynman’s speech was said to be the first account publically in describing the manipulation of matter on a tiny scale. In 1986 Eric Dexler introduced the term “nanotechnology” to the public through his book called Engines of Creation [2]. Ever since then the term nanotechnology rapidly became popular. Today the young field of nanotechnology, scientists and engineers are taking control of atoms and molecules individually by manipulating and putting them to use. Tremendous growth in this emerging technology has opened novel fundamental and applied frontiers, including the synthesis of nanoscale materials and exploration or utilization of their exotic physicochemical and optoelectronic properties. This technology has found a way to bring together chemists, physicists, biologists and engineers under the same principle and methods, and has therefore affected scientific research in different ways. Nanotechnology has gain importance in a number of areas such catalysis, health care and

electronics. The synthesis of nanomaterials is growing rapidly in the research area with a great potential to make technologically advanced and useful materials thus understanding their behaviour and properties will be of great importance.

There have been impressive developments in the field of nanotechnology in the recent past years, with numerous methodologies developed to synthesize nanoparticles of particular shape and size depending on specific requirements. Nanoparticles synthesis and the study of their size, shape and properties are of fundamental importance in the advancement of recent research. New applications of nanoparticles and nanomaterials are increasing rapidly, and some of these nanoparticles have actually proven to be good catalysts that also show bactericidal effects. Hence a high surface to volume ratio is also important. It was found that the optical, electronic, magnetic and catalytic property of metal nanoparticles depends on their size, shape and chemical surrounding. In the synthesis of nanoparticles it is very important to control, not only the particle size, but also morphology and particle size distribution as well [3]. The synthesis of metal nanoparticles and that of semiconductors have been widely reported in the literature.

1.1.1 Silver and silver selenide nanoparticles

Metal nanoparticles mainly those of gold (Au) and silver (Ag) have attracted a lot of attention in recent years due to their unusual physical and chemical properties which differ from their bulk properties. These nanoparticles possess a very strong absorption in the visible region due to surface Plasmon resonance. They show unique properties such as good conductivity, chemical stability and catalytic activity which dependent on the particle size, size distribution and shape [4-6]. Among other metals, silver has often seen as material of choice for the fabrication of nanoparticles for its ease of synthesis and the wide range of application that can be developed based on their synthesis. Nanoparticles of silver have been found to exhibit interesting antibacterial activities [7]. This antimicrobial activity has become a major reason why products containing silver nanoparticles have to be developed. The investigation of this phenomenon has regained importance due to the increase of bacterial resistance to antibiotics, caused by their overuse. Recently, silver nanoparticles exhibiting antimicrobial activity have been synthesized [8]. The antibacterial activity

of the silver containing materials can be used for example, in medicine to reduce infections as well as to prevent bacterial colonization on catheters [9, 10], vascular grafts [11] and etc. Therefore in developing routes of synthesis, an emphasis was made to control the size of silver nanoparticles. Different methods were used to produce more uniform monodispersed silver nanoparticles.

Semiconductor nanoparticles are generally considered to be particles of about 1-20 nm in diameter. They are often referred to as nanoparticles, quantum dots, Q particles, nanocrystals and etc. They fall in an intermediate position between molecular and bulk materials. They also exhibit both physical and chemical properties within an intermediate state of matter. Semiconductor nanoparticles (quantum dots) have the ability to absorb and emit light of different wavelengths from the same material with changing particle size. Different methods were used for the preparation of semiconducting nanoparticles which are micelle route, sol gel route, chemical precipitation route, colloidal route and metal organic route. In many semiconductors, decreasing the size of the material can provide a way to tune the physical properties and observe new phenomena.

Silver selenide (Ag_2Se) is a semiconductor material which belongs to group I-VI compound with the optical band gap of 1.2 eV [12]. Silver selenide (Ag_2Se) has been extensively studied in literature due to its interesting and useful properties [13]. It undergoes a polymorphic phase transition at 133 °C for bulk crystals [14]. The low-temperature orthorhombic phase (β - Ag_2Se , < 133 °C), is a narrow band gap semiconductor and while the high-temperature cubic phase(α - Ag_2Se , > 133 °C) is a superionic conductor [15]. The low temperature phase of silver selenide is a promising candidate for thermoelectric applications because of its relatively high Seebeck coefficient (-150 $\mu\text{V K}^{-1}$ at 300 K), low thermal conductivity and high electrical conductivity [16]. It has also been used as a thermochromic materials and photosensitizers in photographic films. The high temperature can serve as a solid electrolyte in photochargeable secondary batteries.

1.2 Polymer nanocomposites

Polymer hybrid nanocomposite materials have attracted great interest because they often exhibit remarkable improvement in material properties with only a low percentage of inorganic materials. Polymer nanocomposite systems consist of constituent filler materials which are below 100 nm and polymers as major components. Nanoscale fillers such as carbon nanotubes, nanoparticles and nanowires have been electrospun with polymers and these nanofillers can interact with either the solvent or polymer and sometimes both since they act as charge carriers. Nanofillers offer possibilities to improve the physical properties of polymers such as optical, thermal and barrier properties with low loadings while maintaining the processability of the polymer matrix essentially intact [17-19]. Nanofillers can significantly improve or adjust the different properties of the materials into which they are incorporated, sometimes in synergy with conventional fillers. The properties of composite materials can be significantly impacted by the mixture ratio between the organic matrix and the nanofillers. The combination of organic and inorganic materials produces materials that contain properties like flexibility, light weight of organic material, heat resistance and high strength. Therefore with a view to allow nanoparticles to be used as fillers in many devices, their incorporation into polymer matrices is a meaningful objective. Extremely light polymer based coating can be produced using electrostatic coating methods and techniques like electrospinning or droplet (electrospraying) coatings can exploit the polarization force to produce nanoscale polymer fibers from polymer solution or melts. Electrospun fibres with fillers can be applied in a wide variety of applications, such as in catalysts, biosensors, and semiconductors [20-22]. In this case the nanofillers used for this study are silver and silver selenide nanoparticles which will be incorporated into polymer fibres using electrospinning technique.

1.3 Electrospinning

Electrospinning is an electrostatic fibre fabrication technique that has brought more attention to many researchers due to its versatility and potential for application in many fields. Electrospinning uses electrical forces to produce polymer fibres with nanometer-scale diameters. Electrospinning occurs when the electrical forces at the surface of a polymer solution melt or overcome the surface tension and cause an electrically charged jet to be ejected. When the jet dries or solidifies, an electrically charged fibre remains and can be directed or accelerated by electrical forces and then collected in sheets or any other useful geometrical forms. Unlike other conventional fibre spinning techniques (wet spinning, dry spinning, melt spinning, gel spinning), which are capable of producing polymer fibres with diameters down to the micrometer range, electrostatic spinning, or ‘electrospinning’ is capable of producing polymer fibres in the nanometer range, and the resulting coating network has a large specific area. This technique can be utilized to assemble fibrous polymer mats composed of fibre diameters ranging from several microns down to fibres with diameter lower than 100 nm. Both natural and synthetic polymers can be electrospun using this technique. According to previous report, fibres produced by electrospinning have high surface area to volume ratio and have found application in filtration, tissue engineering scaffolding drug delivery and wound dressing [23]. The incorporation of inorganic nanoparticles into polymer nanofibres can be achieved using either electrospinning polymer solution containing metal nanoparticles or by reducing the metal salts or complexes in the electrospun polymer nanofibres [24–27]. The obtained polymer nanofibres might exhibit improved optical, electrical, catalytic, magnetic and thermal properties. These properties of polymer nanofibres depend on the type of incorporated nanoparticles, their size, shape, their concentration and interaction with polymer matrix. Metal and semiconducting nanoparticles have been the material of great interest when it comes to polymer reinforcement due to their exciting properties especially their unusual size-dependent optical properties. These exciting properties of the nanoparticles could be introduced into polymers, by incorporating these nanoparticles into polymers to form composite materials.

The electrospinning process is solely governed by many parameters classified broadly into solution parameters, process parameters and ambient parameters. Solution parameters include concentration, viscosity, molecular weight, conductivity, and surface tension hence process

parameters include applied electric field, tip to collector distance, and flow rate. The setup for electrospinning is shown in **Figure 1**. Each of these parameters significantly affects the formation of fibres morphology obtained as a result of electrospinning and by proper manipulation of these parameters one can get nanofibres of desired morphology and diameters.

Polymers such as (poly methyl methacrylate) PMMA and (poly vinyl pyrrolidone) PVP were used in this study for the preparation of polymer nanocomposites, and nanoparticles such as silver and silver selenide were incorporated into these polymers to form polymer composite fibres. These polymers were chosen because of the following properties: PMMA is a transparent, hard, and stiff material with excellent ultraviolet stability, low water absorption, and outstanding outdoor weathering properties. PVP has a good charge storage capacity, easy processability and excellent transparency. It is a potential material having a good charge storage capacity and dopant-dependent electrical and optical properties. Chemically, PVP has been found to be inert, and non-toxic. It also shows a strong tendency for complex formation with a wide variety of small molecules.

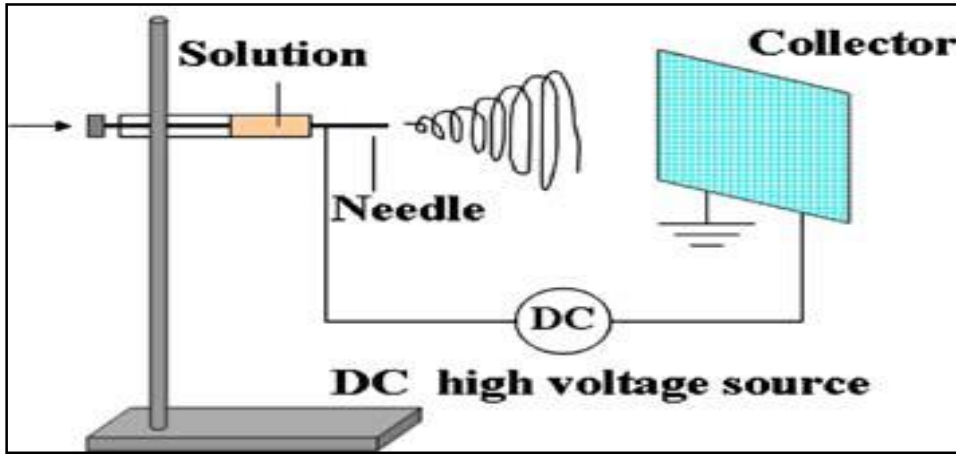


Figure 1: Schematic diagram of electrospinning technique for producing nanofibres

1.3.1 Electrospinning: History and process setup

The behavior of magnetic and electrostatic phenomena was first described by William Gilbert [28] in the late 16th century. In his study, he recorded the first observation of electrospraying after he observed that when a suitably electrically charged piece of amber was brought near a droplet of water it would form a cone shape and small droplets would be ejected from the tip of the cone. However, in 1887 C.V. Boys performed an experiment of electrical spinning and he found that as the stock liquid reached the edge of the dish the fibres could be drawn and this can be made from a number of materials. The electrical spinning apparatus made by Boys consists of a small dish, insulated and connected with an electrical machine [29]. Fifteen years later in 1902 the term electrospinning was patented by J.F Cooley and W.J. Morton [30, 31]. Cooley's patent set up included the use of rotating collector for the fibres produced from the jet directed by an auxiliary electrode [32]. The work was studied in detail by John Zeleny in 1914 where he looked at the behaviour of fluid droplets at the end of metal capillaries [33], and he made an effort to mathematically model the behaviour of fluid under electrostatic forces. Further development was made by Anton Formhals when he published a sequence of patents from 1934 [34] to 1944 [35] describing the process set up for the fabrication of textile yarns. He also came up with various innovative process setups for the production of fibres and collection, which include designs that do not require a spinneret or rotating fibre collection devices, and is been delineated in a series of patents he has published [36-38]. Formhals spinning setup composed of movable thread collecting device to collect threads in a stretched condition, like the one of a spinning drum in convention spinning [39]. However, in 1964 Sir Geoffrey Ingram Taylor was inspired by the work started by Zeleny in 1914 on the formation of jet from droplet. In his work Taylor looked at the behaviour of fluid droplets under the influence of an electric field and initiated mathematical studies on the jet forming process. Taylor discovered that when applying high electric field to a polymer solution, the exposed droplet takes a conical shape and becomes an electrically driven jet [40]. This cone is known as the Taylor cone. He theoretically derived that a perfect cone formed under the influence of an electric field required a semi-vertical angle of 49.3° just before the jet initiate.

With the emergence of nanotechnology in 1990s electrospinning has gained a great deal of attention in the manufacturing of fibres at the nanoscale. Researchers started to overlook at the importance of the electrospinning process in the nanofibres productions and realize that it has a huge potential in the variety of applications. In the fields of bio-medical research, electrospinning has found its way in electronics, catalysis, environmental and energy storage applications which has led to an increased number of scientific publications [41, 42]. Electrospinning has gained much attention ever since then and has become an attractive method for the preparation of polymer nanofibres. The process of electrospinning show many advantages over traditional nanofibre fabrications which include drawing, template synthesis, phase separation, and self assembly, like having control over morphology, porosity and the possibility to develop continuous nanofibres from various polymers. At the present moment it is the only technique that allows fabrication of continuous fibres with dimension in the order of nanometers.

A variety of polymers have been electrospun to form fine nanofibres within the submicron range. These polymers are reported as being from various synthetic and natural polymers. Typical natural polymers include chitosin, gelatine, collagen and cellulose are preferred more when used in biomedical application as compared to synthetic polymers because they exhibit better biocompatibility and low immunogenicity. Advantage for using natural polymers for electrospinning is their ability to bind cells through their protein series, example arginine, glycine and aspartic acid [43]. Despite having a good biocompatibility there has been a concern about denaturation of natural polymers during fabrication of nanofibres. Studies have been conducted on synthetic polymers, and it was found that synthetic polymers have advantage over natural polymers because they can be tailored to give a wider range of properties such as mechanical properties and desired degradation rate [44]. Examples of synthetic polymers include Polystyrene, Polyacrylonitrile, Polycarbonate, Poly (benzimidozal), Poly (vinylidenechloride), Poly (vinylidene fluoride), as well as bio-degradable polymers such as poly (ϵ -caprolactone), poly (L-lactic acid), polyglycolide, and etc [45].

Electrospinning is the technique used to produce fibres with the diameter ranging from nanometer to micrometer. Fibres produced by electrospinning have a larger surface area than those obtained from conventional spinning processes. The technique consists of three major components that is a

high voltage power supply, a needle spinneret and a collector. During this process a polymer solution held by its surface tension at the end of a capillary tube is subjected to an electric field and an electric charge is induced on the liquid surface due to this electric field. When the electric field is applied the repulsive force will overcome the surface tension and a jet is ejected from the tip of the Taylor cone. The electrospinning process consists of three stages:

1. The formation of Taylor cone and the ejection of the jet (jet initiation).
2. Continuous flow of the charge jet towards the ground collector.
3. Bending instability of the jet.

1.3.2 Jet initiation

The jet formation is the crucial step in the electrospinning process since it requires an electric field in order for it to be formed. First the voltage needs to be applied between the nozzle and the collector, in order for the electrons to migrate from the cathode to the anode causing charge on the surface of the polymer solution which forms at the tip of the needle. When the electric field is increased the charged jet of the solution will be ejected from tip of the Taylor cone.

1.3.3 Continuous flow of the jet towards the ground collector

The jet becomes stable at the tip of the spinneret at a certain distance and causes a stretching as it travels down or across the collector plate. As it travels the rapid whipping of the jet occurs at the space between the capillary tip and collector leading to the evaporation of the solvent allowing the polymer to dry.

1.3.4 Bending instability of the jet

Electrospinning utilizes electrical force to move the polymer solution out of the needle in the form of a jet towards the collector. The polymer jet can have an effect on the morphology of the fibres since it determines the manner in which the fibres are deposited on the collector. Bending instability is the region where the jet bends due to the high electrostatic forces on the surface of the jet at the tip of the Taylor cone. During this process, the charged jet of the polymer is stretched and travels for a certain distance towards the ground electrode, then a bending or whipping instability of the jet occurs which then transformed into fibres. The jet motions can results into three different types of instabilities that are:

1. Rayleigh instability, in which the jet breaks into micron-sized droplets.
2. Axisymmetric conduction instability, in which the jet resulted in a bead structure.
3. The bending or whipping instability is responsible for the elongation the jet and forming the nanofibres.

1.3.5 Parameters affecting electrospinning process

The formation of nanofibres depends on the electrospinning parameters. These working parameters are very important in order to understand not only the nature of electrospinning but also the conversion of polymer solutions into nanofibres through electrospinning. These parameters are divided into three parts that is solution parameters, process parameters and ambient parameters. Solution parameters include concentration, viscosity, molecular weight, conductivity and surface tension, process parameters include applied electric field, distance between the tip and collector and flow rate. The environmental ones are referred as ambient parameters include temperature and humidity. Each of these parameters can have an effect on the fibres morphology and by proper control of these parameters fibres of desired morphology and diameters can be obtained. These parameters have a range in which they allow for stable electrospinning of polymer

solutions. However, due to the sensitivity of fibres morphology to small changes in these parameters, it is therefore crucial to optimize these parameters for better process control to yield desired fibre morphologies and diameters. Understanding the effects of each parameter on the process is very important in order to obtain desired morphologies and diameters. These effects are discussed in subsections.

1.3.6 Solution parameters

1.3.6.1 Concentration

For fibre formation to occur in electrospinning a minimum solution concentration is required. The concentrations of polymer solution play an important role in the formation of fibres during the electrospinning. During this time electrospraying occurs instead of electrospinning owing to the low viscosity and high surface tensions of the solution [46]. Increasing concentration resulted in change in the fibre's morphology hence more uniform fibres with increased diameters are formed due to higher viscosity resistance. Optimum solution concentrations is required for electrospinning since low concentration produce beads instead of fibres and with higher concentration the formation of continuous fibres are prohibited because of the inability to maintain the flow of the solution at the tip of the needle resulting in larger fibres formation.

1.3.6.2 Viscosity

Solution viscosity plays a very important role in determining the fibres morphology. It has been confirmed that continuous and smooth fibres cannot be obtained in a very low viscosity only beaded fibres are obtained, and whereas very high viscosity results in the hard ejection of jets from solution, hence the beads shape change from being spherical to more spindle-like and finally uniform fibres are formed. To prevent this difficulty of ejection of jets from occurring optimum viscosity is required for electrospinning. Viscosity of the polymer solution is determined by the molecular weight and concentration of the polymer, though the interaction between the polymer

and the solvent can affect the system. Increasing the viscosity has an effect on the fibres diameters and morphology. Increasing viscosity causes the jet breaking resistance to increases (i.e. chain entanglement increases), while the effect of surface tension exerted by the solvent molecules decreases.

1.3.6.3 Molecular weight

High molecular weight polymer solutions have been used for electrospinning process because they provide desired viscosity for the fibre generation. It has been found that lower molecular weight solution tends to form beads instead of fibres and higher molecular weight solution provides fibres with larger average diameters. Molecular weight of the polymer reflects the entanglement of polymer chains in solutions, namely the solution viscosity.

1.3.6.4 Conductivity/Surface Charge Density

For electrospinning to occur the solution needs to be conductive to enable the surface charges to overcome the surface tension of the droplet and initiate jet flow. According to Hayati et al. [47] they have demonstrated that highly conductive solutions are extremely unstable in the presence of strong electric fields, which results in a dramatic bending instability as well as broad diameter distribution. Generally fibres with the smallest diameter can be obtained with the highest electrical conductivity because it has been found that the decrease in fibres diameter is due to the increased electrical conductivity [47]. Non-conducting solutions may not electrospin, no charges will be formed on the liquid surface even when electrical field is applied. Solution conductivity is mostly determined by the type of polymer and solvent used. Addition of ionic salts is also important since it is known to increase the charge density in electrospinning. Zhong et al. [48] have showed that addition of salt in the polymer solution removed fibre beading, with smallest fibre diameters obtained for solutions containing sodium chloride (NaCl) and largest diameters obtained for solutions containing potassium hydrogen phosphate (KH_2PO_4), while solutions containing sodium hydrogen phosphate (NaH_2PO_4) yielded fibres with intermediate diameters. These observations

are due to the greater elongational force, caused by the greater mobility of the smaller ions, under the influence of the electrostatic field.

1.3.6.5 Surface tension

The formation of polymer jet from the droplet requires the repulsive electrical force to overcome the surface tension acting in the opposite direction. When the jet travels to the collector, the stretching force by the repelling charges have to have a control over the surface tension of the jet to prevent beading of the fibres. Surface tension is commonly determined by the solvent composition and the interaction of the solvent with the polymer, and thus varies depending on the solvent used to dissolve a given polymer. In literature, it is stated that lower surface tension of the spinning solution helps electrospinning to occur at a lower electric field [49], whereas higher surface tension of a solution inhibits the electrospinning process because of instability of the jets and the generation of sprayed droplets [50]. In principle, the formation of droplets, bead and fibres depends on the surface tension of the solution.

1.3.7 Process parameters

1.3.7.1 Applied voltage

Applied voltage is the crucial element in the electrospinning process. Electrospinning only takes place when a minimum threshold voltage is applied to a charged solution and thus forms fibres. The applied voltage causes the charges to be collected on the surface of a droplet and together with the applied electric field the formation of a Taylor cone is induced, and the jet will emanate from the tip of the cone. Generally higher voltage causes greater stretching of the jet due to the increase in columbic force exerted by the charges [45]. Increasing the voltage can lead to the reduction of fibre diameters due to increased stretching, while moving beyond a critical voltage can cause more solution to be ejected from the nozzle, which will leads to formation of fibres with larger diameters [51].

1.3.7.2 Distance between the tip and the collector

The distance between the tip and the collector is another factor that can affect the fibres diameters and morphology. Varying the distance between the tip and the collector will change the flight distance as well as the electric field strength for a given voltage. Therefore if the distance is reduced the field strength that accelerate the jet downwards will be increased as a results there may not be enough time for the solvent to evaporate hence wet fibres will be formed. It has been demonstrated that a minimum distance is required to give the fibres sufficient time to dry before reaching the collector in order to prevent beads from occurring. Buchko et al. [52] reported that flatter fibres can be produced at closer distances but as the distance increases rounder fibres were observed with the spinning of silk-like polymer. Yuan et al. [53] showed that a little long distance favours the thinner fibre diameters. Long distance also tends to form beading of fibres. It is therefore important to find the optimum distance between the tip and collector that is sufficiently high to allow evaporation of the solvent from the fibres.

1.3.7.3 Flow rate

Flow rate of the polymer from the syringe is an important factor as it influences the jet velocity and the material transfer rate. Yuan et al. [53] showed that lower feeding rate is more desirable as the solvent will get enough time to evaporate. It was observed that increasing the feeding rate could lead to increased fibre diameters and pore diameters. Generally high flow rates result in beaded fibres due to unavailability of proper drying time prior to reaching the collector. [53]

1.3.8 Ambient parameters

1.3.8.1 Temperature (Ambient temperature)

The solution temperature influences the solvent evaporation rate and solution viscosity. As a result higher temperatures are shown to yield finer fibres [45]. Mit-uppatham et al. [54] did the study on the effect of temperature on the electrospun polyamide-6 and they have found that increasing temperature favours the thinner fibre diameter with polyamide-6 fibres for the inverse relationship between the solution viscosity and temperature.

1.3.8.2 Humidity

Humidity above a certain level is found to cause pores on the surface or interior of the fibres. The pores sizes were found to increase with increasing humidity, eventually coalescing to form large, non-uniform structures [55]. It has been demonstrated that at very low humidity a volatile solvent may dry rapidly as the evaporation of the solvent is faster. In some cases if the evaporation rate is faster than the removal of the solvent from the tip of the needle this can cause problems in electrospinning. [56]

1.4 Motivation statement

Nowadays increasing demand for special materials led to the conception of composites, since valuable properties of different types of materials can be combined. The combination of organic and inorganic materials produces materials that contain properties like flexibility, light weight of organic material, heat resistance and high strength. Polymer nanocomposites are materials that consist of polymer having nanoparticles or fillers dispersed in the polymer matrix. With the emergence of nanotechnology, researchers became more interested in studying the unique properties of nanoscale materials. The discovery on new nanoscaled material such as nanoclays, carbon nanotubes and others offer the possibility of variety of new composites, adhesives, coatings and sealant materials with specific properties [57–62]. Nanoparticles are presently considered to be high potential filler materials for the improvement of mechanical and physical properties of the polymers and polymer composites. Their incorporation into polymer matrix can significantly affect the properties of the matrix [63, 64]. The obtained nanocomposites might exhibit improved optical, electrical, catalytic, magnetic, mechanical and thermal properties. These properties of polymer composite depend on the type of incorporated nanoparticles, their size and shape, their concentration and interaction with the polymer matrix. However combining nanocomposite as matrix material with fibre reinforcement has been shown to be a possibility, but much work still needs to be done in order to understand how these reinforced materials behaves in a dramatic changes of material properties. Understanding their changes in material property will facilitate their extension to the reinforcement of more complicated anisotropic structures and advanced polymeric composites systems.

1.5 Aim and Objectives of the study

The developments in applications of electrospun composites will require further studies to understand electrospinning of composites and how the fillers interact with their surrounding polymer matrix, and how they behave in a dramatic change of material properties. Understanding

their changes in material property will facilitate their extension to the reinforcement of more complicated structures and advanced polymeric composites system. The study was designed to add to the existing knowledge regarding the properties of composite fibres and their use as an antibacterial killer in the biological applications. The aim of this study was to synthesize nanoparticles and also to determine the effect of different parameters into the electrospun nanofibres.

The following objectives were set to achieve the aim of this project

1. To synthesize and characterize HDA/TOPO capped Ag and Ag₂Se nanoparticles
2. To investigate the effect of temperature on the size and shape of Ag and Ag₂Se nanoparticles.
3. To characterize the nanoparticles using UV-Vis spectroscopy, Photoluminescence, Transmission electron microscopy and X-ray diffraction.
4. To incorporate Ag and Ag₂Se nanoparticles into PVP and PMMA polymers using electrospinning technique
5. To characterize the newly formed composite nanofibres using scanning electron microscopy (SEM) for size and morphology, and also using thermal gravimetric analyser (TGA) for thermal decomposition of this material. The X-ray diffraction (XRD) and Fourier transformer infrared (FTIR) spectroscopy will be used for structural analysis and UV-Vis spectroscopy for optical properties.

1.6 References

- [1] R. P. Feynman, There is Plenty of Room at the Bottom. An Invitation to Enter a New Field of Science, Lecture, Annual meeting of the American Physical Society, California Institute of Technology, December 29, **1959**. <http://www.zyvex.com/nanotech/Feynman.html> (Accessed 15 February 2005)
- [2] K. E. Dexler, Engines of Creation, The Coming Era of Nanotechnology Anchor Books, New York, **1986**.
- [3] R. Das, S. S. Nath, D. Chakdar, G. Gope, and R. Bhattacharjee, Journal of Nanotechnology, **2009**, 5, 1-6.
- [4] D. Kim, S. Jeong, and J. Moon, Nanotechnology, **2006**, 17, 4019-4024.
- [5] R. Zhang, K. S. Moon, W. Lin, and C. P. Wong, Journal of Material Chemistry, **2010**, 20, 2018-2023.
- [6] Y. Xiong, A. R. Siekkinen, J. Wang, Y. Yin, M. J. Kimb and Y. Xia, Journal of Material Chemistry, **2007**, 17, 2600-2602.
- [7] S. Pal, Y. Kyung, and J. M. Song, Applied and Environmental Microbiology, **2007**, 73, 1712-1720.
- [8] A. Panacek, L. Kvitek, R. Prucek, M. Kolar, R. Vecerova, N. Pizurova, V. K. Sharma, T. Nevecna and R. Zboril, Journal of Physical Chemistry B, **2006**, 110, 16248-16253.
- [9] H. Yin, T. Yamamoto, Y. Wada and S. Yanagida, Materials Chemistry and Physics, **2004**, 83, 66-70.
- [10] Z. Zhu, L. Kai and Y. Wang, Materials Chemistry and Physics, **2006**, 96, 447-453.
- [11] A. S. Edelstein and R. C. Cammarata, Nanomaterials, synthesis, properties and Applications, **1996**, Institute of Physics Publishing Bristol and Philadelphia.
- [12] M. Pathan and C.D. Lokhande, Bulletin of Materials Science, **2004**, 27, 85-111.
- [13] M. Kobayashi, Solid State Ionics, **1990**, 39, 121-149.
- [14] G. Sáfrán, L. Malicskó, O. Geszti and G. Radnóczki, Journal of Crystal Growth, **1999**, 205, 153-162.
- [15] F. Shimojo and H. Okazaki, Journal of the Physical Society of Japan, **1993**, 62, 179-182.
- [16] M. Ferhat and J. Nagao, Journal of Applied Physics, **2000**, 88, 813-816.

- [17] G. Beyer, Gummi Fasern Kunstoffe, **2001**, 28, 321, T1-T4.
- [18] E. Manias, A. Touny, L. Wu, K. Strawhecker, B. Lu and T. C. Chung, Chemistry of Materials, **2001**, 13, 3516-3523.
- [19] K. S. Mishra, S. H. Sonowane, R. P. Singh, A. Bendale and K. Patil, Journal of Applied Polymer Science, **2004**, 94, 116-122.
- [20] H. Jia, G. Zhu, B. Vugrinovich, W. Katuphinan, D. H. Reneker and P. Wang, Biotechnology Progress, **2002**, 18, 1027-1032.
- [21] X. Wang, Y. G. Kim, C. Drew, B. C. Ku, J. Kumar and L. A. Samuelson, Nano Letters, **2004**, 4, 331-334.
- [22] A. Mills, S. K. Lee and A. Lepre, Journal of Photochemistry and Photobiology A: Chemistry, **2003**, 155, 199-205.
- [23] W.E. Teo and S. Ramakrishna, Composites Science and Technology, **2009**, 69, 1804-1817.
- [24] D. Li, J. T. MacCann, M. Gratt and Y. Xia, Chemical Physics Letters, **2004**, 394, 387-391.
- [25] M. Wang, H. Singh, T. A. Hatton and G. C. Rutledge, Polymer, **2004**, 45, 5505-5509.
- [26] Q. B. Yang, D. M. Li, Y. L. Hong, Z.Y. Li, C. Wang, S. L. Qiu and Y. Wei, Synthetic Metals, **2003**, 137, 973-974.
- [27] V. Subramanian, E. Wolf and P. V. Kamat, Journal of the American Chemical Society, **2004**, 126, 4943-4950.
- [28] W. Gilbert, On the Magnet and Magnetic Bodies, and on That Great Magnet the Earth, **1628**, Peter Short, London.
- [29] C. V. Boys, Proceedings of the Physical Society, **1887**, 9, 8-19.
- [30] J. F. Cooley, Apparatus for electrically dispersing fluids, **1902**, US Patent 692,631.
- [31] W. J. Morton, Method of dispersing fluids, **1902**, US Patent 0,705,691.
- [32] W. E. Teo, and S. Ramakrishna, Nanotechnology, **2006**, 17, 89–106.
- [33] J. Zeleny, Physical Review 3, **1914**, 2, 69-91.
- [34] A. Formhals, Process and apparatus for preparing artificial threads, **1934**, US Patent 1,975,504.
- [35] A. Formhals, Method and apparatus for spinning, **1944**, US Patent 2,349,950.
- [36] A. Formhals, Method and apparatus for the production of fibres, **1938**, US Patent 2,123,992.

- [37] A. Formhals, A Method and apparatus for the production of artificial fibres, **1943**, US Patent 2,323,025.
- [38] A. Formhals, Method and apparatus for spinning, **1939**, US Patent 2160962.
- [39] T. Subbiah, et al. Journal of Applied Polymer Science, **2005**, 96, 557-569.
- [40] G. Taylor, Proceedings of the Royal Society of London. Series A, Mathematical and Physical Sciences, **1969**, 313, 1515, 453-475.
- [41] A. Greiner, and J. H. Wendorff, Angewandte Chemie International edition in English, **2007**, 46, 5670-5703.
- [42] D. Li, and Y. Xia, Advanced Materials, **2004**, 16, 1151-1170.
- [43] M. D. Pierschbacher and E. Ruoslahti, Nature, **1984**, 309, 30-33.
- [44] M. Hakkarainen, Advance Polymer, **2002**, 157, 113-38.
- [45] S. Ramakrishna, K. Fujihara, W. E. Teo, T. C Lim and Z. Ma, An introduction to electrospinning and nanofibres, **2005**, Singapore: World Scientific Publishing Co. Pvt. Ltd..
- [46] G. Eda and S. Shivkumar, Journal of Applied Polymer Science, **2007**, 106, 475-487.
doi:10.1002/app.25907.
- [47] I. Hayati, A. I. Bailey and T. F. Tadros, Journal of Colloid Interface Science, **1987**, 117, 205-21.
- [48] X. Zong, K. Kim, D. Fang, S. Ran, B. S. Hsiao and B. Chu, Polymer, **2002**, 43, 4403-4412.
- [49] A. K. Haggi and M. Akbari, Physica Status Solidi, **2007**, 204, 1830-1834.
- [50] M. M. Hohman, M. Shin, G. Rutledge and M. P. Brenner, Physics of Fluid, **2001**, 13, 2221-2236.
- [51] M. M. Demir, I. Yilgor, E. Yilgor and B. Erman, Polymer, **2002**, 43, 3303-3309.
- [52] C. J. Buchko, L. C. Chen, Y. Shen and D. C. Martin, Polymer, **1999**, 40, 7397-407.
- [53] X. Yuan, Y. Zhang, C. Dong and J. Sheng, Polymer International, **2004**, 53, 1704–1710.
doi:10.1002/pi.1538.
- [54] C. Mit-uppatham, M. Nithitanakul and P. Supaphol, Macromolecular Chemistry and Physics, **2004**, 205, 2327–2338. doi:10.1002/macp.200400225
- [55] C.L. Casper, et al., Macromolecules, **2003**, 37, 573-578.
- [56] P. K. Baumgarten, Journal of Colloid Interface Science, **1971**, 36, 71-9.
- [57] T. Kashiwagi, E. Grulke, J. Hilding, R. Harris, W. Awad and J. Douglas, Macromolecular Rapid Communications, **2002**, 23, 761-765.

- [58] J. Njuguna and K. Pielichowski, Advance Engineering Materials, **2004**, 6, 193-203.
- [59] J. Njuguna, and K. Pielichowski, Advanced Engineering Materials, **2004**, 6, 204-210.
- [60] R. Andrews, D. Jacques, M. Minot and T. Rantell, Macromolecular Materials and Engineering, **2002**, 287, 395-403.
- [61] J. Njuguna and K. Pielichowski, Advanced Engineering Materials, **2003**, 5, 769-778.
- [62] T. J. Pinnavaia, T. Lan, Z. Wang, H. Shi, P.D. Kaviratna. Clay-Reinforced Epoxy Nanocomposites: Synthesis, Properties, and Mechanism of Formation, ACS Symposium Series, **1996**, 622, 250-261.
- [63] G. Kiekelbick, Progress in Polymer Science, **2003**, 28, 83-114.
- [64] W. Caseri, Macromolecular Rapid Communications, **2000**, 21, 705-722.

CHAPTER 2

LITERATURE REVIEW

2.1 Silver metal nanoparticles

The most effective studied nanoparticles today are those made from noble metal, in particular Ag, Pt, Au and Pd. These nanomaterials have tremendous applications in the area of catalysis optoelectronics, diagnostic biological probe and display devices [1]. In the past several years the investigations of silver nanoparticles have drawn attention to the field of nanotechnology because of their excellent biocompatibility and low toxicity. Today a wide range of research has been reported on silver particles in catalysis, electronics, and spectroscopy. Silver nanoparticles have important application in the field of biology, such as antibacterial, antivirus, antifungal effect and biosensor [2]. There are many synthesizing method of silver nanoparticles that have been reported, one of these methods is the chemical reduction of aqueous silver ions by sodium borohydride solution [3]. Silver nanoparticles are effective germ fighter and they are widely recognized as being effective because of their enormously high surface area. Due to the large number of manufacturers using silver nanoparticles in their products, some concern has arisen about its effects on the environment when they are disposed or washed [4]. Several studies have been shown that silver can easily leach into wastewater during washing, and thus potentially disrupting helpful bacteria used in wastewater treatment facilities or endangering aquatic organisms in lakes and streams. The stability of silver nanoparticles in the environment is determined by many factors such as the type of capping agent used, chemicals used in the synthesis of nanoparticles to prevent aggregation, and the surrounding environmental conditions. Silver nanoparticles have the potential to revolutionize the medical and consumer products industries [5]. These silver particles ranging from 1-100 nm in diameter show unique properties especially against various bacteria, viruses and fungus. Silver has been a potent antibacterial agent that is toxic to fungi, viruses and algae. It has been used to treat infections for centuries, but with the advent of nanotechnology, the use of silver

in nanoparticle form has opened doors for new treatment. Various researchers have found that silver nanoparticles are effective killers of pathogenic bacteria such as *E. coli*, *B. subtilis*, and *S. Aureus* [6]. Current studies have indicated that silver nanoparticles in the range of 1–10 nm attach to HIV proteins can inhibit the virus from binding to cells [6]. The most important and distinct property of nanoparticles is that they exhibit larger surface area to volume ratio. Sonochemical processes have been actively researched for the synthesis of metal nanoparticles and nanostructured materials. Sonochemical processes have been used to synthesize various types of materials such as iron (Fe), cadmium sulphide (CdS), titanium dioxide (TiO₂), palladium (Pd), platinum (Pt) nanoparticles on multi-walled carbon nanotubes, Ag₂Se nanocrystals and hollow lead sulphide (PbS) nanospheres [7].

2.1.2 Silver selenide semiconductor nanoparticles (Ag₂Se)

Nanoparticles derived from semiconductor materials are distinctly different from their metal counterparts as they do not have free conduction electrons. Instead, the electrons are contained in valence band states, and the electronic properties reflect excitation of the valence electrons into conduction band states across an energetic band gap [8, 9]. The spatial confinement of the nanoparticles plays an important role in the size of the band gap and consequently, the optical properties such as absorption and emission depend on particle size and shape [10, 11]. As a result, semiconductor nanocrystals are exciting materials for applications including light-emitting devices, photovoltaics, ultrasensitive photodetectors, nanoscale light sources, and nanoscale photocatalysts [12]. Modern synthesis techniques enable very precise particle morphology, which can lead to desired optical and electronic properties [13, 14].

Semiconductor nanoparticles such as CdSe and CdTe have been extensively studied due to their novel properties which are determined by their size, shape and surface modification [12]. Ag₂Se is a semiconductor of group I – VI, which belong to the family of superionic conductors. It has high carrier concentration and finds attractive applications like magnetic resistive sensors, non-volatile memories, IR detectors photoconductors, photovoltaic cells and electrochemical potential memory devices semiconducting optical devices for visible region [15-17]. Silver selenide undergoes a phase transition from low temperature orthorhombic structure to high temperature

cubic structure. Jeong and Xia [18] have demonstrated that the reversible phase transition associated with Ag_2Se provides a new platform for the fabrication of photonic crystals with thermally switchable stop bands. Leon et al. [19] have studied the effect of nanoscale confinement on the phase transition temperature and they found that it increases with the decrease in the grain size of silver selenide. Silver selenide is found to exhibit only n-type semiconducting properties at 4.2K with 0.37 excess selenium [20]. Ag_2Se semiconductor has been studied and it was shown that the synthesis of high quality Ag_2Se nanocrystals is much less developed than those of other materials. High quality Ag_2Se nanocrystals could lead to new applications or significantly improve the performance of existing application [21]. Xu et al. [22] have observed that silver chalcogenide has linear and large magneto-resistance effect. The absorption spectra of Ag_2Se at very low temperature were studied by Dalven and Gill [20] and they found that the band gap is direct. Damodara and karunakaran [23] have reported the band gap energy of Ag_2Se to be within the range from 0.04 eV to 0.08 eV. Recent studies on optical properties of silver selenide show that optical band gap of silver selenide exists between 1.2 eV and 1.8 eV. Santosh Kumar and Pradeep [24], have reported the optical band gap of reactive evaporated Ag_2Se to be 1.58 eV. Kulkarni et al. [25] did optical studies on the annealed and unannealed films of silver selenide and found the band gap of silver selenide to be 1.3 eV. Optical band gap of silver selenide thin films have been found to be independent of thickness which indicates that there is no charge accumulation at the grain boundaries and the presence of density dislocations are also not dominant. Since the grain size is in the order of thickness of films, the mean free path is about film thickness and hence the quantum size effect does not exist in silver selenide thin films [26].

2.2 Synthetic methods for the preparation of nanoparticles

Synthesis of high quality nanoparticles has been an important topic in the field of material chemistry. Their production requires skills and proper method to work with in order to achieve good quality nanoparticles. There are a number of methods that have been developed for the synthesis of nanoparticles. There are two approaches to the fabrication of nanoparticles that is top-down and bottom-up.

1. Bottom-up approach: It deals with the building up of a material from the bottom which refers to the construction of a structure atom by atom, molecule by molecule or cluster by cluster. The advantage of the bottom-up approach is the possibilities to obtain nanostructures with less defects and more homogeneous chemical compositions.
2. Top-down approach: The principle behind the top-down approach is to take a bulk piece of the material and then modify it into the wanted nanostructure. The typical fabrication techniques which have been developed to work on the nanoscale involves cutting, grinding and etching and this is commonly used in physics.

2.2.1 Colloidal route

This method is achieved by carrying out a controlled precipitation in homogenous solution in the presence of stabilizer and the cessation of growth immediately after nucleation. The synthesis of colloidal nanoparticles is based on three component composed of precursors, organic surfactants, and solvents. When heating a reaction medium to a sufficiently high temperature, the precursors chemically transform into monomers. Once the monomers reach high supersaturation level, the nanocrystal growth starts with a nucleation process. The temperature during the growth process is one of the critical factors in determining optimal conditions for the nanocrystal growth. The synthesis of highly monodispersed micrometric colloids was reported by La Mar et al. [27, 28]. In their study they have mentioned that if the nucleation and growth are properly controlled particles with dimensions of the order of nanometer can be synthesized. The less stable small crystals will dissolve and re-crystallize to form larger crystals by a process called Ostwald ripening.

2.2.2 Metal-organic routes

This method involves rapid injection of a metal alkyl (dimethylcadmium) and a chalcogen source TOP-Se mixed in trioctylphosphine and injected into a hot trioctylphosphine oxide. This method for preparing highly quality, crystalline monodispersed nanoparticles was first reported by Murray et al. [29]. Even though the method produces high quality particles, the reaction requires difficult

conditions such as injection of hazardous metal alkyls, which are toxic and volatile at elevated temperature. In this method TOPO was used as a stabilizer during the synthesis of nanoparticles to prevent them from aggregating. It also allows the reaction to take place above the nucleation temperature and allows the nanocrystals to be soluble in organic solvents. The size distribution of the nanoparticles is controlled by the temperature at which the synthesis is taken place, with larger particles being obtained at higher temperature.

2.2.3 Solvothermal Method

High solvent temperatures and pressures are employed in this method to maintain high solubility of precursors and these conditions are the ones that make it difficult for the method to be used in the industries. Solvothermal synthesis consists of precursors, surfactant and solvent in the reaction system. This method is widely used in the synthesis of zeolite nanocrystals.

2.2.4 Synthesis in confined matrices

Many matrices have been used for the preparation of nanoparticles and they can be viewed as nanochambers, which limit the size to which crystals can grow. Their properties are not only determined by the confinements of the host material but also by that of the system.

2.2.5 Chemical precipitation method

This method involves the formation of a separable solid substance from a solution, by either converting the substance into an insoluble form or by changing the composition of the solvent to diminish the solubility of the substance in it. To prevent agglomeration in these method particles should have low solubility. The nucleation step results in the precipitation of particles followed by the normal Ostwald ripening.

2.2.6 Sol-Gel process

This method is mostly used for the fabrication of metal oxides especially the oxides of silicon and titanium. The process involves conversion of monomers into a colloidal solution that acts as the precursor for an integrated network of either discrete particles or network polymers.

2.3 Applications of nanoparticles

Ag nanoparticles have been used extensively as anti-bacterial agents in the health industry, food storage, textile coatings and a number of environmental applications. Ag nanoparticles as anti-bacterial agents were applied in a wide range of applications from disinfecting medical devices and home appliances to water treatment. An Advance research in the synthesis of high quality monodisperse nanoparticles and their unique properties, has led to the high demand of these materials which are now useful in many areas of applications, that include catalysis, optical recording materials, solar cells, biotechnology, sensor and lasing materials.

2.3.1 Applications of Ag nanoparticles

2.3.1.1 Antibacterial Application

Silver nanoparticles have some potential application like diagnostic biomedical optical imaging, biological implants (like heart valves) and medical application like wound dressings, contraceptive devices, surgical instruments and bone prostheses. Silver containing materials can be used to eliminate microorganisms on textile fabrics or they can be used for water treatment. Silver nanoparticles are also used as effective killers of pathogenic bacteria such as E. coli, B. subtilis, and S. aureus.

2.3.1.2 Catalytic Application

Material that show good catalytic activity must possess high surface area. Nanomaterial catalysts show more reactive crystal planes when exposed to the surface, and hence increases their catalytic performance. In the literature it says that the catalytic activities of nanoparticles differ from the chemical properties of the bulk materials. Kohler and co-workers [30] did a study on the organic dye by applying potassium peroxodisulphate in aqueous solution and they demonstrated that bleaching organic dyes by application of potassium peroxodisulphate in aqueous solution at room temperature enhanced strongly by the application of silver containing nanoparticles. Guo et al. [31] mentioned that Ag nanoparticles were found to catalyze the chemiluminescence from luminol–hydrogen peroxide system with catalytic activity better than that of Au and Pt colloid.

2.3.1.3 Optical Application

The optical properties of a metallic nanoparticle depend mainly on its surface plasmon resonance. The surface plasmon resonance refers to the collective oscillation of the free electrons within the metallic nanoparticle. It is well recognized that the Plasmon resonant peaks and line widths of the nanoparticles are sensitive to size and shape, and the surrounding medium. Silver nanoparticles are used to efficiently harvest light and for enhanced optical spectroscopies including metal-enhanced fluorescence (MEF) and surface-enhanced Raman scattering (SERS).

2.3.2 Applications of Ag₂Se nanoparticles

2.3.2.1 Photovoltaic devices

This application is used for the preparation of photovoltaics and solar cells. The difficulties encountered with photovoltaic devices are the conversion efficiencies of light to energy. Light with a wavelength below the value of a band gap will not be adsorbed nor be converted to energy. Any electron excited with a photon greater than the band gap value will scatter the extra energy as heat. The only way to overcome these difficulties is to combine polymers with inorganic semiconductors

because of the nanoscale nature of light absorption and photocurrent generation in solar energy conversion. The advent of methods for controlling inorganic materials on the nanometer scale opens new opportunities for the development of future generation solar cells.

2.3.2.2 Light emitting devices

Semiconductor nanoparticles or quantum dots have been used as alternative light emitters to organic dyes because they can be tuned to emit light at any wavelength range. Their tunability gives them the ability to emit any frequency of light, and a traditional light emitting diode (LED) lacks this ability. Quantum dot-based LEDs can be crafted in a wide range of form factors. Traditional incandescent bulbs may be replaced using QLED technology, since QLEDs can provide a low-heat, full-spectrum source of light. Semiconductor nanoparticles or Quantum dots can be easily encapsulated into organic polymers because of its small size, which will lead to the development of flexible displays. These advantages make quantum dot LEDs useful in many devices, such as laptop and computers.

2.3.2.3 Biological Applications

The first groups to give details about the use of colloidal quantum dots for biological labelling were Alivisatos [32] and Nie [33] groups. In modern biological analysis, various kinds of organic dyes were used but they were unable to meet the expectation due to low quantum yield or brightness they exhibit because of molecular interactions with themselves, each other and with the solvent. Another drawback of organic dyes is the loss of fluorescence that occurs when dye molecules react irreversibly with each other or the solvent, producing a nonfluorescent product. Quantum dots have quickly filled in the role with the advantages of tunable luminescence, high quantum yield, broad light absorption, narrow emission spectra and high stability. It has been estimated that quantum dots are 20 times brighter and 100 times more stable than traditional fluorescent reporters [34]. Photobleaching is the photochemical destruction of a dye or a fluorophore and in quantum dots is diminished as the same passivating layer that enhances quantum yield, also guards particles from external interactions. During this Photobleaching

quantum dots can exhibit continuous fluorescence for a period of time, in an order of magnitude greater than organic fluorescent dyes [33]. In addition, organic fluorescent dyes normally exhibit fixed narrow excitation spectra. Fluorescent excitation spectra of the quantum dots may be excited in a range of wavelengths selected by their size. These properties of quantum dot have led to applications in diverse biological fields, including biosensing, cellular labelling, and *in vivo* fluorescent detection and therapeutics.

2.3.3 Applications of Electrospinning

2.3.3.1 Filtration applications

Filtration has been used widely in both households and industries for removing solid substances from air or liquid. Polymer nanofibres have been used in air filtration application for more than decade. Filtration was the first commercialized application of nanofibers after electrospinning was discovered. Nanofibres with very small diameters are useful in the air filtration application to filter fine articles. In general tiny particles with very high surface area to volume ratio and the resulting high surface cohesion are easily trapped in the electrospun nanofibrous structured filters and this improves the filtration efficiency. The filtration efficiency is normally influenced by the filter physical structure (fiber fineness, matrix structure, thickness, and pore size), fiber surface electronic properties, and its surface chemical characteristic (e.g. surface free energy). Besides the filtration efficiency, other properties such as pressure drop and flux resistance are also important factors to be assessed for a filter media. Electrospun nanofibre mat provides an improvement in the filtration efficiency at relatively small decreases in permeability. Barhate and Ramakrishna [35] did a comparison study on a commercial high efficiency air filter with nylon-6 electrospun mat and they found that nylon-6 nanofibre mat had slightly higher filtration efficiency of 99.99 % as compared to the commercial filter with 99.97 %. Apart from the application of nanofibres as an air filtration system, they could be used as a supporting scaffold in ultra filtration for oil/water emulsion separation. Gibson et al. [36] did a study on the electrospun mats to see if can trap airborne particles and it was found that electrospun nanofiber mats were extremely effective at trapping airborne particles of (0.5~200 μm).

2.3.3.2 Textile applications

The majority of early patents about electrospinning were meant for textile applications. However, recent development of nanotechnology in textile areas has included textile formation and textile finishing. Electrospinning has a potential to generate non-woven garments by integrating advanced manufacturing with fiber electrospinning. The method of electrospinning fabrication introduces multi-functionalities (flame, chemical and environmental protection) by mixing fibres into electrospun lace, and using electrospinning to join different fibers and coatings to form three dimensional shapes. Carbon nanofibers and carbon black nanonoparticles are among the most commonly used nanosized filling materials. Carbon nanofibers can effectively increase the tensile strength of composite fibers due to its high aspect ratio, while carbon black nanoparticles can improve their abrasion resistance and toughness. Both of them have high chemical resistance and electric conductivity. Clay nanoparticles are composed of several types of hydrous alumina silicates, whereby each type differs in chemical composition and crystal structure. Clay nanoparticles possess electrical, heat and chemical resistance and an ability of blocking ultraviolet (UV) light. Therefore Composite fibers reinforced with clay nanoparticles exhibit flame retardant, anti-UV and anti-corrosive behaviour.

2.3.3.3 Catalysis

Fibre membranes have been shown to be very useful for heterogenous catalysis, and they are commonly prepared in the form of a nonwoven mat via electrospinning [37]. The nonwoven materials have been proven to be an efficient photocatalysts as well as a supports for catalytic metal nanoparticles [38]. Metal nanoparticles on polymeric and carbon fibres have been shown to improve a number of catalytic reactions that include hydrogenation of carbonyls and alkenes. Formo and co-workers [39] demonstrated that nonwoven mat of TiO₂ fibres decorated with Pt nanoparticles could serve as a three dimensional scaffolds to generate Pt nanowires in an effort to further increase the active surface for catalysis. Enzyme can also be used to functionalize the nanofibres for enzyme catalysis and have shown to have high catalytic activity like the normal catalyst [40].

2.3.4 Medical Applications

2.3.4.1 Tissue engineering scaffolds

Tissue engineering is an emerging interdisciplinary and multidisciplinary research field which involves the use of living cells, manipulated through their extracellular environment or genetically to develop biological substitutes for implantation into the body and/or to foster remodelling of tissues in some active manners. The effective scaffold should possess a high degree of porosity, have a large surface area, should be biocompatible and biodegradable, should be non-toxic to cells and interact positively with the cells to promote cell adhesion, migration, and differentiated cell function. These features result in a more biologically compatible environment in which cells can grow and perform their regular functions. In most cases the nanofibrous scaffolds have been used widely as scaffold for tissue engineering such as neural, cartilage, vascular and bone tissue engineering. A number of tissue scaffolds have been engineered from natural, synthetic, composite and functionalized polymers. Polymers such as poly (lactic acid), gelatine poly-L-lactic acid (PLLA) and polymer liquid crystal (PCL) have been used in tissue scaffolds. Yang et al. [41] did a study on the aligned and random PLLA electrospun nanofibrous scaffold for the purpose of neural tissue engineering and they have found that neural stem cell elongated and their neuritis outgrew along the direction of the fibre orientation of the aligned nanofibres. Mo and Weber [42] developed an aligned electrospun nanofibrous scaffold from biodegradable poly (L –lactic acid-co - ε -caprolactone) (PLLA-CL) with the goal of developing constructs for vascular tissue engineering and found that the fabricated nanometric fibres resembled the dimension of natural extracellular matrix, possessed mechanical properties comparable to human coronary artery, and supported smooth muscle cell adhesion and proliferation well.

2.3.4.2 Wound healing

Wound healing is a process of renewing dermal and epidermal tissues. It normally takes time and thus requires proper dressing which will protect the wound from bacteria and any wound contamination. Electrospun nanofiber mat is a good material for wound dressing because of its

unique properties such as high porous mat structure and well interconnected pore that are particularly important for giving off fluid from the wound. Drugs can be added into nanofibres via electrospinning for possible medical treatment and antibacterial purpose. Khil et al. [43] did a study on electrospun polyurethane (PU) mat for wound dressing material and they found that the mat effectively give off fluid from the wound without the fluid accumulating under the mat and no wetness occurred on wound. They showed that PU foams have properties such as mechanical strength, swelling ratio and cell adhesion that aid in wound healing application. Schneider et al. [44] electrospun silk nanofibre mat with epidermal growth factor in order to promote wound healing process and found that functionalized mat increased the wound closure by 90 %. According to Rho et al. [45] they mentioned that electrospun collagen mat showed that the early-stage healing of wound using collagen nanofibre was faster than that of using normal cotton gauze.

2.3.4.3 Nanosensors

Sensors devices have been used to detect chemicals, industrial process control, medical diagnosis, and defences. Good sensors should show high sensitivity, selectivity and reliability [46]. Sensors devices require a large specific surface area and a high porous structure in order to show its high sensitivity and a fast response, and they should be able to conduct electricity. Electrospinning polymer nanofibres with a sensing capability have been the area of interest in the bio-sensing application. Yoon et al. [47] have shown that conjugated polymer embedded electrospun nanofibres were able to sense volatile organic compound based on optical absorption properties. Metal oxide nanoparticles such as iron oxide and zinc oxide were incorporated into PAN nanofibres for use as detector for carbon dioxide [48]. These metal oxides were added to enhance gas adsorption and to improve their sensitivity as gas sensors. A small number of oxides nanofibres such as WO_3 , MoO_3 and TiO_2 have been used for detecting gases like ammonia, nitrogen dioxide and hydrogen. [49-51]

2.4 References

- [1] A. Leela and M. Vivekanandan, African Journal of Biotechnology, **2008**, 7, 3162-3165.
- [2] Z.-C. Zhu, Q.-S. Wu, P. Chen and X.-H. Yang, Journal of Nanoparticle Research, **2011**, 13, 5347-5353.
- [3] S. Praharaj, S. Nath, S. Panigrahi, S. Basu, S. K. Ghosh, S. Pande, S. Jana and T. Pal, Chemical Communications, **2006**, 3836-3838.
- [4] G. J. Maass, Colloidal Science Laboratory, **2008**, 1-9.
- [5] J. Pazol, A. Czyzewski, and A. Barron, Antimicrobial fact, fiction, **2010**, North Western University Press, 112.
- [6] A. V. Vishnevsky, Journal of Education, **2010**, 26, 98-102.
- [7] K. Okitsu, R. Nishimura, International Congress on Acoustics, **2010**, 599-853, Sydney, Australia.
- [8] C. Kittel, Introduction to Solid State Physics, **2005**, John Wiley & Sons Inc.
- [9] A. L. Rogach, Semiconductor Nanocrystal Quantum Dots: Synthesis, Assembly, Spectroscopy, and Applications, **2005**, Springer Wien New York.
- [10] A. Efros and M. Rosen, Annual Review of Material Science, **2000**, 30, 475-521.
- [11] A. P. Alivisatos, Science, **1996**, 271, 933-937.
- [12] N. Mntungwa, V. S. R. Rajasekhar Pullabhotla and N. Revaprasadu, Material Chemistry and Physics, **2011**, 126, 500-506.
- [13] D. V. Talapin, J. S. Lee, M. V. Kovalenko, and E. V. Shevchenko, Chemical Reviews, **2010**, 110, 389-458.
- [14] P. V. Kamat, Journal of Physical Chemistry B, **2002**, 106, 7729-7744.
- [15] D. T. Schoen, C. Xie, and Y. Cui, Journal of the American Chemical Society, **2007**, 129, 4116-4117.
- [16] R. Chen, D. Xu, G. Guo and Y. Tang, Journal of Material Chemistry, **2002**, 12, 1437-1441.
- [17] M. Wuttig, Nature Materials, **2005**, 4, 265-266.
- [18] U. Jeong and Y. Xia, Angewandte Chemie International Edition, **2005**, 44, 3099-3103.
- [19] V. Leon, Y. Ren and M. L. Saboungi, Journal of Applied Physics, **2008**, 103, 0161051.
- [20] R. Dalven and R. Gill, Journal of Applied Physics, **1967**, 38, 753-756.

- [21] P. Hoyer and H. Weller, *Chemical Physics Letter*, **1994**, 224, 78-80.
- [22] R. Xu, A. Husmann, T.F. Rosenbaum, M.L. Saboungi, J. E. Enderby and P. B. Littlewood, *Nature London*, **1997**, 390, 57-60,
- [23] V. Damodara Das and D. Karunakaran, *Journal of Applied Physics*. **1990**, 68, 2105-2111.
- [24] M.C. Santhosh Kumar and B. Pradeep, *Semiconductor Science and Technology*, **2002**, 17, 261-265.
- [25] A. B. Kulkarni, M. D. Uplane, C. D. Lokhande, *Thin Solid Films*, **1995**, 260, 14-18.
- [26] M. Pandiaraman, N. Soundararajan, C. Vijayan, C. Kumar and R. Ganesan, *Journal of Ovonic Research*, **2010**, 6, 285 – 295.
- [27] V. K. La Mer and R. H. Dinegar, *Journal of American Chemical Society*, **1950**, 72, 4847.
- [28] R. J. Hunter, *Foundation of Colloid Science*, **1993**, 1, 13-17, Oxford University Press, 6 edition, Oxford.
- [29] C. B. Murray, D. J. Norris and M. G. Bawendi, *Journal of American Chemical Society*, **1993**, 115, 8706-8715.
- [30] J. Kohler, L. Abahmane, J. Albert, and G. Mayer, *Chemical Engineering Science*, **2008**, 63, 5048-5055.
- [31] J. Guo, H. Cui, W. Zhou, and W. Wang, *Journal of Photochemistry and Photobiology A: Chemistry*, **2008**, 193, 89-96.
- [32] M. Jr. Bruchez, M. Moronne, P. Gin, S. Weiss, A. P. Alivisatos, *Science*, **1998**, 281, 2013-2016.
- [33] W. C. W. Chan, S. Nie, *Science*, **1998**, 281, 2016-2018
- [34] M. A Walling, N. Shepard, *Internation Journal of Molecular Sciences*, **(2009-02)**, 10, 441–491.
- [35] R.S. Barhateand S. Ramakrishna, *Journal of Membrane Science*, **2007**, 296, 1-8.
- [36] P. Gibson, H. Schreuder-Gibson, and D. Rivin, *Physicochemical and Engineering Aspects*, **2001**, 187-188, 469-481.
- [37] M. Graeser, E. Pippel, A. Greiner and J. Wendroff, *Macromolecules*, **2007**, 40, 6032-6039.
- [38] S. Zhan, D. Chen, X. Jiao and Y. Song, *Chemical Communications*, **2007**, 57, 2043-2045.
- [39] E. Formo, E. Lee, D. Campbell and Y. Xia, *Nano Letters*, **2008**, 8, 668-672.
- [40] J. Xie and Y. L. Hsieh, *Journal of Material Science*, **2003**, 38, 2125.

- [41] F. Yang, R. Murugan, S. Wang and S. Ramakrishna, *Biomaterials*, **2005**, 26, 2603–2610.
- [42] X. Mo and H. J. Weber, *Macromolecules*, **2004**, 21, 413–416.
- [43] M. S. Khil, D. I. Cha, H. Y. Kim, I. S. Kim, N. and Bhattacharai, *Journal of Biomedical Materials Research, Part B: Applied Biomaterials*, **2003**, 67, 675-679.
- [44] A. Schneider, X. Y. Wang, D. L. Kaplan, J. A. Garlick and C. Egles, *Acta Biomaterialia*, **2009a**, 5, 2570-2578.
- [45] K. S. Rho, L. Jeong, G. Lee, B. M. Seo, Y. J. Park, S. D. Hong, S. Roh, J. J Cho, W. H. Park and B. M. Min, *Biomaterials*, **2006**, 27, 1452-1461.
- [46] M. Y. Faizah, A. Fakhru'l-Razi, R. M. Sidek and A. G. Liew Abdullah, *International Journal of Engineering and Technology*, **2007**, 4, 106-113.
- [47] J. Yoon, S. K. Chae and J. M. Kim, *Journal of the American Chemical Society*, **2007**, 129, 3038-3039.
- [48] R. Luoh and H. T. Hahn, *Composites Science and Technology*, **2006**, 66, 2436-2441.
- [49] G. Wang, Y. Ji, X. Huang, X. Yang, P. I. Gouma and M. Dudley, *Journal of Physical Chemistry B*, **2006a**, 110, 23777-23782.
- [50] P. I. Gouma *Reviews on Advanced Materials Science*, **2003**, 5, 147-154.
- [51] I.D. Kim, A. Rothschild, B.H. Lee, D.Y. Kim, S. M. Jo and H. L. Tuller, *Nano Letters*, **2006**, 6, 2009-2013.

CHAPTER 3

MATERIALS AND METHODS

3.1 Materials

All chemicals were purchased from Sigma Aldrich. These are silver nitrate (99 %), selenium powder (99.5 %, 100 mesh), tri-n-octylphosphine (TOP), hexadecylamine (HDA) (90 %) and trietylphosphine oxide (TOPO) (90 % technical grade), poly (vinyl pyrrolidone) (PVP, $M_w=40,000$ g/mol), poly (methyl methacrylate) (PMMA, $M_w = 96000$ g/mol). The solvent ethanol and N, N- dimethylformamide (DMF) were also from Sigma Aldrich. Analytical grades of methanol and toluene were obtained from CC Immelman. All chemicals were used as received.

3.2 Instrumentation

3.2.1 Optical characterization

The optical measurements were carried out using Perkin-Elmer Lambda 25 UV/VIS spectrophotometer (ELICO-SL-150). The samples were dissolved in toluene and placed in quarts cuvettes (1 cm path length) for analysis using toluene as a reference solvent. The PVP composite fibres were dissolved in ethanol while the PMMA composite were dissolved in DMF and placed in quartz cuvettes for analysis as the nanoparticles. Ethanol and DMF were used as reference solvent for the composites fibres of PVP and PMMA respectively. A Perkin Elmer LS 45 fluorimeter was used to measure the photoluminescence of the particles at the excitation wavelength of 200 nm. The samples were placed in quartz cuvettes (1cm path length) for analysis.

3.2.2 Transmission electron microscopy (TEM)

The TEM images were recorded using HITACHI JEOL 100 S transmission microscope operated at 80 kV. The nanoparticles were dissolved in toluene and a droplet of solution was placed on a carbon-coated copper grid. The sample was dried at room temperature prior to analysis.

3.2.3 X-ray diffraction (XRD)

The powder X-ray diffraction patterns were recorded by a BRUKER D2 diffractometer at 40kV/50mA using secondary graphite monochromated Co K α radiation ($\lambda = 1.7902$). Measurements were taken at high angle 2θ range of $5 - 90^\circ$ with a scan speed of $0.01^\circ 2q \text{ s}^{-1}$.

3.2.4 Scanning electron microscopy (SEM)

The FE-SEM (Leo, Zeiss) scanning electron microscopy operated at 1.00 kV electron potential difference was used to study the fibre morphologies. The composite fibers were prepared by placing them in the sample holders coated with a carbon tape and dried at room temperature.

3.2.5 Infrared spectrophotometer

Infrared spectra of the composite fibres were recorded on Perkin-Elmer spectrum 400 FT-IR spectrometer ranging from 650-4000 cm $^{-1}$ IR region. The samples were placed onto the universal ATR sample holder and pressed on top by gauge force arm for analysis.

3.2.6 Thermogravimetric analysis (TGA)

Thermogravimetric analysis of the fibres and the composite fibres were performed using Perkin Elmer STA 6000 simultaneous thermal analyzer under nitrogen with a flow rate of 20 °C/min. The samples were heated from 30 to 800 °C at a heating rate of 10 °C/min.

3.2.7 Electrospinning

The electrospinning of the polymer was performed using (KES Kato Tech Co. LTD, Japan) to make polymer fibres. The polymer solution prepared was placed in a 20 ml plastic syringe fitted with a stainless steel needle of tip-dimensions of 1.20938 mm. A high-voltage power supply was used to set the voltage with the distance of 10 cm between the nozzle and the collector. A syringe pump was used to feed the polymer solution into the needle tip at a rate of 0.050 mm/min.

3.3 Experimental procedures

3.3.1 Synthesis of Ag nanoparticles

In a typical experiment, silver nanoparticles were prepared by dissolving AgNO_3 (0.5 g) in tri-n-octylphosphine (TOP) (5 mL) and injected into hot hexadecylamine (HDA) or tri-n-octylphosphine oxide (TOPO) (6 g) at various temperatures of (130, 160 and 190 °C for HDA) and (160, 180 and 200 °C for TOPO) to yield HDA-capped or TOPO-capped nanoparticles. The reaction was stirred for 1 hour under the flow of nitrogen gas and cooled to about 70 °C. Methanol was added to precipitate the silver nanoparticles formed. The resulting nanoparticles were separated by centrifugation and washed with methanol to remove excess capping agent. The nanoparticles were left to dry for further characterization.

3.3.2 Synthesis of Ag_2Se nanoparticles

Selenium powder (0.5 g) and AgNO_3 (0.5 g) were separately dissolved in TOP to obtain the solution of TOP-Se and TOP-Ag respectively. The prepared TOP-Se was then injected into 6 g solution of hot HDA or TOPO, followed by the addition of TOP-Ag at a specific reaction temperature of 130, 160 and 190 °C for HDA-capped and at 180, 200 and 250 °C for TOPO-capped under constant flow of nitrogen gas. The solution was stirred for 1 hour and cooled to 70 °C. The Ag_2Se nanoparticles formed were precipitated with methanol and separated by

centrifugation. The resultant brown/black precipitates were washed with methanol to remove excess HDA/TOPO. The schematically diagram for this preparation is shown in **Figure 2**.

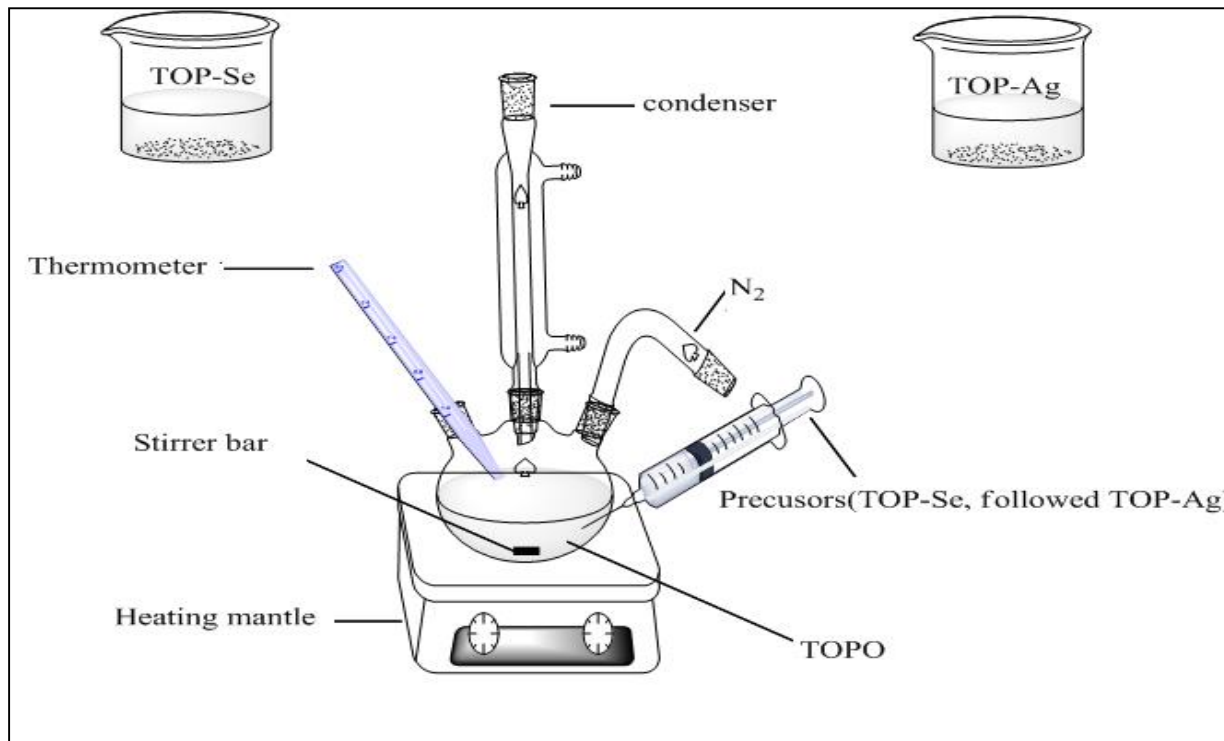


Figure 2: Schematic diagram showing the synthesis Ag₂Se nanoparticles.

3.3.3 Electrospinning of Ag₂Se/PVP/PMMA

A PVP solution was prepared by dissolving a PVP powder in a mixture of ethanol/DMF (1:1) at various concentrations ranging from (35, 40 and 45 wt%) with stirring at room temperature for 1 hour. QDs (0.2 and 0.6 wt%) were added directly to the prepared solution of (40 wt%) and stirred for 2 hours. The PMMA solution were prepared the same way using different polymer concentrations ranging from (8, 10 and 12 wt%) and the nanoparticles loading ranging from 0.2 to 0.6 wt%. The prepared composite solutions were then electrospun to produce composite fibers. The polymer solution was placed in a 20 ml plastic syringe fitted with a stainless steel needle of tip-dimensions of 1.20 x 38 mm. A high voltage power supply was used to produce the voltages ranging from 11 to 20 kV and the distance between the nozzle and the collector screen was kept at

10 cm. A syringe pump was used to feed the polymer solution into the needle tip at a rate of 0.050 mm/min. The optimum conditions for PVP fibres were 40 wt%, distance of 10 cm, and a voltage of 17 kV. The concentration of PMMA nanofibres was kept at 8 wt% at a distance of 10 cm, and a voltage of 15 kV. **Figure 3** shows the schematic illustration of nanoparticles incorporated into polymer and the process of electrospinning to form nanofibres.

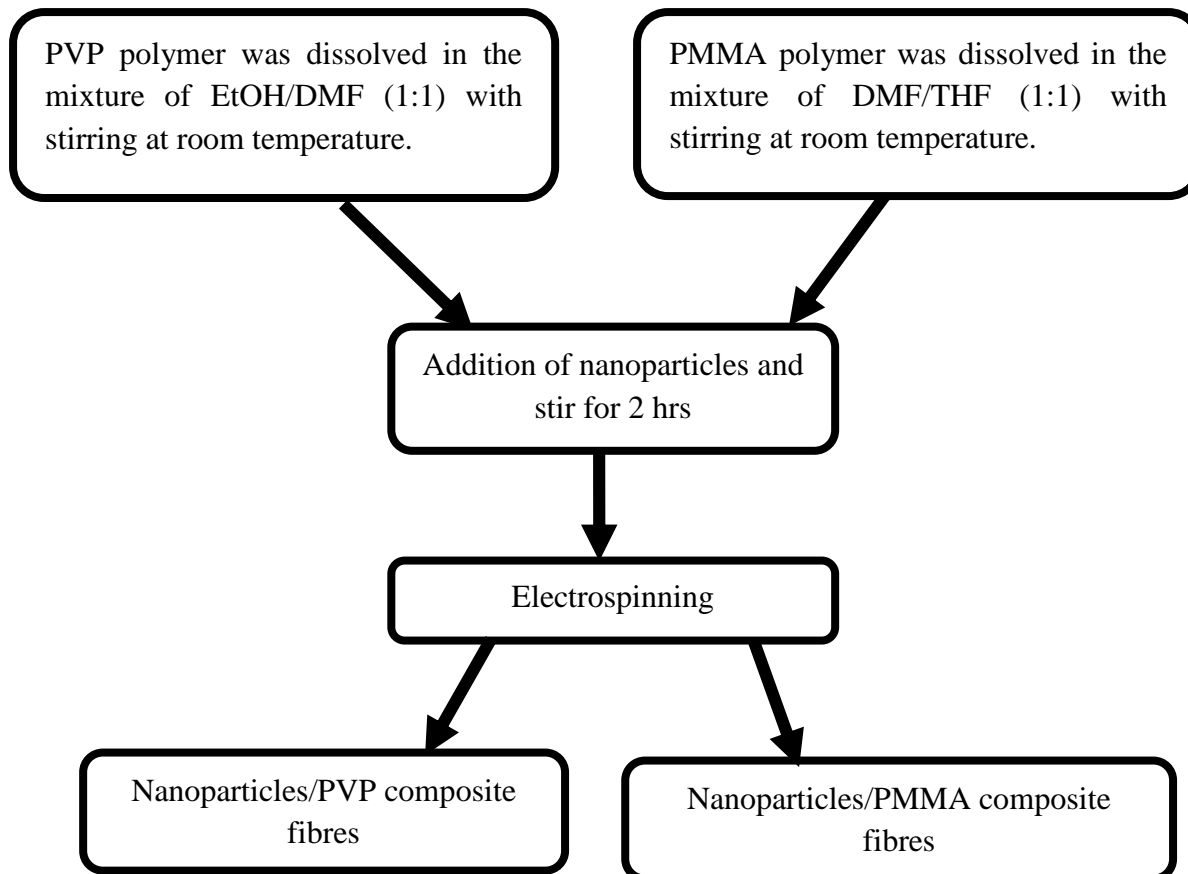


Figure 3: schematic illustration of the nanoparticles incorporated into PVP and PMMA polymers

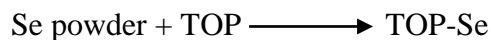
RESULTS AND DISCUSSIONS

CHAPTER 4

NANOPARTICLES

4.1 Synthesis and characterization of Ag₂Se nanoparticles

Silver selenide nanoparticles were synthesized using tri-n-octylphosphine (TOP) as solvent, tri-n-octylphosphine oxide (TOPO) and hexadecylamine (HDA) as capping agent. Silver selenide was prepared by reacting silver nitrate with tri-n-octylphosphine (TOP) to form TOP-Ag solution and Se powder with TOP to form TOP-Se solution. The solutions were thermolysed at different temperatures ranging from 180 to 250 °C for TOPO and the temperature was kept between 130 to 190 °C for HDA. In our study TOP was used as a solvent to dissolve the precursors. It has been reported that the addition of TOP to the precursors result in the release of free phosphine ligands into the solution as the precursors decomposes [1]. Therefore, at lower temperature the phosphine ligands stabilize the precursors and hinder the degradation process which leads to the decrease of the rate of nucleation process. The action scheme of the dissolved precursors is shown below:



4.1.1 Capping molecules

The choice of an effective coordinating solvent is very important because the surface passivation of the nanocrystals by organic molecule have been shown to control the growth rate and particle size. Some of the examples of coordinating solvent include alkyl phosphine oxides, alkyl phosphonic acids, alkyl phosphones, fatty acids and amines. All these molecules contain the metal

coordinating groups and these coordinating groups are usually electron-donating to allow coordination to electro-deficient metal atoms at the nanocrystal surface. These prevent further growth and aggregation of the nanoparticles. In our study TOPO and HDA were used as coordinating solvents and to prevent aggregation. These coordinating solvent can cause changes in particle size and shape. The choice of TOPO as coordinating solvent let the reaction to take place above the nucleation temperature since it has a high boiling point. TOPO is an organophosphorus compound with a high polarity which results from the dipolar phosphorus oxygen bond which allows it to bind to metal compound. It has a bulky nature which provides increased steric hindrance. In contrast HDA is a primary amine with less steric hindered and a larger capping density which enhance surface passivation and increase the luminescence efficiency [2]. **Figure 4** shows the structures of TOPO and HDA.

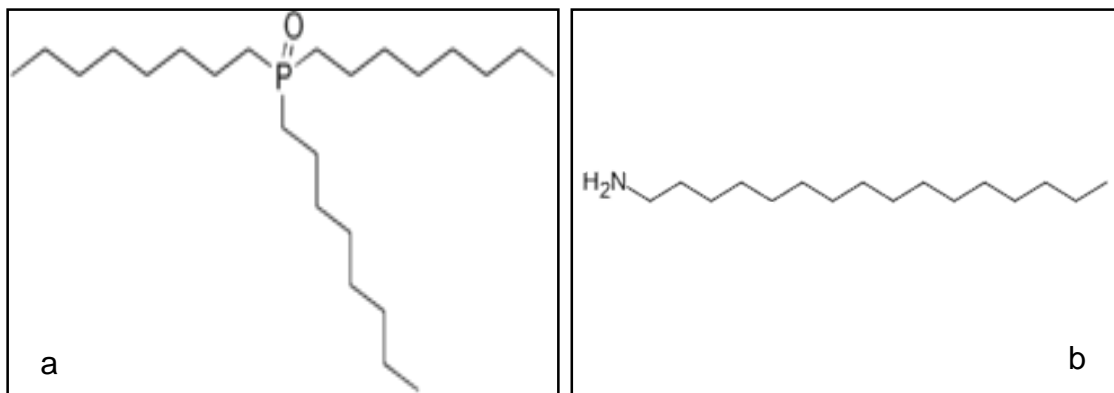


Figure 4: Structures of coordinating solvent (a) TOPO (tri-octylphosphine oxide) and (b) HDA (hexadecylamine)

4.2 TOPO-capped Ag_2Se nanoparticles

4.2.1 Effect of temperature

4.2.1.1 Optical properties

Temperature is one of the major factors that influence the particle size, growth rate and luminescent properties. Increasing the temperature greatly decreases the stability of the intermediate complexes formed in solution and the binding of the surfactants to the nanocrystal surface, while increasing

the diffusion rates of the complexes. This favours nucleation and growth of the nanocrystals. Higher growth temperature leads to faster growth rates and induce faster surface degradation. Higher temperature also favours the formation of larger particles and this has been attributed to the rate at which a ligand attaches and detaches itself from the surface of the metal [3]. Moloto et al. [4] have studied the optical properties of CdS on the reaction temperature and observed that temperature also affects the shapes of the nanoparticles due to the competition between the kinetic and thermodynamic growth regime.

The absorption and emission spectra for the synthesized Ag₂Se nanoparticles at temperature ranging from 180 to 250 °C are shown in **Figure 5**. A comparison between the absorption spectra of the particles prepared at different temperatures show differences in their band edges. **Figure 5 (a) (i), (ii) and (iii)** shows an increase in the band edges as the temperature was increased from 180, 200 and 250 °C with the band edges of 290, 330 and 340 nm, respectively showing large blue shift from the bulk band gap of 1035 nm. This signifies that as the temperature was increased the nanoparticle sizes also increased. The increase in nanoparticle sizes was observed due to Ostwald ripening. **Figure 5 (b)** shows the emission peaks of the above reported temperature, and they were all red shifted from their corresponding absorption band edges. **Figure 5 (b) (i) and (ii)** shows a shift from the lower wavelength of (444 nm) to the higher wavelength of (448 nm) as the temperature was raised from 180 to 200 °C. **Figure 5 (b) (iii)** showed a shift to a lower wavelength of (443 nm) as the temperature was further increased to 250 °C which suggest a change in morphology of particles. This change in the optical properties for nanoparticles prepared at 250 °C was found to correlate with the structural analysis in **Figure 6 (e)**. Increasing the temperature from 180 to 250 °C pushed the reaction away from the thermodynamic equilibrium to kinetics as observed when the morphology of the particles changed from sphere to hexagonal shape.

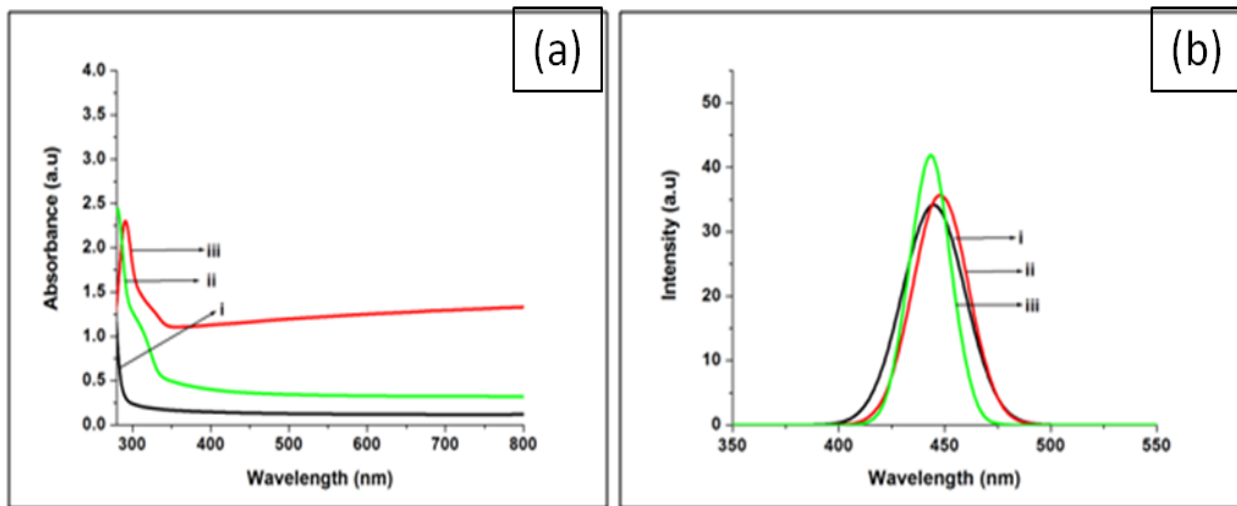


Figure 5:(a) Absorption and (b) Emission spectra of TOPO-capped Ag_2Se nanoparticles prepared at different temperatures (i) 180 °C (ii) 200 °C and (iii) 250 °C

4.2.1.2 Structural characterization

Figure 6 shows the TEM images for TOPO-capped Ag_2Se nanoparticles prepared at temperature 180, 200 and 250 °C. The TEM image and particle size distribution for particles prepared at 180 °C is shown in **Figure 6 (a) and (b)**. It was observed that uniform, polydispersed, spherical shapes were formed for TOPO-capped Ag_2Se nanoparticles with the particle size distribution of 8 to 20 nm. When the reaction temperature was raised to 200 °C, uniform spherical nanoparticles were also observed with the particle size distribution ranging from 20 to 40 nm as shown in **Figure 6 (c) and (d)**. As the temperature was further increased to 250 °C, the nanoparticle's shape changed from spherical to hexagonal shape with an increased particles size. The particles size distribution was found in the range of 30 to 120 nm as shown in **Figure 6 (e) and (f)**. It can be seen that as the temperature was raised from 180-250 °C, the particles size increased and the particle shape changed drastically at 250 °C, and this could be due to the faster growth rate of nuclei at higher temperature. It is evident that temperature plays a measure role on the formation of nanoparticles, this is demonstrated by the evolution of different sizes and shapes as the temperature was varied between 180 and 250 °C.

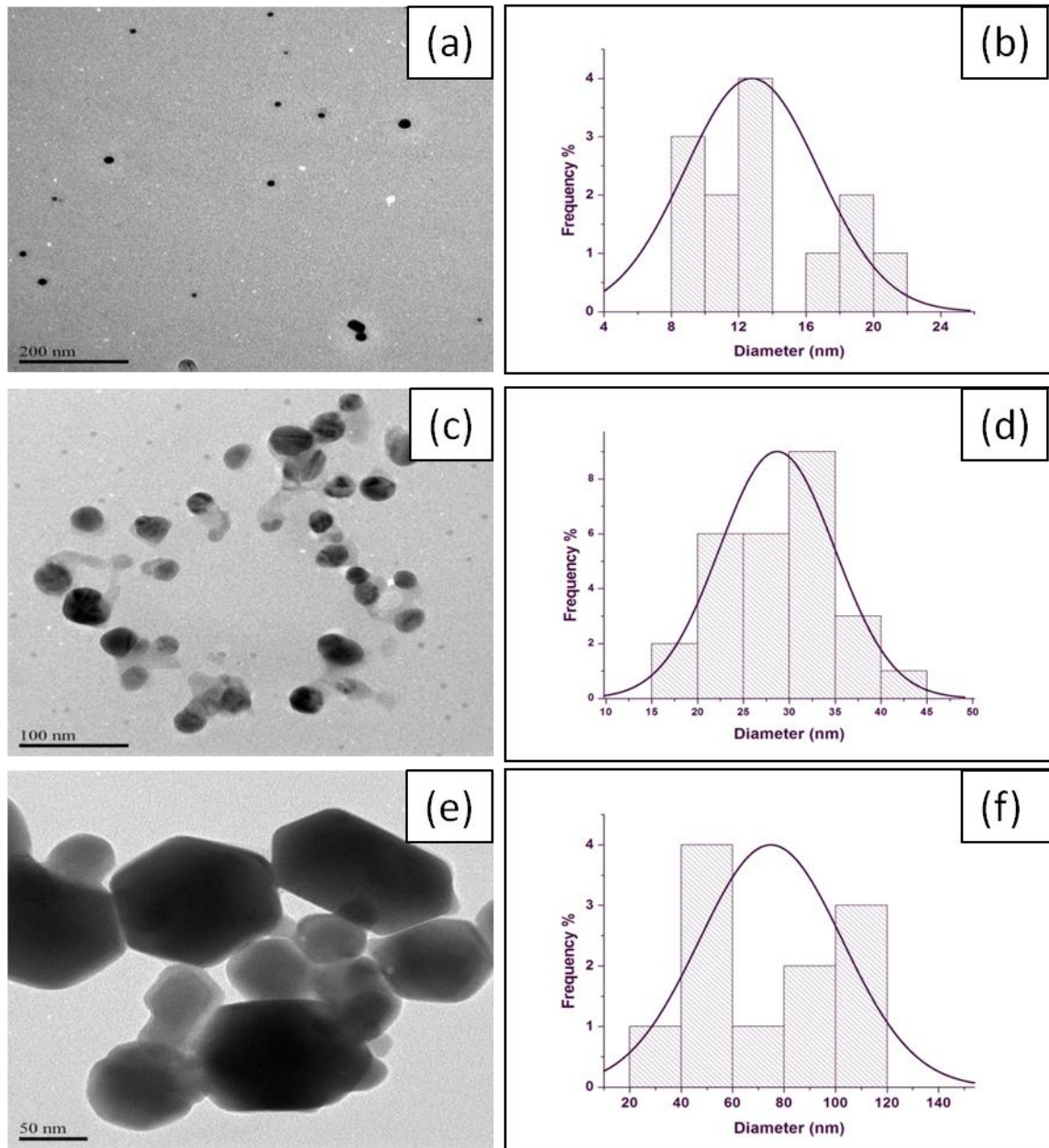


Figure 6: TEM images and histogram of TOPO-capped Ag₂Se nanoparticles prepared at different temperatures (a, b) 180 °C, (c, d) 200 °C and (e, f) 250 °C

Figure 7 (a), (b) and (c) shows XRD patterns for TOPO-capped Ag₂Se nanoparticles synthesized at different temperatures (180, 200 and 250 °C). Ag₂Se nanoparticles can exist as either cubic or an orthorhombic phase. According to Kumashiro et al. [5] they say that nonstoichiometric excess Ag occurred in Ag₂Se it dissolves in Ag₂Se. During the cooling process, the sample experiences an $\alpha \rightarrow \beta$ phase transition. They also mention that Ag has lower solubility in β -phase than in α -phase [5], therefore excess Ag will dissociate and form Ag particles and/or the segregation of Ag metal. The observed peak at $2\theta = 52.1^\circ, 76.1^\circ$ in **Figure 7 (a)** correspond to (211) and (222) planes which confirms the body centered cubic phase of α - Ag₂Se (JCPDS, 01-076-0135). The sharp peak at $2\theta = 44.5^\circ$ correspond to (111) plane which indicate the presence of silver in the face centered cubic phase (JCPDS, 03-065-2871). The presence of silver in this material suggest that the availability of silver during its reduction from silver nitrate by TOP was stoichiometrically more than selenium, with the ratio 2:1 for Ag and selenium. The calculated sizes of Se and Ag are 103 and 165 pm, respectively. This confirms that the material has excess silver which is well supported by the presence of silver peak in the XRD measurement. **Figure 7 (b)** and **(c)** correspond to (211) and (222) planes which also confirms the body centered cubic phase of α - Ag₂Se. The same sharp peak for a face centered cubic phase of silver was observed at $2\theta = 44.5^\circ$ in both **Figures 7 (b)** and **(c)** which corresponds to (111) plane.

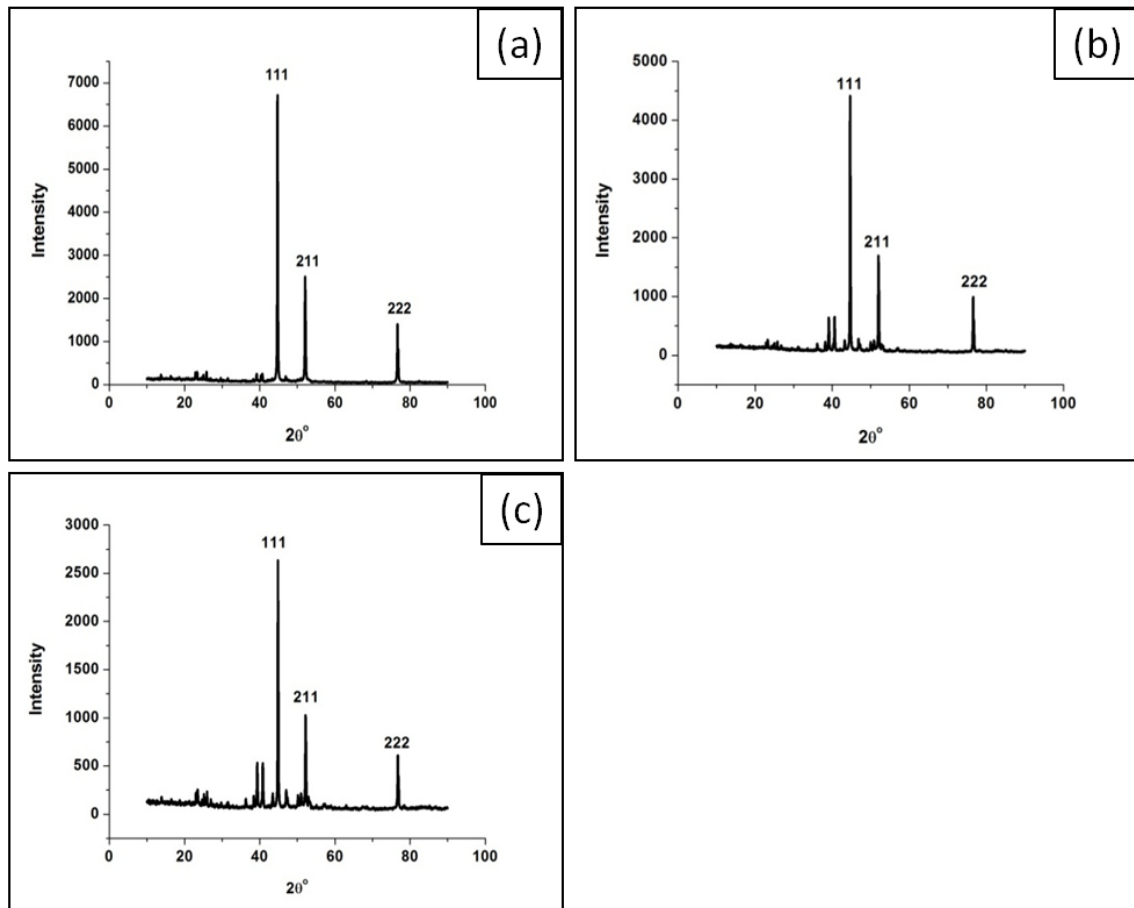


Figure 7:X-ray diffraction patterns of TOPO-capped Ag_2Se nanoparticles at different temperatures (a) 180 °C, (b) 200 °C and (c) 250 °C

4.3 HDA-capped Ag_2Se nanoparticles

4.3.1 Effect of temperature

4.3.1.1 Optical properties

Silver selenide nanoparticles were synthesized using HDA as a capping agent. The effect of temperature was investigated in HDA-capped Ag_2Se nanoparticles using the same conditions used in TOPO-capped Ag_2Se nanoparticles. The temperature variation was performed during this experiment to check the effect of temperature on the formation of nanoparticles in terms of size

and shape. The effect of temperature was investigated by varying the temperature from 130, 160 and 190 °C.

Figure 8 (a) and **(b)** shows absorption and emission spectra of HDA-capped Ag₂Se nanoparticles synthesized at different temperatures (130, 160 and 190 °C). The absorption spectra in **Figure 8 (a)** shows a blue shift from the bulk band gap of 1035nm with the band edge increasing as the temperature increases. **Figure 8 (a) (i)** show a blue shift from the bulk with the band edge of 284 nm. At higher temperatures of (160 and 190 °C) in **Figure 8 (a) (ii)** and **(iii)** an increase in the absorption band edges were observed at about 290 and 330 nm respectively indicating change in relation to their particle size with temperature increase. The growth of the particle size was observed due to Ostwald ripening. **Figure 8 (b)** shows emission peaks which were all red shifted from their corresponding absorption band edges. **Figure 8 (b) (i)** and **(ii)** show a slight shift from the lower wavelength to the higher wavelength as the temperature was increased from 130 °C (424 nm) to 160 °C (425 nm). As the temperature was further increased to 190 °C in **Figure 8 (b) (iii)** there was a slight decrease of the maximum emission wavelength towards the lower wavelength of 423 nm and this could be due to the change in morphology of the particles forming small crystal at higher temperature with increased particles size and this is confirmed by TEM image in **Figure 9 (e)**. The reaction favoured thermodynamic rather than kinetics since the most stable form of nanocrystals with spherical shaped were formed when temperature was increased from 130 to 190 °C with an increased particle size as observed in the TEM.

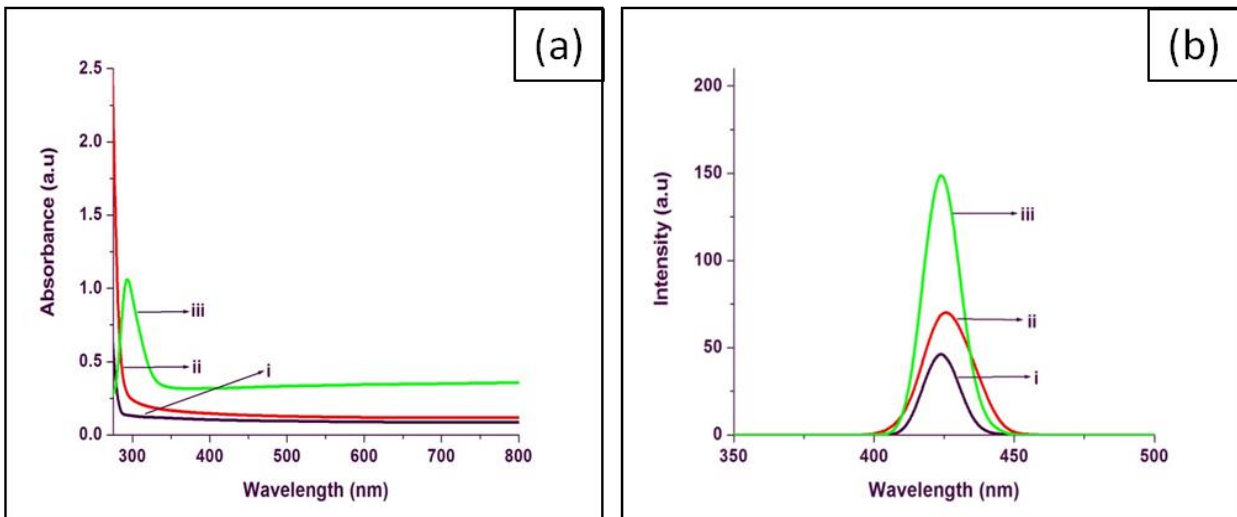


Figure 8: (a) Absorption and (b) emission spectra of HDA-capped Ag_2Se nanoparticles prepared at different temperatures (i) $130\text{ }^\circ\text{C}$, (ii) $160\text{ }^\circ\text{C}$ and (iii) $190\text{ }^\circ\text{C}$

4.3.1.2 Structural characterization

The TEM images in **Figure 9** show HDA-capped Ag_2Se nanoparticles prepared at different growth temperatures of (130 , 160 and $190\text{ }^\circ\text{C}$). The morphologies of nanoparticles prepared at 130 , 160 , and $190\text{ }^\circ\text{C}$ were all spherical in shape. The diameter of this nanoparticles increases with an increase in temperature. The TEM image in **Figure 9 (a)** shows uniform, spherical nanoparticles which were prepared at $130\text{ }^\circ\text{C}$ for HDA-capped Ag_2Se nanoparticles with the particle size distribution of 2 to 12 nm as shown in **Figure 9 (b)**. When the injection temperature was increased to $160\text{ }^\circ\text{C}$ uniform spherical shapes were also observed with the size distribution ranging from 4 to 16 nm as shown in **Figure 9 (c)** and **(d)**. As the temperature was further increased to $190\text{ }^\circ\text{C}$ the nanoparticle sizes also increased with the size distribution ranging from 4 to 18 nm as shown in **Figure 9 (e)** and **(f)**. This increase in nanoparticle sizes is as a result of Ostwald ripening. Ng et al. [1] have studied the effect of HDA on the morphology of Ag_2Se nanoparticles at high temperature and they found that nanoparticles prepared with high amine concentration at high temperature are mainly small faceted crystals since more nuclei were produced under those conditions.

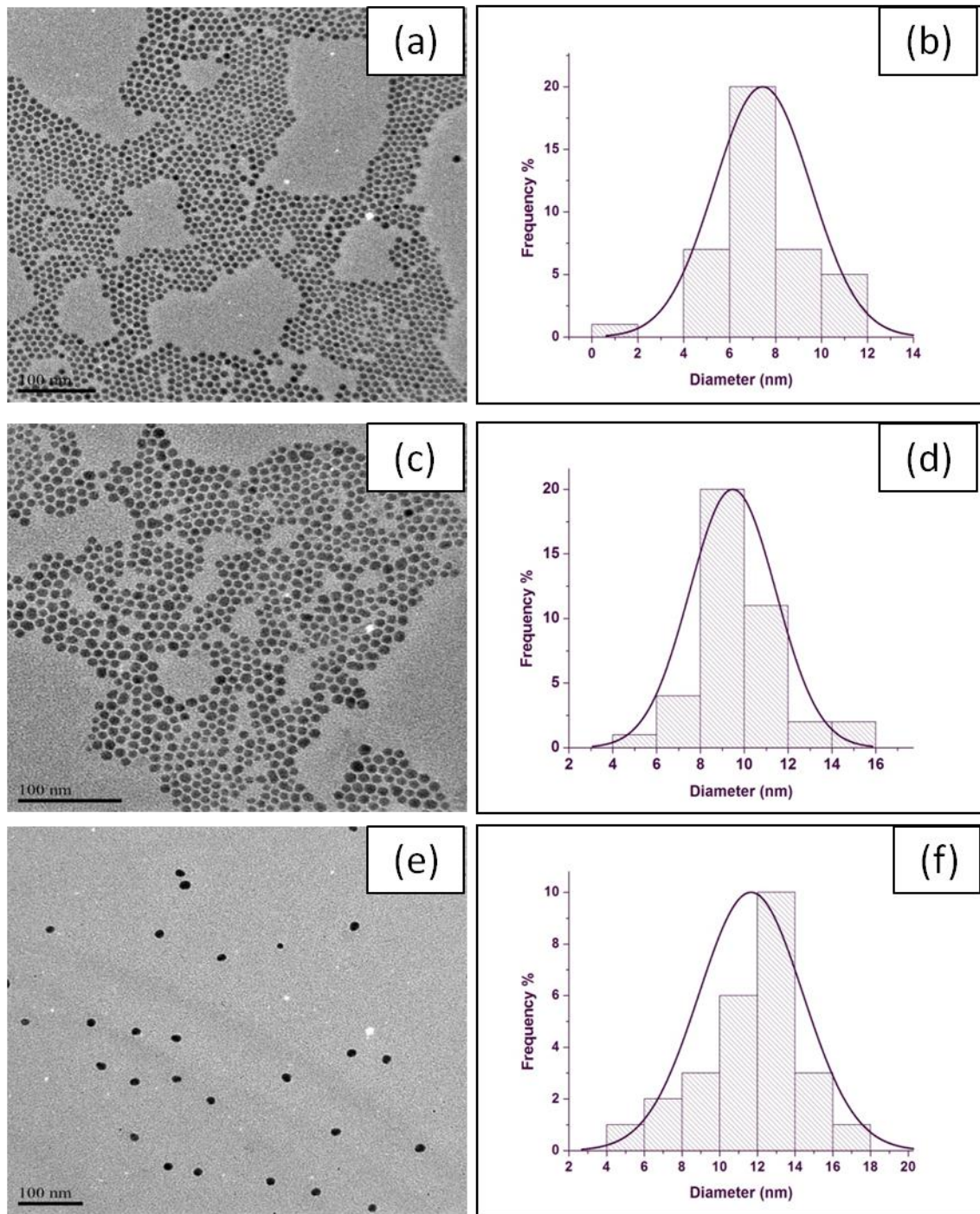


Figure 9: TEM images of HDA-capped Ag₂Se nanoparticles prepared at different temperatures (a, b) 130 °C, (c, d) 160 °C and (e, f) 190 °C

The XRD patterns shown in **Figure 10 (a), (b) and (c)** represent HDA-capped Ag₂Se nanoparticles prepared at different temperatures (130, 160 and 190 °C). The peaks at $2\theta = 52.1^\circ, 76.1^\circ$ in **Figure 10 (a)** correspond to (200) and (222) planes confirming the body centered cubic of α -Ag₂Se (JCPDS, 01-076-0135). The sharp peak at $2\theta = 44.5^\circ$ correspond to (111) plane indicating the presence of silver in face centered cubic (JCPDS, 03-065-2871). The same peak at $2\theta = 44.5^\circ$ were observed for all the temperatures and it became more prominent as the temperature was increased from 130 to 190 °C. **Figure 10 (b)** and **(c)** correspond to (200) and (222) planes which also confirms the body centered cubic phase of α -Ag₂Se. The intensities of the peaks became more prominent for all the temperatures as the temperature was increased.

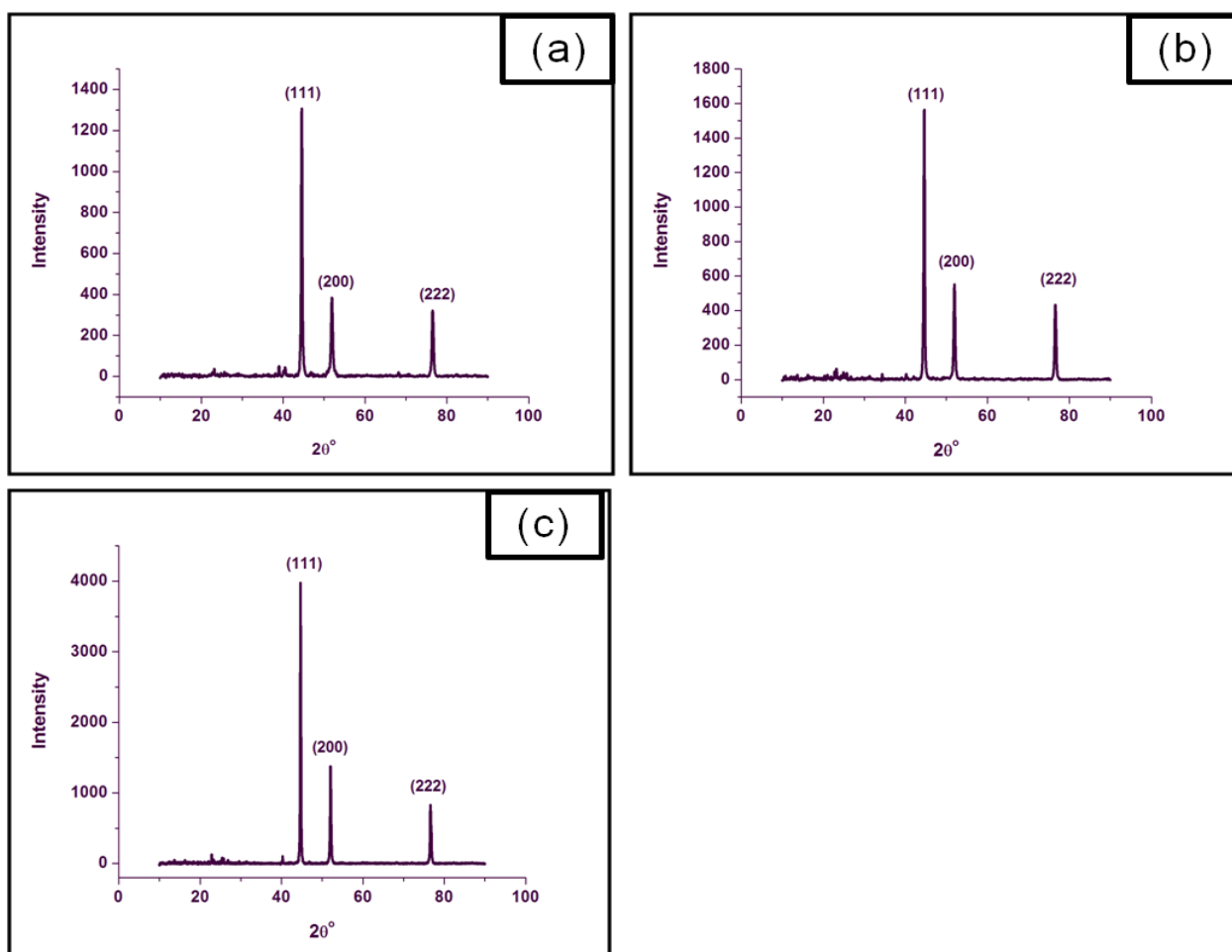


Figure 10: XRD pattern of HDA-capped Ag₂Se nanoparticles prepared at different temperatures (a) 130 °C, (b) 160 °C and (c) 190 °C.

Capping molecules (HDA and TOPO) play an important role in the formation of nanoparticles and they are known to influence the particle's growth and stability giving rise to different shapes and sizes. Their effect was evaluated on Ag₂Se nanoparticles. In this study higher temperatures were used for TOPO as compared to HDA. The shape of TOPO-capped nanoparticles changed from sphere to hexagonal as the temperature was increased which also had an impact on the size of these nanoparticles compared to HDA-capped which favoured spherical shapes for all temperatures. Narrow size distributions were observed for HDA-capped nanoparticles compared to TOPO-capped nanoparticle. HDA-capped nanoparticles show significant luminescence intensity compared to TOPO-capped nanoparticles because of its larger capping density and less steric hindered. The absorption and PL spectra display sharp band-edge luminescence and weaker, broader luminescence peaks at lower temperatures for HDA-capped compared to TOPO-capped nanoparticles. Some peaks were observed in the XRD structures for TOPO which may be due to impurities compared to HDA with no impurities.

4.4 Ag Nanoparticles

Metal nanoparticles have been the subject of great interest in the field of research. Nanoparticles of silver exhibit interesting antibacterial activities due to their large surface to volume ratio. The study was based on established silver nanoparticles with their antibacterial activity applied in different forms and the intention was to incorporate them into fibres to make nanocomposite fibres for potential use in wound dressing. The use of inorganic precursors to synthesize metal nanoparticles at high temperature has been reported. Green and co-workers [6] have reported the synthesis of trialkyl-phosphine oxide and amine stabilized silver nanocrystals. Nath et al. [7] also reported the synthesis of HDA-capped silver organosols which were reproducibly stable for over a year. Chen et al. [8] developed a method for the synthesis of monodispersed silver nanoparticles using tri-octylphosphine (TOP) as a reducing agent, solvent, and surfactant. In their method they used single-phase system whereby silver nitrate was dissolved in TOP and heated to a destined temperature range of 160 – 200 °C. In our work, Ag nanoparticles were synthesized using HDA and TOPO as capping agent. These capping molecules were used because of their solubility and stability in organic solvents. The nanoparticle's solubility is provided by the shell of the capping molecules. AgNO₃ was reacted with TOP to form TOP-Ag and the solution was injected into a hot

HDA/TOPO at different temperature range of (130, 160 and 190 °C) for HDA and (180, 200 and 250 °C) for TOPO. Due to the solubility of the capping molecules and the solvent used, Ag nanoparticles prepared by HDA were isolated and very small yields were obtained which we were able to do the analysis such as UV-Vis spectroscopy and TEM only. Other analysis like XRD were not performed due to the small yield obtained. On the other hand when TOPO was used as a capping agent the experiment was unsuccessful because it was difficult to isolate the nanoparticles from the solution. The reason could be that the nanoparticles are either too small that they cannot be isolated by the standard solvent/non solvent precipitation techniques or it might be that TOPO is binding too strongly to Ag. According to Moloto et al. [4], they say that a molecule that binds too strongly to the surface of the crystal is not suitable as it would not allow the crystal to grow. Due to the reasons mentioned above Ag nanoparticles was not incorporated into PVP and PMMA nanofibres.

4.4.1 Effect of temperature

4.4.1.1 Optical properties

The temperature variation was performed for HDA-capped Ag nanoparticles to check the effect of temperature on the formation of nanoparticles in terms of size and shape. The temperatures were varied from 130, 160 and 190 °C.

Figure 11 shows the absorption spectra of HDA-capped Ag nanoparticles synthesized at different temperature of 130, 160 and 190 °C. **Figure 11 (i) and (iii)** show similar absorption band at 418 nm for both 130 and 190 °C. This behaviour is confirmed by TEM where the particles size distribution show more or less the same frequency for the nanoparticles.

Figure 11 (ii) show a broad absorption band at 428 nm as the temperature was increased to 160 °C. Similar studies were conducted where they reported the synthesis of silver nanoparticles and nanowires with the Surface Plasmon Resonance (SPR) band at 410 nm for the diameter of 20 to 30 nm. [9]

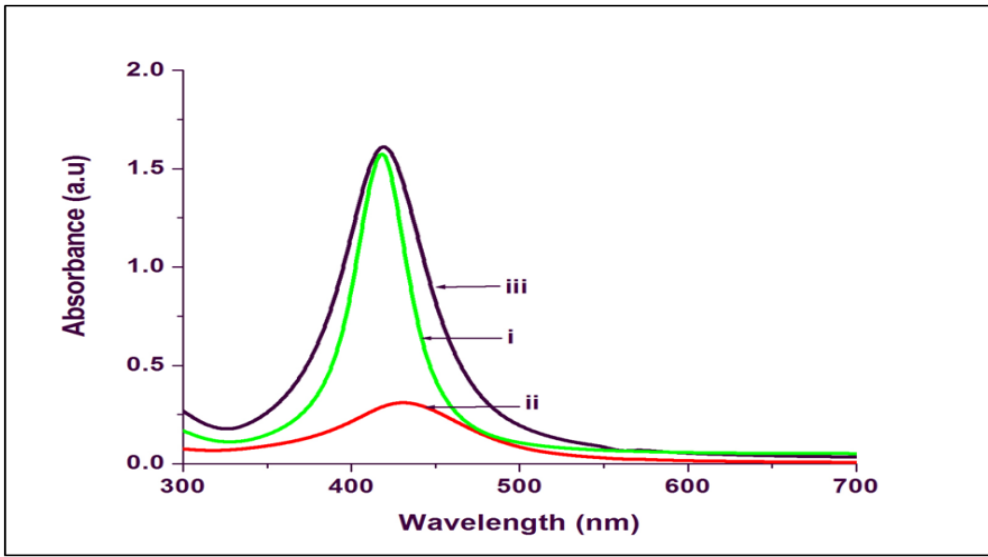


Figure 11: Absorption spectra of HDA-capped Ag nanoparticles prepared at different temperatures (i) 130, (ii) 160 and (iii) 190 °C

4.4.1.2 Structural properties

The TEM images in **Figure 12** show HDA-capped Ag nanoparticles prepared at different temperatures of (130, 160 and 190 °C). The TEM images of all the temperatures show spherical nanoparticles. It can be observed from **Figure 12** that as the temperature was increased, the diameter of the nanoparticles increased as well. The TEM image in **Figure 12 (a)** show uniform, monodispersed spherical particles were observed at 130°C for HDA-capped Ag nanoparticles with the particle size distribution ranging from 6 to 18 nm as shown in **Figure 12 (b)**. As the reaction temperature was increased to 160 °C scattered particles were observed with broader size distribution showing an increase in particles size with the range of 12 to 14 nm as shown in **Figure 12 (c)** and **(d)**. When the temperature was further increased to 190 °C the nanoparticle sizes also increased with the particle size distribution ranging from 8 to 20 nm as shown in **Figure 12 (e)** and **(f)**. This increase in particles size is as a result of Ostwald ripening.

The size distribution of the particles prepared at 130 and 190 °C show frequencies which are close to one another and this gives a reason why their absorption band occurred at the same wavelength.

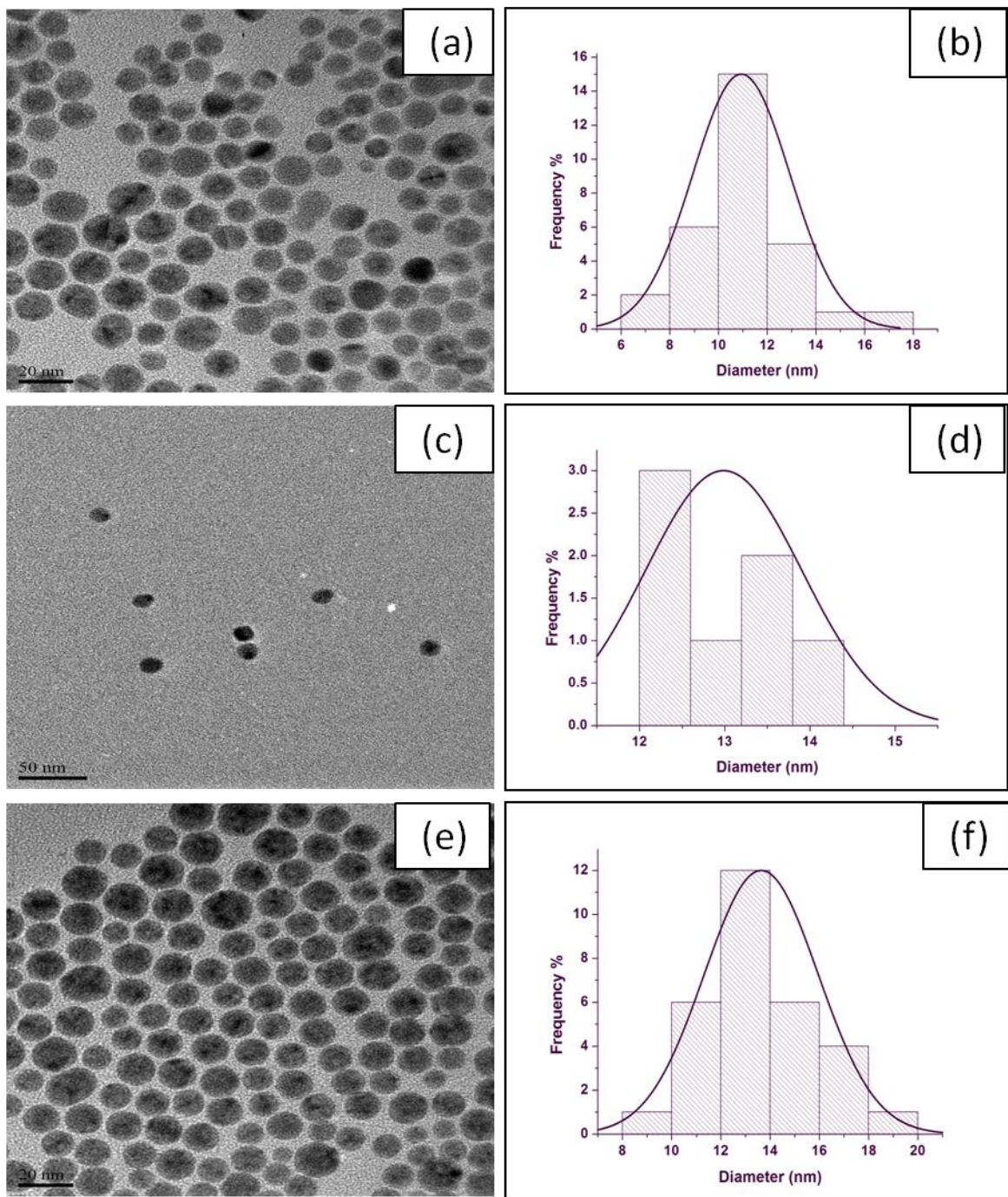


Figure 12: TEM images of HDA-capped Ag nanoparticles prepared at different temperatures (a, b) 130 °C, (c, d) 160 °C and (e, f) 190 °C

4.5 Conclusions

Ag_2Se nanoparticles were successfully prepared in TOPO and HDA as coordinating agent. Uniform, monodispersed spherical silver selenide nanoparticles were prepared in HDA rather than in TOPO. The prepared particles seem to depend on the reaction temperature where the increase in temperature led to an increase in particle sizes. This increase in particle size was observed due to Ostwald ripening. These temperature variations were found to influence the optical properties of silver selenide nanoparticles. The particles prepared in TOPO changed from sphere to hexagonal shape when the temperature was increased. Furthermore, the size and shape of these nanoparticles can be tuned by changing the HDA or TOPO concentration, since these capping agents are also known to influence the particle growth and stability giving rise to different shapes and sizes. In conclusion, TOPO has a poor capping capacity than HDA since the nanoparticles prepared by TOPO showed the tendency of agglomeration with increase in temperature. HDA is more stable as compared to TOPO.

HDA-capped Ag nanoparticles were successfully prepared using the metal-organic route method. The produced Ag nanoparticles were found to be affected by temperature variation. Uniform spherical shapes were observed for both 130 and 190°C. Scattered particles were obtained at 160°C. The absorption spectra of HDA-capped silver nanoparticles at different temperatures show a surface Plasmon resonance (SPR) band in the regions 418 - 428 nm. The synthesis of TOPO-capped Ag nanoparticles was unsuccessful during this study since none of the particles were isolated from the solution due to its lower capping density and it may be that TOPO is binding too strongly to Ag.

4.6 References

- [1] M. T. Ng, C. Boothroyd and J. J. Vittal, Chemical Communications, **2005**, 30, 3820-3822
- [2] M. A. Hines, and P. Guyot-Sionnest, Journal of Physical Chemistry B, **1998**, 102, 3655-3657
- [3] R. He and H. Gu, Physicochemical and Engineering Aspects, **2006**, 272, 111-116.
- [4] N. Moloto, N. Revaprasadu, P. L. Musetha, and M. J. Moloto, Journal of Nanoscience and Nanotechnology, **2008**, 9, 1-7.
- [5] Y. Kumashiro, T. Ohachi, and I. Taniguchi, Solid State Ion, **1996**, 86-88, 761–766.
- [6] M. Green, N. Allsop, G. Wakefield, P. J. Dobson and J. L. Hutchison, Journal of Material Chemistry, **2002**, 12, 2671-2674.
- [7] S. Nath, S. Praharaj, S. Panigrahi, S. Kundu, S. K. Ghosh, S. Basil and T. Pal, Colloids and Surfaces A: Physicochemical Engineering Aspects, **2006**, 274, 145-149.
- [8] Z. Chen and L. Gao, Materials Research Bulletin, **2007**, 42, 1657-1661
- [9] D. B. Zhang, L. M. Qi, J. H. Yang, J. M. Ma, H. M. Cheng and L. Huang, Chemistry of Materials, **2004**, 16, 872-876.

CHAPTER 5

POLYMER FIBRES

5.1 Properties of PVP and PMMA polymers

Poly (vinylpyrrolidone) (PVP) is a water-soluble polymer composed of N-vinylpyrrolidone monomers [1]. It is an important synthetic polymer that was first reported in a patent almost 60 years ago, with good complexation and adhesion properties. Its amorphous structure provides a low scattering loss, which makes it as an ideal polymer for composite material for different applications. It has good environmental stability with good mechanical strength. It has a good charge storage capacity and dopant-dependent electrical and optical properties. Chemically it has been found to be inert and non-toxic. It exhibits a strong tendency for complex formation with a wide variety of small molecules [2-4]. It binds exceptionally well to polar molecules. It is well known to be of great importance in pharmaceutical industries since it is been used as a binder for tablets. PVP is also known to be a hydrogen bond acceptor because it contains carbonyl group that is capable of donating electrons. Each vinylpyrrolidone has one hydrogen bond active site, and it can form hydrogen bonds between carbonyl side groups of its repeating units and the terminal hydroxyl group of the other co-monomer functional groups.

Poly (methyl methacrylate) PMMA is a clear polymer which belongs to the important family of acrylic resins. Chemically it is a synthetic polymer of methyl methacrylate. PMMA uses the carboxylate functional group for chemical bonding with the metal ions. PMMA is a transparent and rigid plastic most often used as a light weight or shatter resistant alternative to glass. It has high mechanical strength and low elongation. It is one of the hardest thermoplastics and is also highly scratch resistant. It exhibits low moisture and water absorbing capacity, due to which products made of it have good dimensional stability. It is one of the polymer that is most resistant

to direct sunshine exposure. It has excellent chemical, physical, biological, mechanical, optical and thermal properties [5-7]. It exhibits very good optical properties meaning it can be able to transmit more light up to 93 % of visible light than glass and is used extensively for optical application. It has a good degree of compatibility with human tissue, and can be used for replacement of intraocular lenses or for contact lenses. Lastly it is mostly used in research for studies based on polymers and composites. **Figure 13 (a)** and **(b)** shows the structures of the chosen polymers.

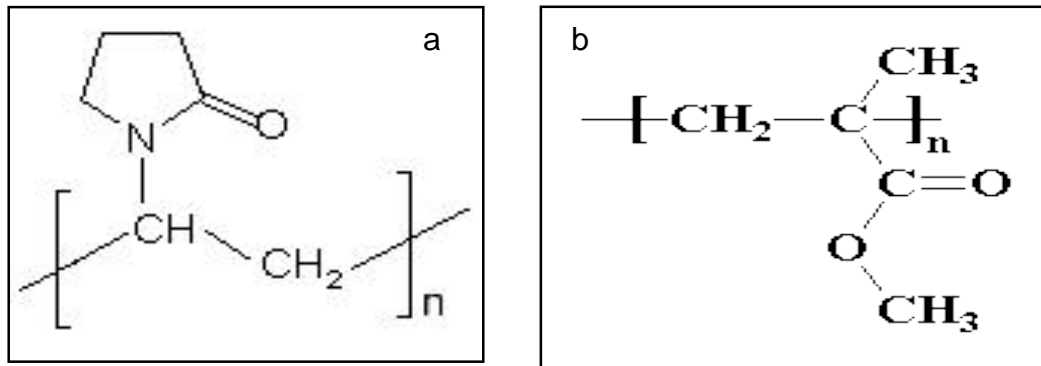


Figure 13: Structure of (a) PVP and (b) PMMA polymers.

5.2 Electrospinning of PVP and PMMA polymer fibers

5.2.1 Polymer nanofibers

The electrospinning process is governed by many parameters classified broadly into solution parameters, process parameters and ambient parameters. It is well known that the morphology and size of electrospun nanofibers strongly depend on solution properties such as viscosity, conductivity, molecular weight, and surface tension. Process parameter such as applied electric field, tip to collector distance and feeding or flow rate are also known as parameters which can influence the formation of nanofibers. Each of these parameters significantly affects the fibers morphology obtained as a result of electrospinning and by proper manipulation of these parameters nanofibers of desired morphology and diameters can be obtained. The influence of some of these

parameters was studied and presented in subsections i.e. by varying the polymer concentration, applied voltage and finally by varying the amount of silver selenide nanoparticles loaded on the polymer solution. Addition of silver selenide nanoparticles prepared at 180 °C for TOPO and the one prepared at 160 °C for HDA were effective only under the conditions of 40 wt% PVP concentration, with a voltage of 17 kV and a spinning distance of 10 cm respectively. The same procedure was used for PMMA polymer except that the nanoparticles added for both TOPO and HDA were effective at 8 wt% PMMA concentration, with the voltage of 15 kV and a spinning distance of 10 cm. With the PVP polymer the parameter called voltage was further investigated hence not done in PMMA polymer.

5.2.2 Effect of PVP and PMMA concentration the electrospun polymer fibers

It is known that the solution concentration is a key factor in determining nanofibre diameter. At low viscosities, solution surface tension is the dominant influence on fibre morphology and below a certain concentration drops will be formed instead of fibres. At high concentration the formation of continuous fibres are prohibited because of the inability to maintain the flow of the solution at the tip of the needle resulting in the formation of larger fibres [8]. In addition a higher polymer concentration tends to stabilize the jet and results in fewer beads and more uniform fibres. The molecular weight of the polymer also plays a major role in the preparation of the polymer solution, since it affect the viscosity of the polymer at any given concentration. Polymers with higher molecular weight result in a higher viscosity and the one with lower molecular weight results in lower viscosity. Their differences in molecular weight accounts for a difference in the range of concentration when they are being electrospun using conditions mentioned in the study. The viscosity of PVP solution was lower than that of the PMMA solution due to lower molecular weight. Therefore higher concentrations for PVP polymer were chosen for electrospinning instead of lower concentration.

Figure 14 (a), (b), (c) and (d) shows the SEM images and average fibre distribution of the PVP fibres electrospun at different concentrations of 35 wt%, 40 wt% and 45 wt% with a voltage of 17 kV and a distance of 10cm. At 30 wt% droplets were formed due to lower concentration and higher surface tension. Hohman et al. [9] reported that high surface tension of a solution inhibits the electrospinning process because of instability of the jets and hence the formation of sprayed droplets will be generated. At concentration higher than 45 wt% it was difficult to electrospin fibers due to the higher viscosity of the solution. However a mixture of beads and fibres were obtained at 35 wt% with an average fibre diameter of 358 nm. As the concentration was increased to 40 wt% the shape of the beads changed from spindle-like to more uniform fibres with an average diameter of 653 nm. As the concentration was further increased to 45 wt% more uniform fibres were obtained with an increased average diameter of 1012 nm. It is evident that the increase in fibre diameters does depend on the solution concentration.

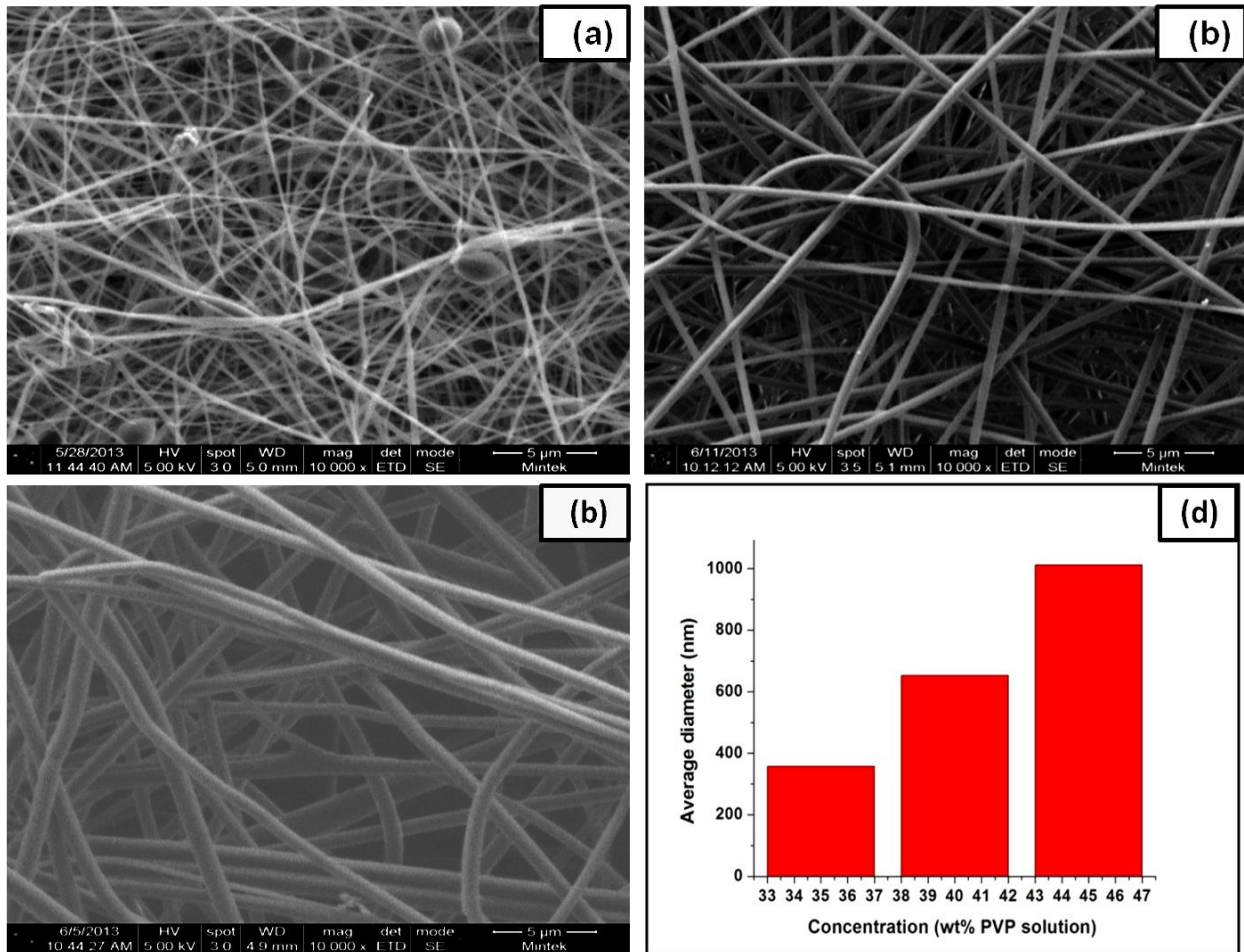


Figure 14: SEM images and average fiber distribution of PVP nanofibers at different polymer concentrations of (a) 35 wt%, (b) 40 wt% and (c) 45 wt%

The same principle as above was applied here with the concentration of PMMA ranging from (8-12 wt%) with the voltage of 15 kV and a spinning distance of 10 cm. The SEM images on the effect of concentration for PMMA polymer fibres were not available for discussion. PMMA polymer was electrospun at lower concentrations compared to PVP because of the higher viscosity produced as a results of higher molecular weight. PMMA nanofibres have been electrospun before by other researchers and similar trend were observed when the concentration of PMMA were varied. Wang and co-workers [10] reported on the electrospun PMMA nanofibres. Their observation showed that the diameter of the fibres decreased from 1260, 857, and 764 nm for 30, 26, and 22 wt% respectively. This observation showed that the diameter of the fibres decreased

with decreasing the concentration. Mthethwa et al. [11] reported on the effect of concentration on PMMA polymer. In their observation they found that as the concentration of the polymer solution increase the fibres diameter also increases with the value ranging from 371 to 644 nm for 4 to 6 wt% PMMA. The same trend was observed with PVP solution, this observable difference was due to the increase in concentration which turned to increase the fibre diameter.

5.3 Effect of applied voltage

The applied voltage is a crucial element which influences the fiber diameter. Researchers have suggested that when higher voltages are applied, there is more polymer ejection and this facilitates the formation of a larger fibre diameter [12]. Other researchers have shown previously in their studies that increasing the applied voltage did not have much influence on the diameter and morphology of the nanofibres for certain polymers [13]. Yordem et al. [14] have reported that applied voltage influences the fibres diameter, but its level of significance varies with the polymer concentration and on the distance between the tip and the collector.

In this study the voltage seemed to have an effect on both the diameter and the morphology of electrospun fibres. **Figure 15 (a), (b), (c), (d) and (e)** shows the SEM images and average fibre distribution of PVP nanofibres at different voltages, with a PVP concentration of 40 wt% and a distance of 10 cm. The influence of voltage on morphology and diameter of the nanofibres were investigated. **Figure 15** shows that the fibre diameter of the nanofibres increased gradually from 423 to 497, 506 and 653 nm as the voltage was increased from 11 to 13, 15 and 17 kV, respectively. As the voltage was further increased to 20 kV, the diameter of the nanofibres decreased significantly to 512 nm, which could be due to voltage resulting in the complete disappearance of the droplet at the needle tip. In most cases higher voltage can cause a greater stretching of the solution due to the greater columbic forces in the jet as well as a stronger electric field, and these effects can lead to the reduction of fibre diameter and also a rapid evaporation of solvent from the fibres. The SEM images in **Figure 15** showed a uniform morphology with no beads at all voltages.

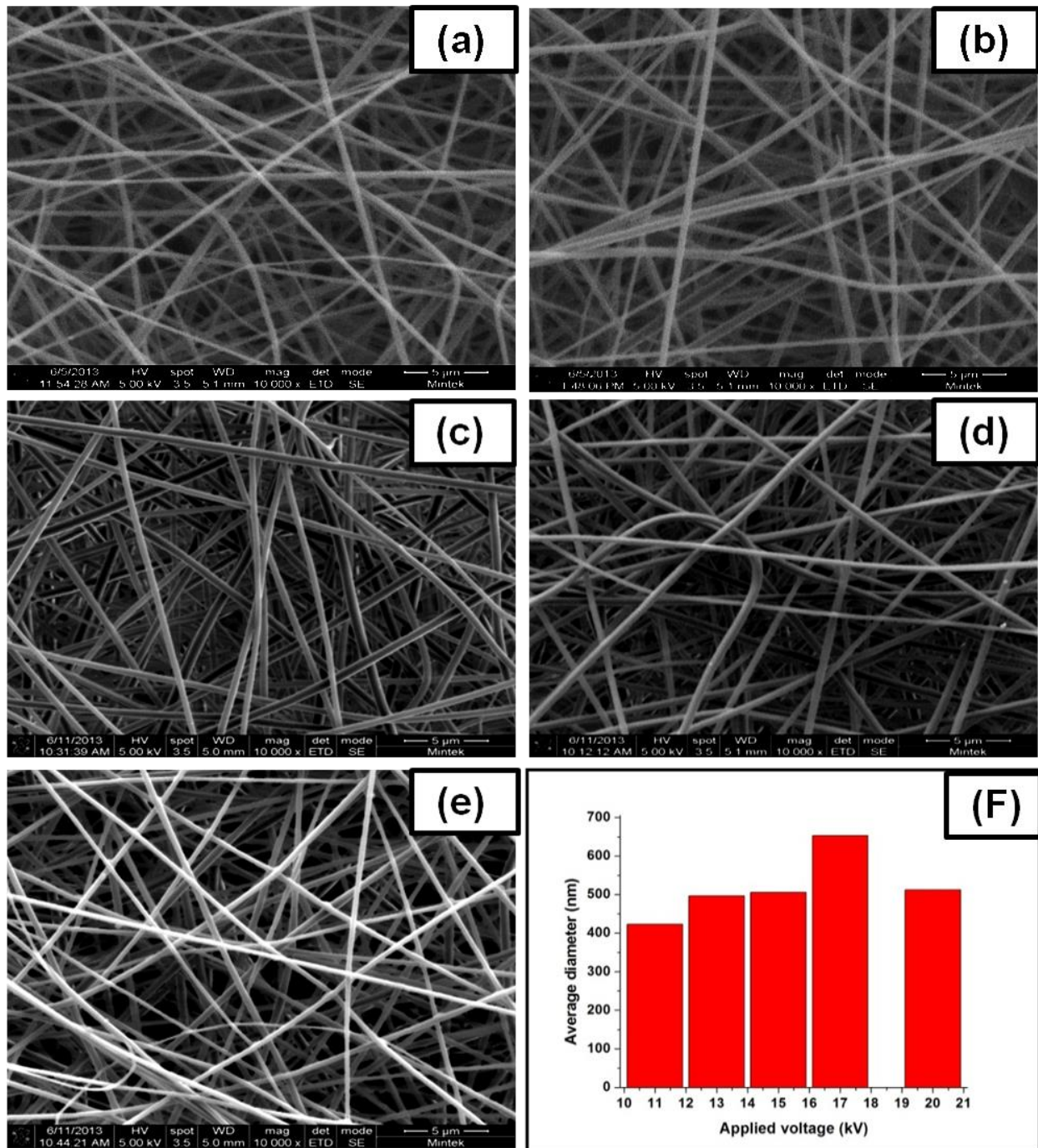


Figure 15: SEM images and fibres distribution of 40 wt% PVP at different voltages (a) 11 kV, (b) 13 kV, (c) 15 kV, (d) 17 kV and (e) 20 kV (f) Fibre size distribution

5.4 PVP/PMMA/Ag₂Se composite fibres

5.4.1 Incorporation of TOPO-capped Ag₂Se nanoparticles into PVP and PMMA nanofibers

The synthesis of Ag₂Se nanoparticles was reported in chapter 3 and discussed in chapter 4. During the synthesis small yield of Ag₂Se nanoparticles were obtained. These nanoparticles were used as additives or fillers in the preparation of nanocomposite fibres. Their dispersion into polymer fibres was reported in chapter 3 and discussed in chapter 5. During their incorporation into PVP and PMMA polymers lower percentages (0.2 and 0.6 wt%) were used due to the small yield obtained. For the preparation of PVP and PMMA polymer solutions, higher percentages were used to maintain the desired viscosity for electrospinning. The effect of nanoparticles loading on the morphology of the fibres for both PVP and PMMA polymers were investigated. SEM results for PMMA incorporated Ag₂Se nanoparticles are not shown in the study. Other techniques like XRD, FTIR spectroscopy, TGA, and UV-Vis spectroscopy have been shown and discussed fully.

5.4.2 Structural properties of the composite fibres

5.4.2.1 SEM analysis of the composite fibres

The properties of composite materials can significantly be impacted by the ratio of a mixture of an organic matrix and the additive. In electrospinning, additive may be added to a polymer solution to influence its viscosity, surface tension and conductivity. The fact that the conductivity of a solution has major influence on the electrospinning, the effect of loaded QDs/Ag₂Se nanoparticles on the morphology and diameter of the fibres was therefore investigated. Zong et al. [15] studied the effect of ions on the morphology and fibre diameter of electrospun fibres by adding ionic salts, and they found that addition of ionic salts to the polymer solution produced beadless fibres with smaller diameters.

Figure 16 show the SEM images and fibre distribution of pure PVP and its (PVP/Ag₂Se) composite fibres prepared from a 40 wt% PVP solution with different loadings of QD's ranging from (0.2 and 0.6 wt%) respectively. The voltage used was 17 kV and a spinning distance of 10 cm. By comparison, it was observed that the diameter of pure PVP nanofibres (653 nm) in **Figure 16 (a)** was thicker than those of Ag₂Se/PVP composite fibres. Addition of Ag₂Se nanoparticles into 40 wt% PVP solution resulted in an improved fibre morphology with a decreased average diameter of 372 nm for 0.2 wt% as shown in **Figure 16 (b)**. As the concentration of Ag₂Se nanoparticles was further increased to 0.6 wt% the fibre uniformity improved further with a decrease in fibre diameter of 361 nm as shown in **Figure 16 (c)**. This was also illustrated by the fibre distribution in **Figure 16 (d)**. The sudden reduction in fibre diameter is as a result of increased conductivity in the polymer solution due to the presence of nanoparticles added. According to the literature, it has been reported that when the dopant is added to the polymer solution for electrospinning an interaction between the dopant and polymer makes the nanofibres thicker [16]. However, if the dopant increases the conductivity of the polymer solution the nanofibres become thinner [17].

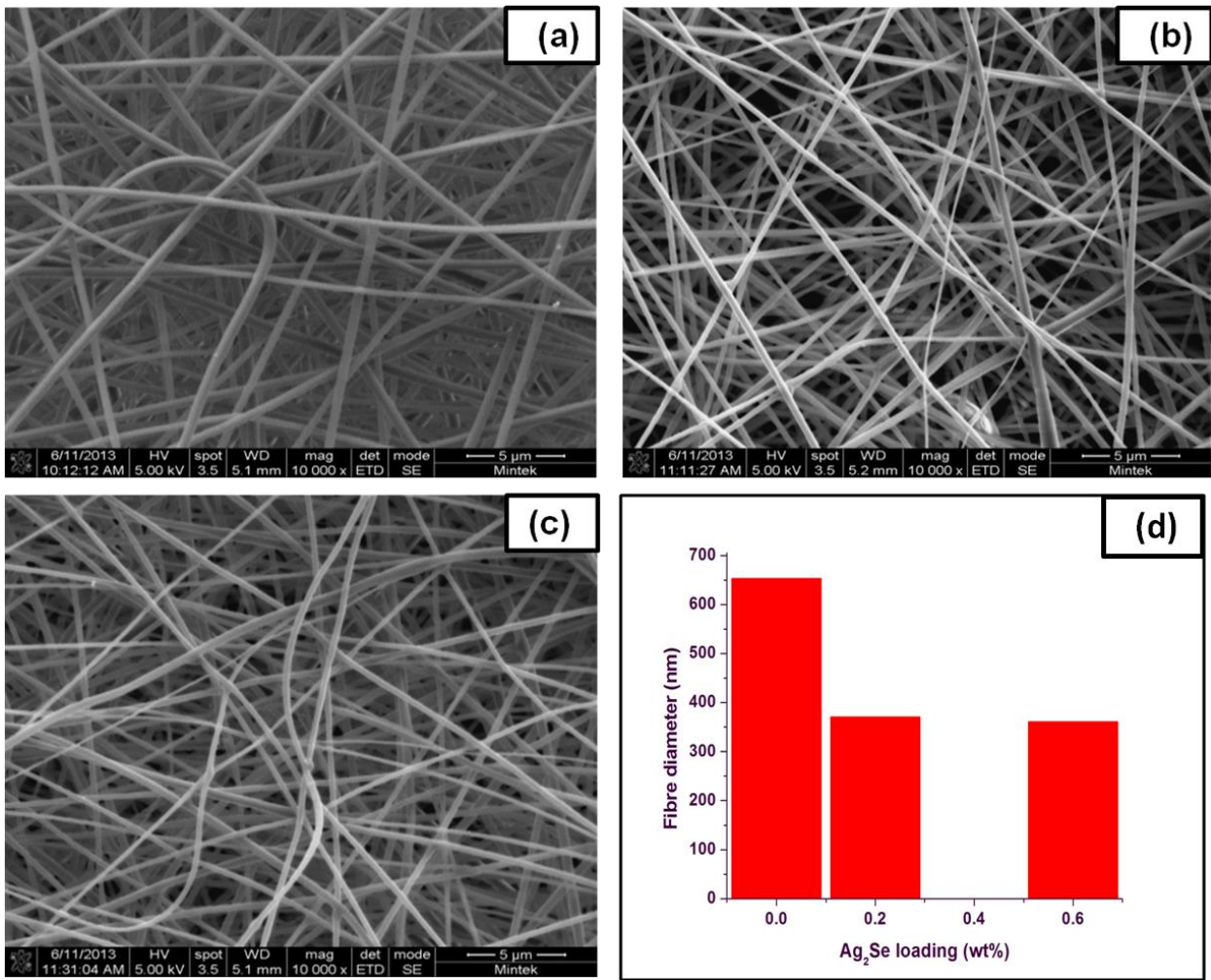


Figure 16: SEM images and fibre distribution of (40 wt%) PVP with different loading of the nanoparticles (a) 0 wt% (b) 0.2 wt% and (c) 0.6 wt%.

The same procedure used for PVP was also applied here though the conditions were different with concentration of PMMA being 8 wt%, voltage of 15 kV and a distance of 10 cm (SEM not shown). The nanoparticles /quantum dots loaded range between 0.2 and 0.6 wt%. The UV-Vis spectra of the composite fibres, shows that the composite fibres are red shifted from the nanoparticles added which indicate a slight growth of the nanoparticles in the composites fibres. Mthethwa et al. [11] again reported on the effect of CdS/CdSe quantum dots added on the fibre morphology of PMMA and they found that addition of quantum dots to the polymer solution increased the diameter of the electrospun fibres and further improved fibres uniformity. Wei et al. [18] did a study on the electrospun PMMA and its composites PMMA/CdSe/Zn. They observed that large quantity of fine

uniform and defect free fibres were obtained at low concentrations of PMMA with 0.1 wt% quantum dots added.

5.4.2.2 XRD analysis of the pure polymer and the composite fibres

The XRD analysis of the electrospun PVP polymer and its composite fibres ($\text{Ag}_2\text{Se}/\text{PVP}$) were performed to investigate the presence of Ag_2Se nanoparticles in the polymer fibres, and to investigate the influence of the nanoparticles loading on the structure of the polymer. The XRD patterns in **Figure 17 (a)** shows the amorphous peaks for both the polymer and its composite fibres at $2\theta = 12^\circ$ and 22° . There were no peaks observed for Ag_2Se nanoparticles in the composite due to lower concentration (0.2 and 0.6 wt%) Ag_2Se nanoparticles added into 40 wt% polymer fibre.

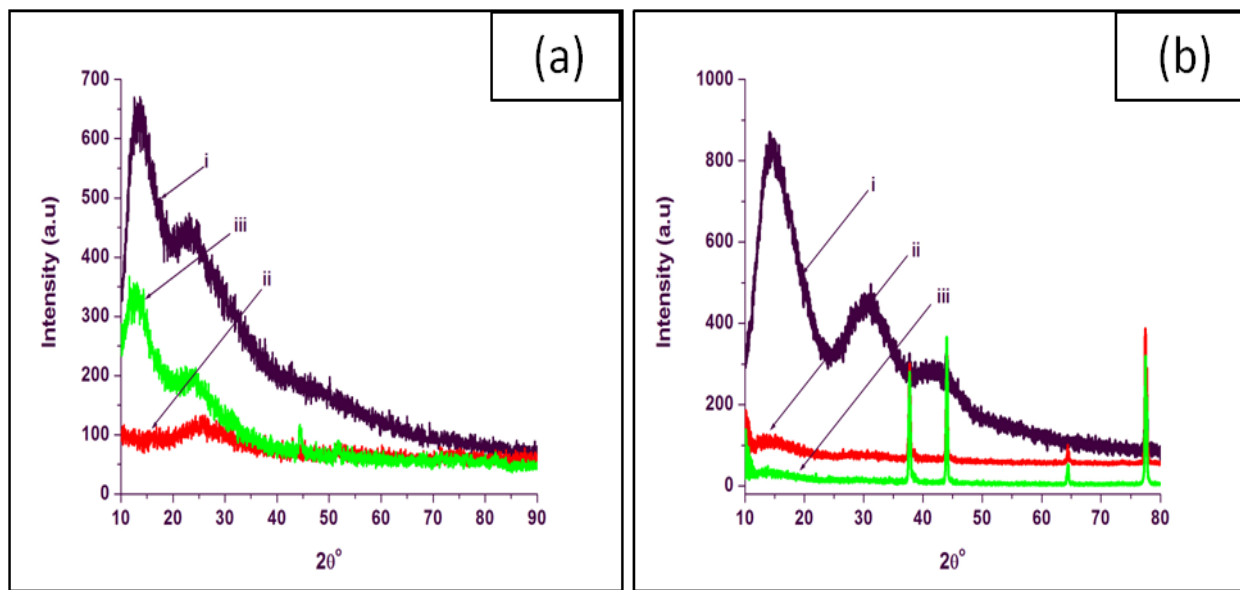


Figure 17: XRD patterns of (a) PVP, (i) 0wt%, (ii) 0.2 wt% and (iii) 0.6 wt% and (b) PMMA, (i) 0 wt%, (ii) 0.2 wt% and (iii) 0.6 wt% $\text{Ag}_2\text{Se}/\text{PVP}/\text{PMMA}$.

Figure 17 (b) shows the XRD patterns of PMMA and its composite fibres ($\text{Ag}_2\text{Se}/\text{PMMA}$). The XRD diffractogram of PMMA shows a broad peak at $2\theta = 14.2^\circ$, and two broad peaks with low intensities at $2\theta = 30.5^\circ, 43.1^\circ$. These broad peaks show the amorphous nature of the polymer. The XRD diffractogram of the composite fibres has peaks at $2\theta = 38.0^\circ, 44.0^\circ, 64.4^\circ$ and 77.4° which corresponds to the diffraction patterns of (111),(200) (220) and (311) respectively, confirming the presence of silver in the face centered cubic. The presence of silver in this material indicates that the availability of silver via reduction of silver nitrate by trioctylphosphine (TOP) was stoichiometrically in excess than selenium. The mole ratio of silver to selenium is (2:1) meaning the material will always be rich in Ag. The calculated sizes of Se and Ag are 103 and 165 pm, respectively.

5.4.2.3 FTIR spectral analysis of the polymer and the composites fibres

The composite fibres were characterized using FTIR spectroscopy to determine if there are any changes in the structure's functionality of the composite fibres. **Figure 18 (a)** shows the FTIR spectra of PVP polymer and composite fibres. According to the literature the stretching frequency for the carbonyl functional group in PVP was observed at 1680 cm^{-1} . In this study the strong C=O absorption peak from the carbonyl group of free PVP was observed at 1651 cm^{-1} which could be due to the moisture present in the sample. It has been shown that the frequency of the carbonyl stretch is very sensitive to hydrogen bond formation with water molecules, therefore as the concentration of adsorbed water is increased, the wavenumber (C=O) shifts from 1680 to 1651 cm^{-1} . The peaks assigned to the C-N group were observed at 1285 and 1074 cm^{-1} . The C-H stretching and bending vibrations were observed at 2952 cm^{-1} and 1424 cm^{-1} respectively. The FTIR spectra of $\text{Ag}_2\text{Se}/\text{PVP}$ composite fibres and PVP polymer itself gave almost identical features. There were no peaks observed for TOPO in the composite fibre which was attributed to the polymer chains displacing TOPO as capping agent.

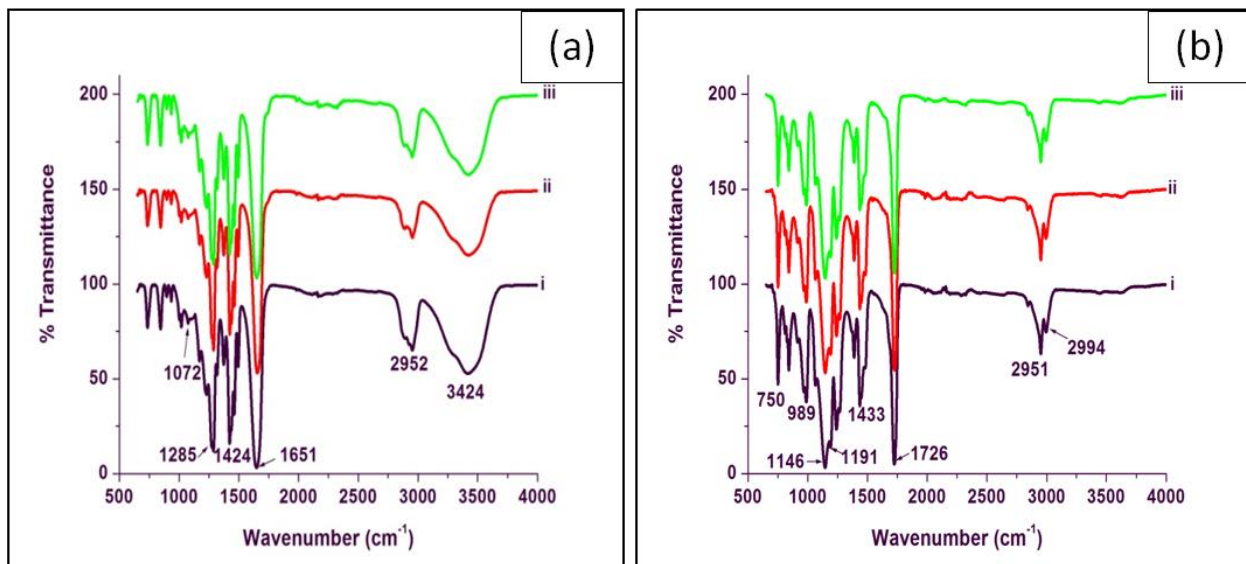


Figure 18: FTIR spectra of (a) PVP, (i) 0 wt%, (ii) 0.2 wt% and (iii) 0.6 wt% and (b) PMMA, (i) 0 wt%, (ii) 0.2 wt% and (iii) 0.6 wt% Ag₂Se/ PVP/PMMA

Figure 18 (b) shows the FTIR spectra of the electrospun PMMA and its composites fibres. The electrospun fibres were prepared from the concentration of 8 wt% PMMA with 0.2 and 0.6 wt% of Ag₂Se nanoparticles. The peaks observed at 2951 cm⁻¹ and 2994 cm⁻¹ correspond to the C-H stretching vibrations. The strong sharp peak at 1726 cm⁻¹ corresponds to the C=O stretching vibration and the peak at 1433 cm⁻¹ is from the CH₃ bending vibration. The peak observed at 1146 cm⁻¹ correspond to CH₂ bending and the peak at 1191 cm⁻¹ is from the C-O-C stretching vibration. The peak at 989 cm⁻¹ corresponds to the bending vibration of C-H and the peak at 750 cm⁻¹ is attributed to the vibration of PMMA chains.

5.5 Thermogravimetric analysis (TGA) of the polymers and the composites fibres

Figure 19 (a) indicates a weight loss of 11 % below 100 °C for pure PVP, due to the moisture present. The major decomposition observed from the pure PVP occurs between 370 and 472 °C. These results are close to the values reported by Silva and co-workers. According to Silva et al.

[19] they reported that the thermal decomposition of pure PVP start at 250 °C and a sharp mass loss occurs between 370 and 430 °C. The thermal decomposition occurs in one stage only beside the moisture observed below 100 °C, showing purified and stable PVP. The same trend was observed for 0.2 wt% and 0.6 wt% Ag₂Se/ PVP composite fibres, because they showed no significant effect on the thermal stability of the polymer due to the lower concentration of Ag₂Se nanoparticles added into the 40 wt% polymer solution.

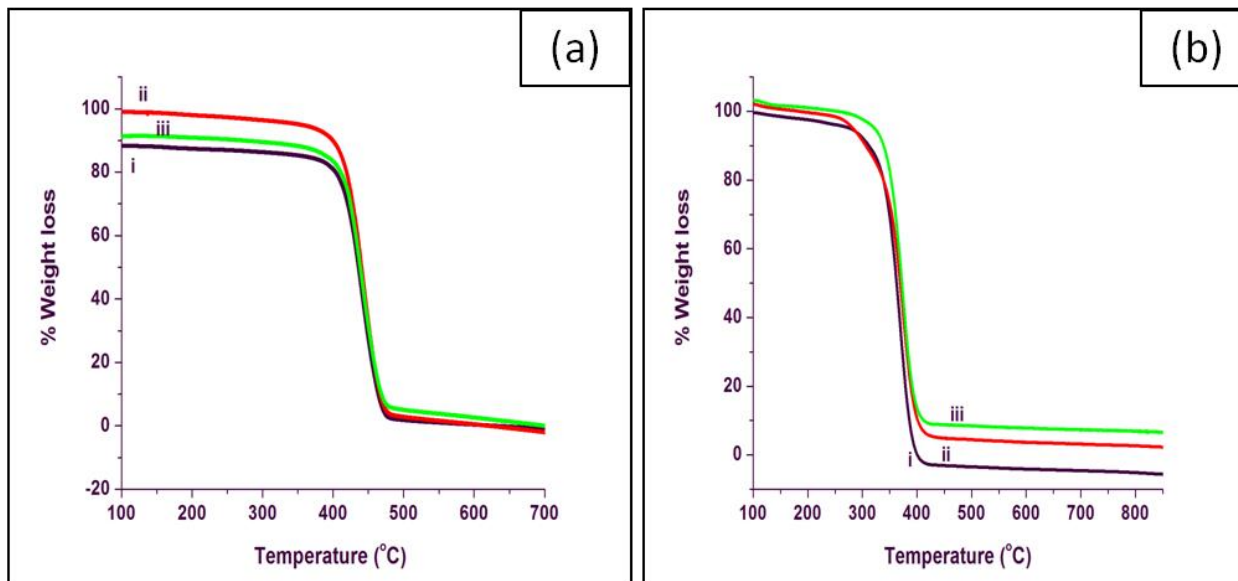


Figure 19: TGA curve of (a) PVP, (i) 0 wt%, (ii) 0.2 wt% and (iii) 0.6 wt% and (b) PMMA, (i) 0 wt%, (ii) 0.2 wt% and (iii) 0.6 wt% Ag₂Se/ PVP/PMMA

Figure 19 (b) shows the TGA curves of the electrospun PMMA and the composites fibres. PMMA decomposes in two stages, i.e. degradation of allylic chain ends followed by the main chain scission [20]. The polymer starts to degrade at 200 °C, followed by a second stage commencing at 340 °C. For pure PMMA the first decomposition stage occurred at 280 °C and could be due to the terminal C=C bond scission which normally occur at 220 °C for powdered polymer, and while the second decomposition occurred at 415 °C showing the complete decomposition of PMMA polymer. This value is close to the one reported by Dong et al. According to Dong et al. [21] they found that the thermal decomposition of PMMA at the second decomposition stage is 440 °C and

is due to the complete decomposition of PMMA polymer. The TGA curves for both composite fibres show a residue of 5 % for 0.2 wt% and 8 % for 0.6 wt% Ag_2Se nanoparticles.

5.6 Optical properties of the polymer and the composite fibres

TOPO-capped Ag_2Se nanoparticles were dispersed in PVP solution (40 wt%) by varying the amount of nanoparticles loaded from 0.2 and 0.6 wt%. **Figure 20 (a)** shows the optical properties of the electrospun PVP and composite fibres ($\text{Ag}_2\text{Se}/\text{PVP}$). The absorption bands of the composite fibres show a blue shift from pure Ag_2Se nanoparticles which have a band edge of 290 nm as explained in **Figure 5 (a) (i)**. UV-Vis spectra of nanoparticles and the composite fibres showed absorption band that were blue shifted from the bulk of Ag_2Se (1035 nm), with the band edge of 266 nm for 0.2 wt% and 273 nm for 0.6 wt% indicating the presence of nanoparticles in the fibres even at lower concentration of Ag_2Se nanoparticles. In comparison, the $\text{Ag}_2\text{Se}/\text{PVP}$ nanocomposite fibres show an improved optical property as compared to unmodified PVP.

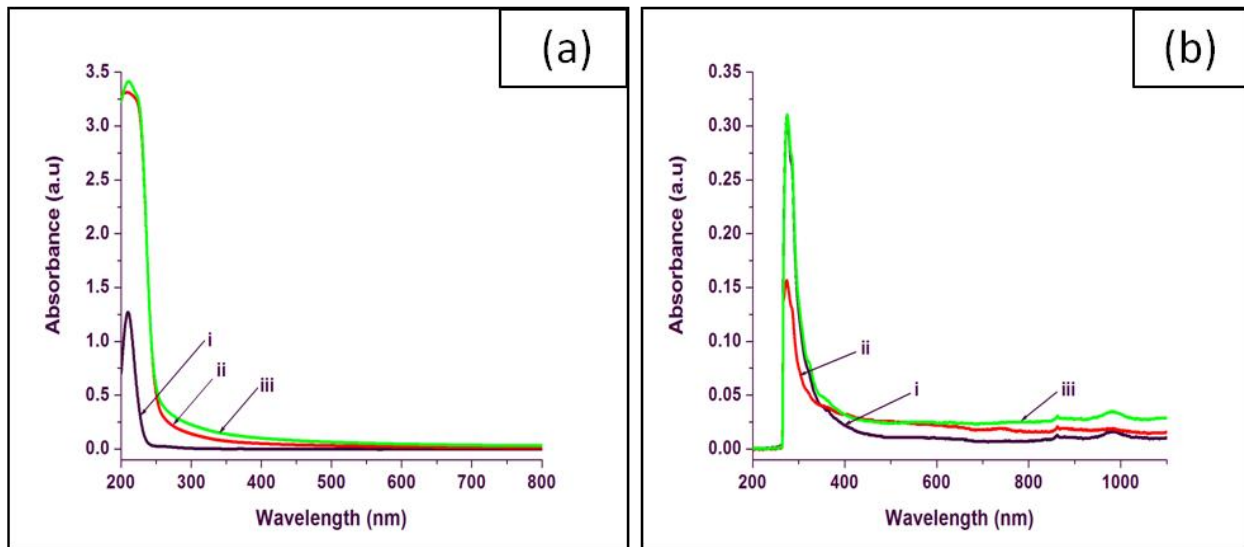


Figure 20: Absorption spectra of (a) PVP, (i) 0 wt%, (ii) 0.2 wt% and (iii) 0.6 wt% and (b) PMMA, (i) 0 wt%, (ii) 0.2 wt% and (iii) 0.6 wt% $\text{Ag}_2\text{Se}/\text{PVP}/\text{PMMA}$

Figure 20 (b) shows the absorption spectra of the electrospun PMMA and the composite fibres. The absorption features of the composite fibres show a red shift from the pure Ag₂Se nanoparticles which absorb at 290 nm as seen in **Figure 5 (a) (i)**. These red shifts could be due to the polymer displacing the capping agent TOPO which results in the growth of nanoparticles. The red shifted spectrum can be attributed to the poor distribution of the nanoparticles within the surface of the fibres. Though Ag₂Se nanoparticles were incorporated in order to enhance the interaction between the additive particles and the polymer, formation of agglomeration cannot be prevented more especially for high concentration of the additives. Both the nanoparticles and the composites fibres are blue shifted from the bulk band gap of Ag₂Se nanoparticles with the value of 1035 nm. The composite fibres show the absorption band edges at 335 nm for 0.2 wt% and 347 nm for 0.6 wt%.

5.7 Incorporation of HDA-capped Ag₂Se nanoparticles into PVP and PMMA nanofibers

Composite materials for HDA-capped Ag₂Se nanoparticles were prepared following the same method used for the incorporation of TOPO-capped Ag₂Se nanoparticles into PVP and PMMA polymers. The nanoparticles were prepared at 160 °C and have the size distribution ranging from 4 to 16 nm. These nanoparticles were found to be monodispersed, uniform and have spherical shapes. They were used as fillers to form composite fibres. It was demonstrated that when the nanoparticles were introduced into polymer solution, they increase the possibility of different kind of interaction within the solution. In this study both PVP and PMMA composite fibres produced with TOPO-capped and HDA-capped nanoparticles seemed to have no difference in what so ever, more especially on the XRD and FTIR structures. The SEM images for Ag₂Se/PVP/ PMMA composite fibres were not available for discussion.

5.7.1 XRD analysis of the pure polymer and the composite fibres

The XRD patterns in **Figure 21 (a)** shows the amorphous peaks for both the polymer and its composite fibres at $2\theta = 12^\circ$ and 22° . **Figure 21 (b)** shows the XRD patterns of PMMA and its composite fibres ($\text{Ag}_2\text{Se}/\text{PMMA}$). The pure PMMA shows a predominant and broad peak at $2\theta = 14.2^\circ$, with two other broad peaks but low intensity at $2\theta = 30.5^\circ$ and 43.1° . These broad peaks indicate the amorphous nature of the polymer. From the XRD patterns of the composite fibres the peaks appear at $2\theta = 38.0^\circ$, 44.0° , 64.4° and 77.4° correspond to the diffraction patterns of (111), (200), (220) and (311) respectively, confirming the presence of silver in the face centered cubic.

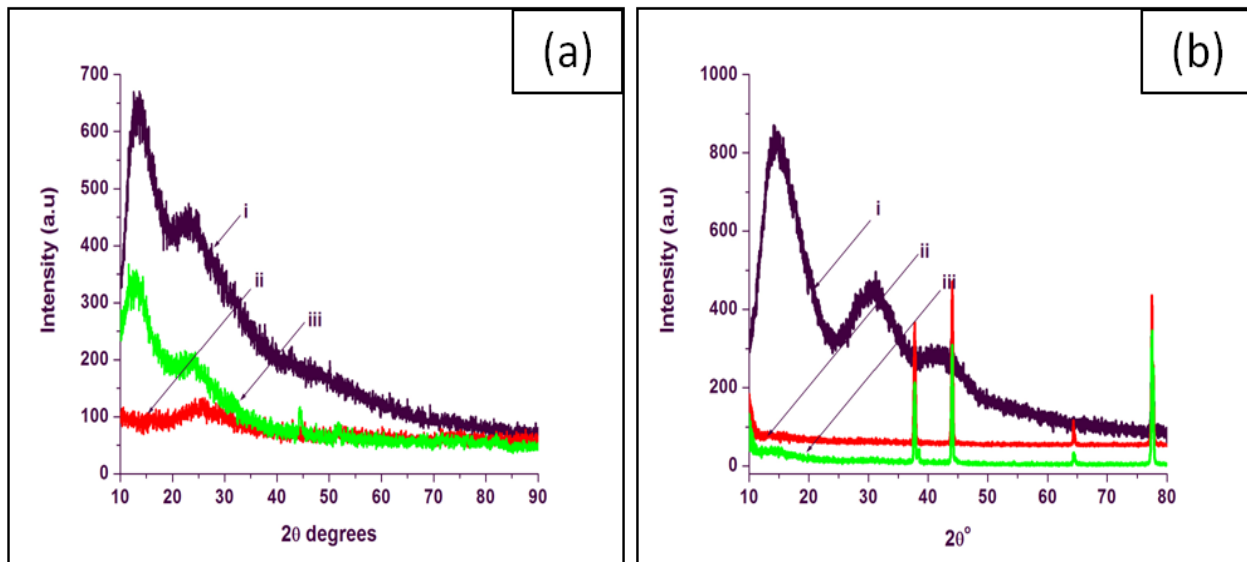


Figure 21: XRD patterns of (a) PVP, (i) 0 wt%, (ii) 0.2 wt% and (iii) 0.6 wt% and (b) PMMA, (i) 0 wt %, (ii) 0.2 wt% and (iii) 0.6 wt% $\text{Ag}_2\text{Se}/\text{PVP/PMMA}$

5.7.1.2 FTIR spectral analysis of the polymer and the composites fibres

The FTIR spectra of pure PVP polymer and composite fibres are shown in **Figure 22 (a)**. The strong C=O absorption peak from amide group of PVP is observed at 1651cm^{-1} . The peaks assigned to the C-N group were observed at 1285 cm^{-1} and 1074 cm^{-1} . The C-H stretching and bending vibrations were observed at 2952 cm^{-1} and 1424 cm^{-1} respectively. The FTIR spectra of $\text{Ag}_2\text{Se}/\text{PVP}$ composites fibres and PVP polymer gave almost identical features.

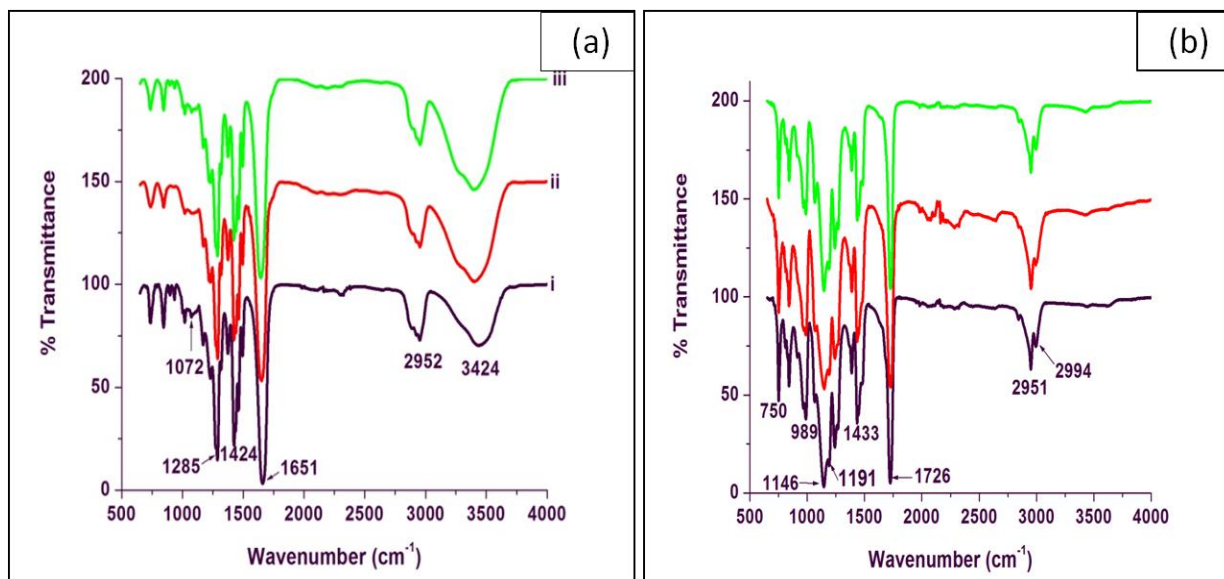


Figure 22: FTIR spectra of (a) PVP, (i) 0 wt%, (ii) 0.2 wt% and (iii) 0.6 wt% and (b) PMMA, (i) 0 wt%, (ii) 0.2 wt% and (iii) 0.6 wt% $\text{Ag}_2\text{Se}/\text{PVP}/\text{PMMA}$.

Figure 22 (b) shows the FTIR spectra of PMMA fibres and $\text{Ag}_2\text{Se}/\text{PMMA}$ composite fibres electrospun from 8 wt% PMMA solution and the nanoparticles loading of 0.2 and 0.6 wt% respectively. The peaks observed at 2951 cm^{-1} and 2994 cm^{-1} correspond to the C-H stretching vibration. The peak observed at 1146 cm^{-1} corresponds to the H-C-H bending, and the peak at 1433 cm^{-1} is from the CH_3 bending vibration. The sharp peak at 1726 cm^{-1} corresponds to the C=O stretching and the peak assigned to C-H bending vibration occurred at 989 cm^{-1} . The peak at 750

cm^{-1} is assigned to the vibration of the polymer chains. The peak observed at 1191 cm^{-1} corresponds to the C-O-C stretching vibrations. The FTIR spectra of the free PMMA and $\text{Ag}_2\text{Se}/\text{PMMA}$ composite fibres were almost identical. No any other peaks were observed for TOPO and the nanoparticles in the composite materials. The FTIR spectra showed no difference on the structural properties of the $\text{Ag}_2\text{Se}/\text{PVP}/\text{PMMA}$ composites fibres due to the lower concentration (0.2 and 0.6 wt%) of Ag_2Se nanoparticles added.

5.8 Thermogravimetric analysis (TGA) of the polymers and the composites fibers

The TGA analysis of the polymer and the composite fibres were also carried out. **Figure 23 (a)** indicates a weight loss of 11 % below $100\text{ }^{\circ}\text{C}$ for pure PVP, due to the moisture present. The major decomposition observed from the pure PVP occurs between 370 and $472\text{ }^{\circ}\text{C}$. The thermal decomposition occurs in one stage only beside the moisture observed below $100\text{ }^{\circ}\text{C}$, showing purified and stable PVP. The same trend was observed for 0.2 wt% composite fibres ($\text{Ag}_2\text{Se}/\text{PVP}$), and there was no significant effect on the thermal stability of the polymer fibres due to the lower concentration of Ag_2Se nanoparticles added into 40 wt% polymer solution. A residue of 3 % was observed for TGA curve of 0.6 wt% composite fibres indicating the presence of nanoparticles in the material.

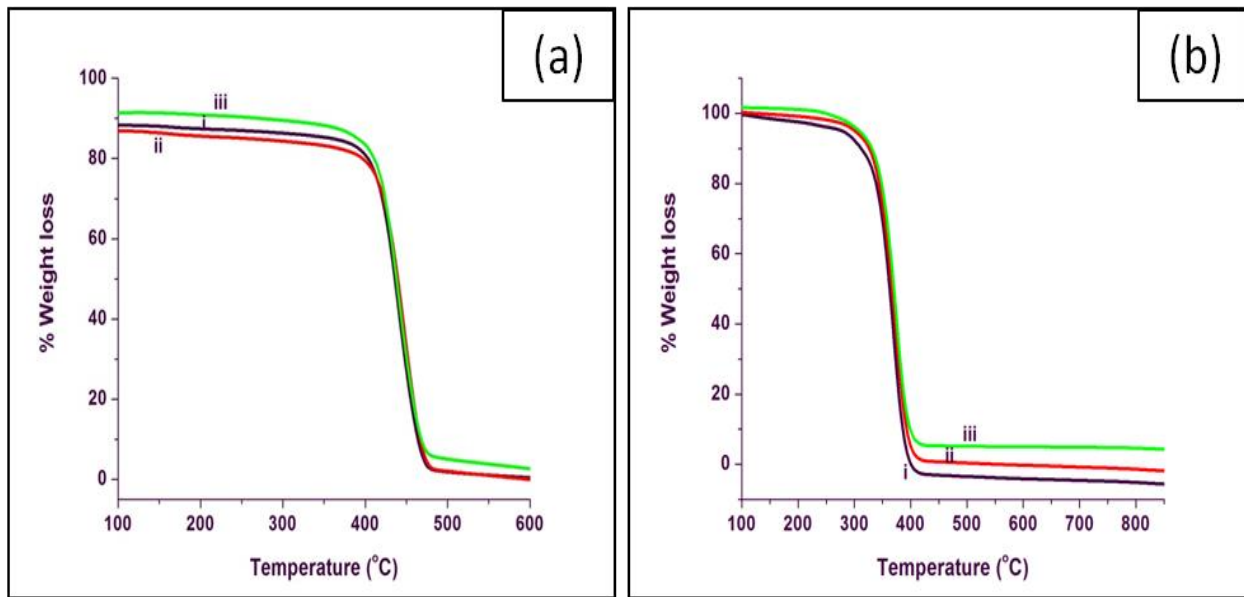


Figure 23: TGA curve of (a) PVP, (i) 0 wt%, (ii) 0.2 wt% and (iii) 0.6 wt% and (b) PMMA, (i) 0 wt%, (ii) 0.2 wt% and (iii) 0.6 wt% Ag₂Se/ PVP/PMMA

Figure 23 (b) shows the TGA curves of the electrospun PMMA and the composites fibres. For pure PMMA, the first decomposition stage occurred at 266 °C and could be due to the head-to-head linkage initiated by terminal C=C bond, which is known to appear at a lower temperature of about 220 °C for powder PMMA [22]. The second decomposition occurred at 412 °C indicating the complete decomposition of PMMA polymer fibres. The TGA of 0.6 wt% composite fibres (Ag₂Se/PMMA) show a residue of 8 % which could be due to the nanoparticles present in the material. The TGA curve for 0.2 wt% composite fibres has a left over residue of 2 % due to the nanoparticles present. Addition of Ag₂Se nanoparticles into PMMA fibres improved the thermal stability of the polymer.

5.9 Optical properties of the polymers and the composite fibres

HDA-capped Ag₂Se nanoparticles were dispersed in PVP solution (40 wt%) by varying the amount of nanoparticles loaded from 0.2 and 0.6 wt%. **Figure 24 (a)** shows the optical properties of the electrospun PVP and composite fibres (Ag₂Se/PVP). The absorption bands of the composite fibres show a blue shift from pure Ag₂Se nanoparticles which have a band edge of 290 nm as observed in **Figure 8 (a) (ii)**. The nanoparticles and the composite fibres show a blue shift from the bulk of Ag₂Se (1035 nm), and this is a consequence of quantum confinement effect of the incorporated nanoparticles. The band edges for the composite fibres are 248 nm for 0.2 wt% and 259 nm for 0.6 wt%.

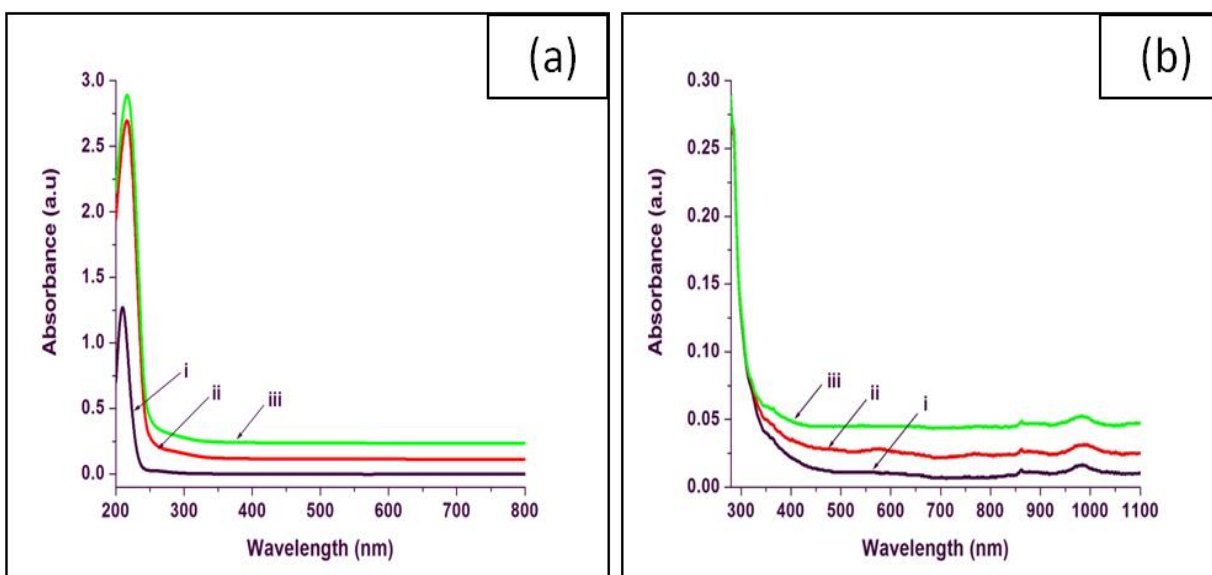


Figure 24: Absorption spectra of (a) PVP, (i) 0 wt%, (ii) 0.2 wt% and (iii) 0.6 wt% and (b) PMMA, (i) 0 wt%, (ii) 0.2 wt% and (iii) 0.6 wt% Ag₂Se/ PVP/PMMA

Figure 24 (b) shows the absorption spectra of the electrospun PMMA and the composite fibres. HDA-capped Ag₂Se nanoparticles were dispersed in the solution of 8 wt% PMMA. The effect of nanoparticles loading was also investigated here by varying the amount of Ag₂Se nanoparticles or quantum dots (0.2 to 0.6 wt%) added into PMMA solution. The absorption features of the composite fibres show a red shift from the pure Ag₂Se nanoparticles which absorb at 290 nm as seen in **Figure 8 (a) (ii)**. These red shifts come from the poor distribution of the nanoparticles within the surface of the fibres. The nanoparticles and the composites fibres are blue shifted from the bulk band gap of Ag₂Se nanoparticles with the value of 1035 nm. The absorption band edges for composite fibres are 338 nm for 0.2 wt% and 342 nm for 0.6 wt%.

5.10 Conclusions

Ag_2Se nanoparticles were successfully prepared using TOPO and HDA as capping agents. The effect of temperature on the optical properties, morphology and size of the nanoparticles was also investigated and appears to have an influence on the shape and size of the nanoparticles. PVP and PMMA polymer fibres were prepared successfully using electrospinning technique at room temperature. The prepared polymer fibres were found to be affected by the solution concentration, voltage and the amount of nanoparticles or additives loaded. The incorporation of Ag_2Se nanoparticles into PVP and PMMA nanofibres have been prepared successfully by electrospinning. For PVP, at lower concentration beads and fibres were formed, whereas at higher concentration the shape of the beads changed to more uniform fibres. The SEM results showed that an increase in PVP concentration resulted in a more uniform fibers with an increased average diameters. Upon addition of nanoparticle into 40 wt% PVP solution the fibers uniformity improved and further decreased the diameters. Hence increasing the voltage decreases the fibre diameters. The absorption bands showed blue shifts, from the bulk, and the appearance of the bands in composites confirm the presence of nanoparticles at the lowest concentration. The electrospun composite fibres for PVP show improved optical properties as compared to the pure PVP polymer. The XRD patterns show the amorphous peaks for both the polymer and its composites fibres. TGA curves showed no significant effect on the thermal properties of the polymer and its composites due to the lower concentration of Ag_2Se nanoparticles added into 40 wt% PVP solution. The FTIR spectra of the composite and pure PVP gave almost identical features.

PMMA incorporated TOPO-capped Ag_2Se nanoparticles was also prepared successfully using electrospinning technique. The XRD patterns of the composite fibres confirmed the presence of Ag in the material. The FTIR spectra showed no significant difference on the structural functionality of the pure polymer and its composite fibres. The absorption band of the composite fibres showed a red shift from the pure Ag_2Se nanoparticles but blue shifted from the bulk of Ag_2Se . TGA curves showed an increase in the thermal stability of the composite fibres ($\text{Ag}_2\text{Se}/\text{PMMA}$) upon addition of the nanoparticles. The very same study was performed for PVP

and PMMA incorporated HDA-capped Ag₂Se nanoparticles. The nanoparticle prepared with HDA appears to have no significant difference on the structural functionality of the composite fibres. Both composites fibres prepared by TOPO and HDA appears to have similar observations on XRD and FTIR structures and also on UV-VIS spectra. TGA of both PVP and PMMA incorporated HDA-capped nanoparticles showed a residue with increasing the amount of Ag₂Se nanoparticles.

In comparison the absorption bands for PVP composite fibres show a blue shift from the pure Ag₂Se nanoparticles whereas on the PMMA composite, it shows a red shift from the pure Ag₂Se. The XRD analysis of the PVP composite fibres shows no significant difference upon addition of Ag₂Se nanoparticles, whereas on PMMA composite it shows peaks which were due to Ag in the face centered cubic phase. TGA curves showed no significant effect on the thermal properties of the PVP polymer and its composite fibres, whereas on the PMMA composite fibres it shows an increase in the thermal stability of the polymers upon addition of Ag₂Se nanoparticles.

5.11 References

- [1] F. Haaf, A. Sanne, and F. Straub, *Polymer*, **1985**, 17, 143-152.
- [2] D. Wohrle, *Angewandte Chemie International Edition*, **2005**, 44, 7500-7502.
- [3] P. R. Majhi, S. P. Moulik, S. E. Burke, M. Rodgers, and R. Palepu, *Journal of colloid and interface Science*, **2001**, 235, 227-234.
- [4] H. D. Wu, I. D. Wu, and F. C. Chang, *Polymer*, **2005**, 42, 555.
- [5] M. A. Witek, S. Wei, B. Vaidya, A. A. Adams, L. Zhu, W. Stryjewski, *Lab Chip*, **2004**, 4, 464-72.
- [6] S. A. Soper, S. M. Ford, S. Qi, R. L. McCarley, K. Kelly, and M. C. Murphy, *Anal Chem*, **2000**, 72, 642 A - 651 A.
- [7] R. L. McCarley, B. Vaidya, S. Wei, A. F. Smith, A. B. Patel, and J. Feng, *Journal of American Chemical Society*, **2005**, 127, 842-843.
- [8] J. M. Deitzel, J. Kleinmeyer, D. Harris, and N. C. B Tan, *Polymer*, **2011**, 42, 261-272.
- [9] M. M. Hohman, M. Shin, G. Rutledge, and M. P. Brenner, *Physics of Fluids*, **2001**, 13, 2221-2236.
- [10] H. Wang Q. Liu Q. Yang, Y. Li, W. Wang, L. Sun, C. Zhang, and Y. Li, *Journal of Material Science*, **2010**, 45:1032–1038
- [11] T. P. Mthethwa, M. J. Moloto, A. De Vries, and K. P. Matabola, *Materials Research Bulletin*, **2011**, 46, 569-575.
- [12] T. J. Sill, and H. A. Von Recum, *Biomaterials*, **2008**, 29:1989-2006.
- [13] H. Jin, X. Du, and Y. Jiang, *Proceedings of SPIE*, **2009**, 7508, 750841.
- [14] O. S. Yordem, M. Papila, and Y. Z. Menceloglu, *Mater Des*, **29**, **2008**, 34-44.
- [15] X. Zong, K. Kim, D. Fang, S. Ran, and B. Chu, *Polymer*, **2002**, 43, 4403-4412.
- [16] Q. B. Yang, D. M. Li, and Y. L. Hong, *Synthetic Metals*, **2003**, 137, 973-974.
- [17] W. K. Son, J. H. Youk, and T. S. Lee, *Macromolecular Rapid Communications*, **2004**,

25, 1632.

[18] S. Wei, J. Sampathi, Z. Guo, N. Anumandla, D. Rutman, A. Kucknoor, L. James and A. Wang, *Polymer*, **2011**, 52, 5817-5829.

[19] M. F. Silva, C. A. da Silva, F. C. Fogo, E. A. G. Pineda, and A. W. Hechenleitner, *Journal of thermal Analysis and Calorimetry*, **2005**, 79, 367-370.

[20] N. Grassie, *Chemistry of high polymer Degradation Processes*, **1956**, John Wiley & Sons, Inc. New York.

[21] Z. Dong, S. J. Kennedy and Y. J. Wu, *Power Sources*, **2011**, 196, 4886 – 904.

[22] W. R. Zeng, S. F. Li, and W. K. Chow, *Journal of Fire Sciences*, **2002**, 20, 401-434.

CHAPTER 6

SUMMARY AND RECOMMENDATION

6.1 Summary

The synthesis of Ag₂Se nanoparticles was done successfully using TOPO and HDA as capping agent. The effect of temperature and capping group on the morphology of Ag₂Se nanoparticles were investigated. Uniform, monodispersed spherical Ag₂Se nanoparticles were prepared in HDA as compared to TOPO. Temperature variation had an influence on the morphology and size of the nanoparticles, where an increase in particles was observed due to Ostwald ripening. An increase in temperature for TOPO-capped Ag₂Se nanoparticles favoured the kinetic reaction since the morphology of the nanoparticle changed from sphere to hexagonal shape. The nanoparticles prepared in HDA favoured thermodynamic reaction since no change in the morphology of the nanoparticles was observed, the particles remained spherical regardless of the increase in temperature. In the XRD results of Ag₂Se nanoparticles the peak that belongs to Ag was observed for both TOPO and HDA.

Polymer composite fibres have been prepared directly by electro-spinning at room temperature. Lower concentrations of the nanoparticles were used in the study due to small yield obtained during the synthesis. The nanoparticles were incorporated into PVP and PMMA to make composite fibres. High concentration (40 wt%) of the polymer solution were used for PVP polymer solution and lower concentration (8 wt%) were used for PMMA composite fibres. The increase in PVP concentration resulted in a uniform fibres with an increased fibre diameters. Increasing the voltage decreases the fibre diameters. Incorporation of Ag₂Se nanoparticles into PVP fibres decreased the fibre diameters as a result of an increased conductivity. Addition of HDA-capped Ag₂Se nanoparticles into PVP and PMMA fibres improved the thermal stability of the polymer fibres,

whereas on TOPO-capped nanoparticles it improved the thermal stability of PMMA fibres. This could be due to the fact that TOPO has a poor capping density and since PVP concentration was very high in the solution its polymer chains might displace TOPO as capping agent. That is why there were no traces of TOPO-capped nanoparticles in the composite fibres ($\text{Ag}_2\text{Se}/\text{PVP}$). The polymer composites fibres produced were characterize by UV-VIS spectrometry for optical properties, SEM for morphology and size, XRD and FTIR for the structural analysis lastly TGA for thermal study. The study was supposed to show how the interaction occurs between the polymer and the organically capped nanoparticles, since it is a challenging subject to all researchers. However introducing nanoparticles into the polymer could improve some of the properties that the polymer contains.

6.2 Recommendations

Further studies needs to be done in order to understand electrospinning of composites and how additives/fillers interact with their surrounding polymer matrix, and how they behave in a dramatic change of material properties. The study also needs to be done to understand about the dispersity of the nanoparticles in the polymer solution and how to prevent their agglomeration.

The study on synthesis of Ag nanoparticles was also performed using the metal organic route method. This method must not be used when synthesizing Ag nanoparticles because it produces small yields. The nanoparticles prepared were for HDA only and nothing was obtained for TOPO. Analyses were only performed on TEM and UV-VIS spectroscopy. XRD analysis was not done because there were not enough yields. The study on the incorporation of HDA-capped Ag nanoparticles into polymer fibres was unsuccessful due to small yield obtained during the synthesis of nanoparticles. Other method that can give high yields can be looked at for the preparation of Ag nanoparticles.